Order Number 9200458

The hydraulic fracturing of soil

Murdoch, Lawrence Corlies, III, Ph.D.
University of Cincinnati, 1991

U·M·I
300 N. Zeeb Rd.
Ann Arbor, MI 48106

THE HYDRAULIC FRACTURING OF SOIL

A Dissertation submitted to the

Division of Graduate Studies and Research
of the University of Cincinnati

in partial fulfillment of the
requirements for the degree of

DOCTOR OF PHILOSOPHY

in the Department of Geology
of the College of Arts and Sciences

1991

by

Lawrence Corlies Murdoch III

B.S., Pennsylvania State University, 1980
M.S., University of Cincinnati, 1983
M.S., University of Cincinnati, 1988

Committee Chair: Arvid M. Johnson

UNIVERSITY OF CINCINNATI

4 May 19 91

I hereby recommend that the thesis prepared under my supervision by Lawrence Corlies Murdoch III

entitled The Hydraulic Fracturing of Soil

be accepted as fulfilling this part of the requirements for the degree of Doctor of Philosophy

Approved by:

Arnold M. Johnson

David B. Nash

Thomas C. Lamb

ABSTRACT

Little is known about the hydraulic fracturing of soil, although the technique holds potential for several environmental engineering applications. The dissertation research consists of laboratory experiments, where hydraulic fractures were created by injecting dyed glycerin into colluvium contained in a triaxial pressure cell, and a field test, where hydraulic fractures were created by injecting guar gum gel at shallow depths in glacial drift. The laboratory tests showed that hydraulic fractures are readily created in clayey-silt colluvium. Furthermore, hydraulic fractures created in soil with positive pore pressure were filled with two fluids: one injected to create the fracture, and pore fluid that infiltrates into the fracture tip. The length of the infiltrated tip increases with increasing fracture length.

The water content of soil markedly affects the fracturing process. In particular, the transition from negative to positive pore pressure results in an abrupt decrease in fracture toughness and modulus, and a decrease in the amount of leakoff. Increasing water content causes fracture propagation to become more stable. A theoretical analyses, based on laboratory observations and formulated using linear elastic fracture mechanics, is developed to explain the forms of pressure records and to predict essential details of the experiments.

A field test was conducted during June 1988 at a site underlain by Pleistocene glacial drift near Cincinnati, Ohio. Oil-field service equipment was used to create fractures at 10 boreholes 2 to 4 m deep. Excavation following the tests revealed that the fractures were slightly elongate in plan (2:3 aspect) and dipped gently (14° to 25°) toward their parent borehole. The largest covered 90 m^2 and extended 13.5 m from the borehole when it vented. More typically, however, the fractures covered roughly 20 m^2 and extended 5 to 8 m from the borehole. Sand

pumped into the fractures was a maximum of 9 mm thick. This research shows that hydraulic fractures of useful size can be created and filled with sand at shallow depths in glacial drift.

ACKNOWLEDGEMENTS

This dissertation has been far from a solo venture. Professor Arvid Johnson, chairman of the dissertation committee, trained me to use the professional tools that were necessary to conduct the dissertation research. He also reviewed various drafts and suggested details that proved to be insightful and significant. Professor David Nash has been an enthusiastic advocate throughout the research project. He, along with Professor Tom Lowell, reviewed drafts of the dissertation and provided helpful suggestions as members of the committee.

The research described in this dissertation was conducted as part of a project funded by the U.S. Environmental Protection Agency while I was working at the University of Cincinnati Center Hill Solid and Hazardous Waste Research Facility. I would like to express my gratitude to the many individuals at both the USEPA and Center Hill who have helped with this project. Doug Ammon, formerly of the USEPA, recognized merit in my early proposals and was instrumental in initiating the project. It was the consistent support of Herb Pahren and Mike Roulier of the USEPA, however, that made the project possible. Gerry Roberto, manager of the Center Hill Facility, provided encouragement and advice, but, most of all, was understanding during the times when the academic aspects of completing the dissertation overlapped with the professional aspects of fulfilling the requirements of the funded project. John Stark and the management of the ELDA Landfill gave me permission to conduct a field test on their property, and they generously provided assistance during the tests. Gary Weiss of the University of Cincinnati helped with the derivation in Appendix C.

I had the privilege of interacting with many talented individuals at Center Hill during the course of this dissertation. Bruce Patterson played a key role during

the field tests at the ELDA Site. He and Bruce Braswell provided patience and care during the many, often tedious, laboratory experiments. Glenn Milenkevich and Patti Strube conducted the geotechnical soil tests. Various computer codes, apparatuses, electronic circuits, and other gadgetry were designed, created and implemented by the talented Phil Cluxton. Bill Harrar and George Losonsky contributed to the field test, and Bill offered some useful insights during the laboratory tests. Joe Wilmhoff drafted many of the figures.

My family deserves special appreciation. My mother, Pat Gibbon, and my father, Larry Murdoch Jr., provided the early schooling that sparked my curiosity, and remained an enthusiastic force throughout my education. More than anyone else, however, it was Nan Genther who provided the inexhaustible support and patient understanding without which this dissertation would probably still be an unfinished draft.

To the many others who contributed but were not mentioned above; thanks.

TABLE OF CONTENTS

LIST OF FIGURES

LIST OF TABLES

INTRODUCTION

The recovery of hazardous chemicals from contaminated ground is often difficult and sometimes impossible using established techniques, so earth scientists have begun to turn to related fields for innovative ideas. The problem of recovering hydrocarbons from reservoirs in petroleum engineering is analogous to the problem of recovering contaminants from aquifers in environmental engineering. Petroleum engineers have developed a wide range of techniques to enhance the recovery of oil from reservoirs, and one of the most effective is hydraulic fracturing. Thus my research has focused on the similarities and differences of hydraulic fracturing in rock and in soil.

Most remedial systems requiring fluid flow either into or out of the subsurface could benefit from hydraulic fracturing. Pump and treat systems are obvious candidates because they employ procedures resembling those used in petroleum recovery, where the benefits of hydraulic fractures are without question. The yields of vapor-producing wells, such as those recovering natural gas or steam, are improved by hydraulic fracturing, so by analogy vapor extraction systems should benefit from this technology. Similarly, hydraulic fracturing could be used in conjunction with steam stripping--a process developed to improve yields of oil wells and currently being tested under remedial conditions. Horizontal, sheet-like hydraulic fractures placed below a contaminated region could be used as gravity drains to intercept the leachate from soil flushing systems (Murdoch and others, 1987). Bio-remediation systems stand to benefit in particular because nutrients for microorganisms, or the microorganisms themselves, could potentially be delivered as fine-grained solids in hydraulic fractures.

The basic process of hydraulic fracturing, as it is used in the petroleum industry, begins with the injection of fluid into a well until the pressure of the fluid exceeds a critical value and a fracture is nucleated. A granular material, which is usually sand and is termed a *proppant*, is pumped into the fracture as it grows away from the well. Transport of the proppant is facilitated by using a viscous fluid, usually a gel formed from guar gum and water, to carry the proppant grains into the fracture. After pumping, the proppant holds the fracture open while the viscous gel breaks down into a thin fluid. The thinned gel is then pumped out of the fracture, creating a permeable channelway suitable for either the delivery or recovery of liquid or vapor.

Experience in the oil industry suggests that hydraulic fracturing might increase flow rates from wells used to recover ground water contaminants. However, to realize this increase, hydraulic fractures would have to be created and filled with sand under the conditions of contaminated regions. Oil reservoirs are typically deeper and are composed of different materials than contaminated regions, so the applicability of fracturing methods used by petroleum engineers is unknown.

Contaminants commonly occur in soils[1] that are weaker and more compliant than limestone or sandstone typical of oil reservoirs. Effects of the higher plasticity of soil on hydraulic fracturing are difficult to anticipate based on the results of studies of hydraulic fracturing in brittle rock.

Hydraulic fractures virtually never vent when they are created in oil reservoirs, which are several hundred to several thousand meters deep, but the

---

1 The term *soil* is used in this work to mean an unlithified, or uncemented sediment.

practical problem of creating fractures at shallow depths has yet to be addressed. Most contaminants occur at shallow depths (several meters to several tens of meters), so hydraulic fractures in soil will tend to intersect the ground surface and vent, severely limiting the length, and thus the performance of the fractures.

As a result, little is known about the basic problem of hydraulic fracture propagation in soil and the applied problem of creating useful hydraulic fractures at shallow depths.

The approach of this research was to adapt methods proven from studies of hydraulic fracturing of rock to applications of hydraulic fracturing of soil. Laboratory experiments were conducted by creating hydraulic fractures in rectangular samples of remolded clayey-silt confined in a triaxial pressure cell. Results of the experiments were analyzed using methods of linear elastic fracture mechanics, a branch of elasticity theory that is widely used to analyze hydraulic fracturing in rock and other engineering materials.

Field experiments were performed by creating hydraulic fractures in Pleistocene glacial till at depths of between two and four meters. The experiments were conducted in collaboration with a subcontractor, who used equipment designed to create hydraulic fractures from oil wells. Hydraulic fractures were successfully created during the field tests, and then were exposed in the walls of trenches dug with a backhoe. Detailed descriptions of exposures document the geometries of the fractures.

The dissertation contains four chapters and several appendices. Direct observations of hydraulic fractures are described in Chapter One, as are the experimental techniques and equipment. A conceptual model that explains the observations is discussed at the close of Chapter One. Indirect observations,

particularly the records of injection pressure from the experiments are described in Chapter Two. Fracture toughness, a material property identified by workers in fracture mechanics, is used in Chapter Two to account for a close relationship between the pressure records and the water content of the soil enveloping a fracture. Taken together, Chapters One and Two outline the descriptive information obtained from the experiments. A theoretical analysis that is based on observations from Chapter One and seeks to explain the pressure records in Chapter Two is derived and tested in Chapter Three. A comparison between the theoretical analysis and the information obtained from the laboratory concludes Chapter Three. The final chapter, Chapter Four, outlines the methods and results of the field test. Possible applications of hydraulic fractures are outlined in Appendix A, along with some preliminary estimates on the effects of hydraulic fractures during remediation. A review of other work on hydraulic fracturing is presented in Appendix B, and a solution to the flow of water to a well intersecting a vertical hydraulic fracture of finite conductivity is derived in Appendix C.

CHAPTER ONE

OBSERVATIONS DURING LABORATORY EXPERIMENTS

The way that hydraulic fractures grow in soil has been largely ignored. Only their initiation has been of concern because the problem is to prevent them from happening at all. They are a nuisance to engineering projects such as injection of grout, permeability testing, deep-well injection, or dam construction. As a result of the focus on fracture initiation little is known about the physical appearance, mechanical behavior, or methods of analyzing the growth of a hydraulic fracture in soil.

The goal of this chapter is to apply methods of studying hydraulic fractures in rock to aid in understanding hydraulic fractures in soil. Laboratory tests were conducted using a bench scale apparatus designed to create hydraulic fractures. During the laboratory tests, hydraulic fractures were created by injecting fluid into samples confined within a triaxial loading cell. The traces of the fractures were observed directly by looking through a transparent loading plate in the experimental apparatus, and phenomena related to fracturing were observed indirectly by measuring the pressure and volume of injected fluid as a function of time. The direct observations, combined with descriptions of fracture surfaces from samples split open after testing, yield important details of the appearance of a hydraulic fracture.

Before the observations can be described, it will be necessary to explain the design of the apparatus, the techniques of preparing a sample, and the procedures of conducting a test.

EXPERIMENTAL DESIGN

The experiments were designed to create hydraulic fractures by injecting glycerin into rectangular blocks of soil confined in a triaxial pressure cell. Rhodamine dye was added to the glycerin to highlight areas of the fracture surface wetted by the glycerin. The pressure of the injection fluid was monitored as a function of time to develop insights into the initiation and propagation of the fractures.

Apparatus

The experimental apparatus consists principally of a pump, a fracture cell, and a data acquisition computer (Fig. 1.1). The pump is used to inject fluid at a constant rate into a sample contained in the fracture cell. Typically, the pressure of the injected fluid increases until fracturing occurs, then decreases during fracture propagation. The computer is used to monitor injection fluid pressures as a function of time and to control the flow rate of the pump.

The fracture cell is a rectangular chamber (inside dimensions are 10 cm by 10 cm by 39 cm) with one moveable side that is used as a loading plate (Fig. 1.2). The loading plate is transparent, so that the interior of the cell can be inspected during a test. The other five sides of the chamber are lined with neoprene bladders which can be inflated with air. The three principal stresses on the sample are controlled independently by adjusting air pressures in the bladders. Three sets of pressure gauges and regulators provided independent control of each of the confining stresses. Pressure in the bladders rarely exceeded 105 kPa (15 psi) during this study.

A hole in the loading plate allows access to a soil sample inside the chamber. A spacer plate, placed between the loading plate and the sample, contains a

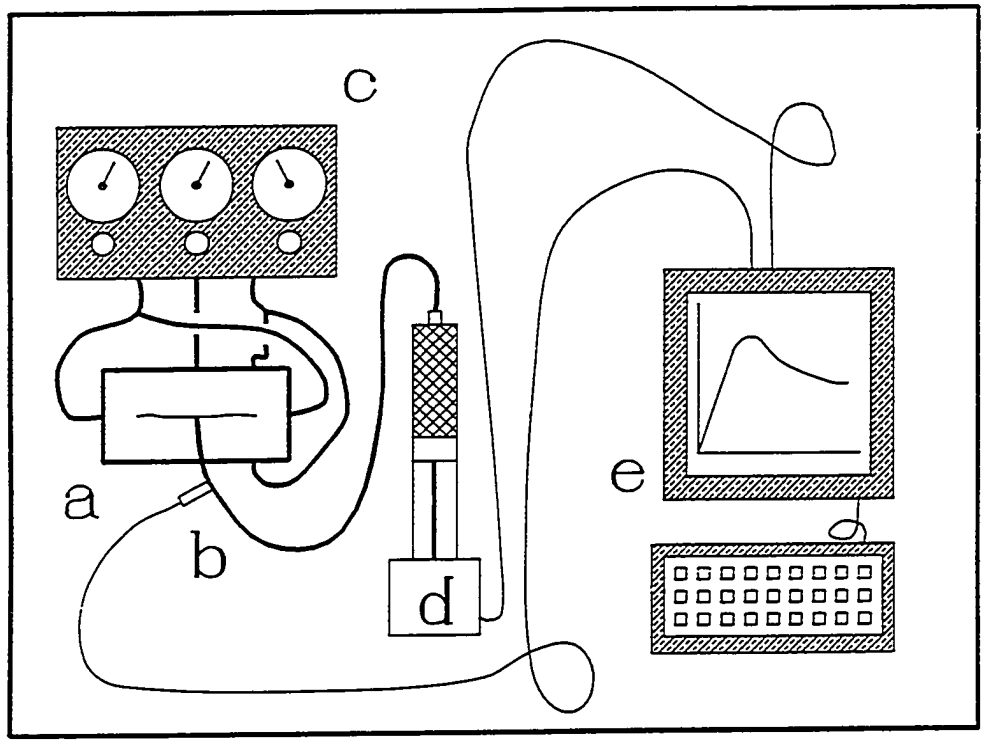

Figure 1.1. Apparatus used during hydraulic fracturing experiments. A. Fracturing cell; B. Pressure Transducer; C. Gauges and regulators of confining pressure; D. Syringe pump; E. Data acquisition computer.

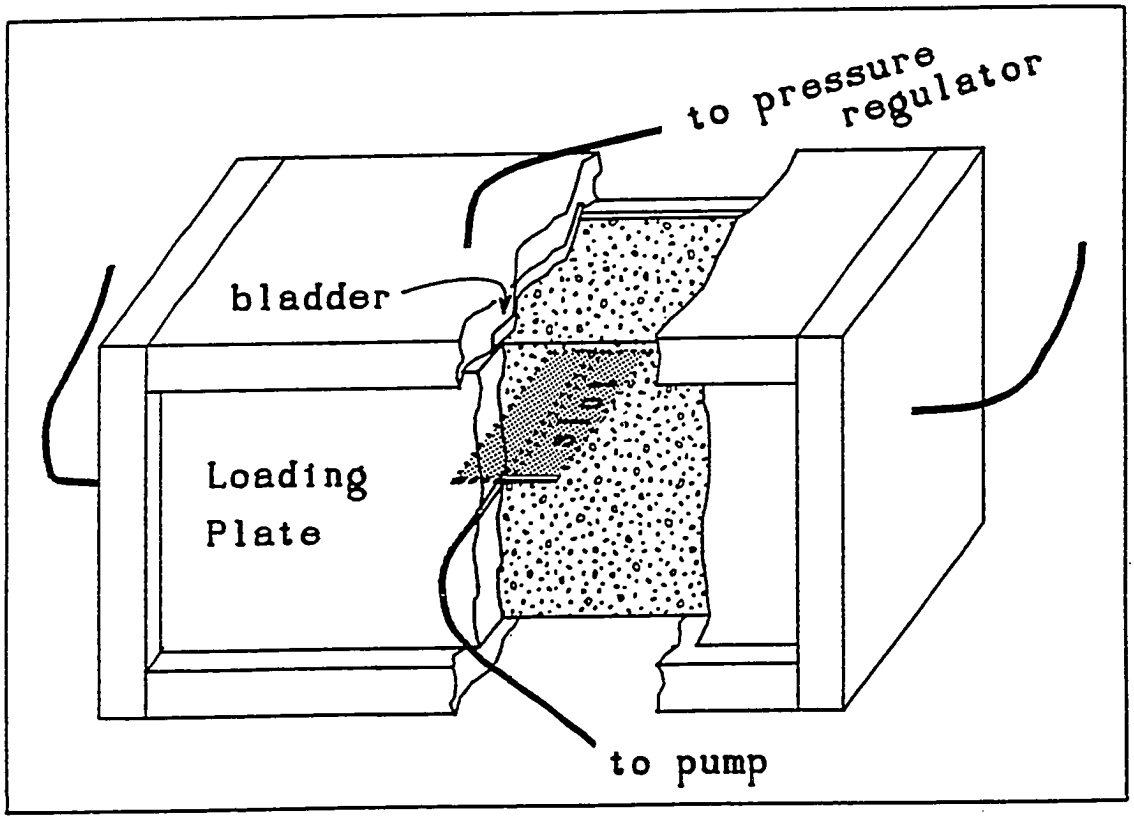

Figure 1.2. Cut-away sketch of hydraulic fracturing cell.

pressure-tight fitting for tubing three mm in diameter. The tubing extends from the pump through the loading and spacer plates and into a thin slot cut in the sample (Fig. 1.2). The slot is the initial hydraulic fracture.

The pump (Fig. 1.1) used to inject fluid into the slot is a syringe-like device consisting of a piston driven by a threaded rod attached to a stepper motor. The flow rate of the pumping system is controlled by regulating the rate of rotation of the motor. Other details of the design and operation of the pumping system are given in Murdoch and others (1990).

A flow rate of 0.033 cm^3/sec was used for the tests described in the following pages. The Reynolds Number associated with flow of glycerin in the starter slot at that flow rate is 0.1, and in hydraulic fractures it was less because the aperture of the fractures was less than that of the slot, so laminar flow is assumed to occur in the fractures.

Glycerin was used as the injection fluid for all the tests. Rhodamine dye, which stains soil a deep red, was added at roughly 1:100. The dyed glycerin has a viscosity of 175 cp at 21 °C, and the viscosity is constant over the strain rates anticipated in the apparatus, according to laboratory measurements made with a rotational viscometer.

Pressure of the injection fluid as a function of time was recorded during each test. A transducer, accurate to 300 Pa, positioned roughly 20 cm upstream of the slot was used to measure pressure every 0.2 sec. Pressure losses due to flow from the transducer to the tip of the starter slot are on the order of the accuracy of the transducer, according to calculations using standard methods (Streeter, 1971), so the pressure measured at the transducer will be taken to be the pressure within the slot.

Physical Characteristics of the Soil

The experiments were conducted using a yellow-brown clayey silt colluvium collected at a depth of 0.7 to 1.0 m from a pit adjacent to the Center Hill Research Facility, Cincinnati, Ohio. The colluvium is weathered from undifferentiated shale and limestone overlying the Bellevue Formation. It is similar to the colluvium involved in shaliow landslides throughout the Cincinnati area (Fleming and others, 1980). The colluvial soil will be termed the Center Hill clay.

Both the results of hydraulic fracturing of soil and many of the physical characteristics of Center Hill clay have a strong dependence on water content θ, the ratio of the weight of water to the weight of solids. For the purposes of this work, we will identify three fundamental conditions based on water content and designate them Conditions *A*, *B*, and *C*. The Conditions are marked by significant changes in either pore pressure or degree of saturation. The transition from negative (with respect to atmospheric pressure) to positive pore pressure at a water content of approximately 0.23 marks the boundary between *A* and *B*, whereas the transition from partial to fully saturated pores at a water content of 0.27 marks the boundary between *B* and *C* (Fig. 1.3). Thus, the water content conditions are defined as

Condition *A*: Partly-saturated, negative pore pressure

Condition *B*: Partly-saturated, positive pore pressure

Condition *C*: Fully-saturated, positive pore pressure

To obtain data shown in Figure 1.3, the degree of saturation R_s was determined from

$$R_s = (\gamma_{solid}\ \gamma_{dry}\ \theta)/\ \gamma_w(\gamma_{solid} - \gamma_{dry}) \qquad (1.1)$$

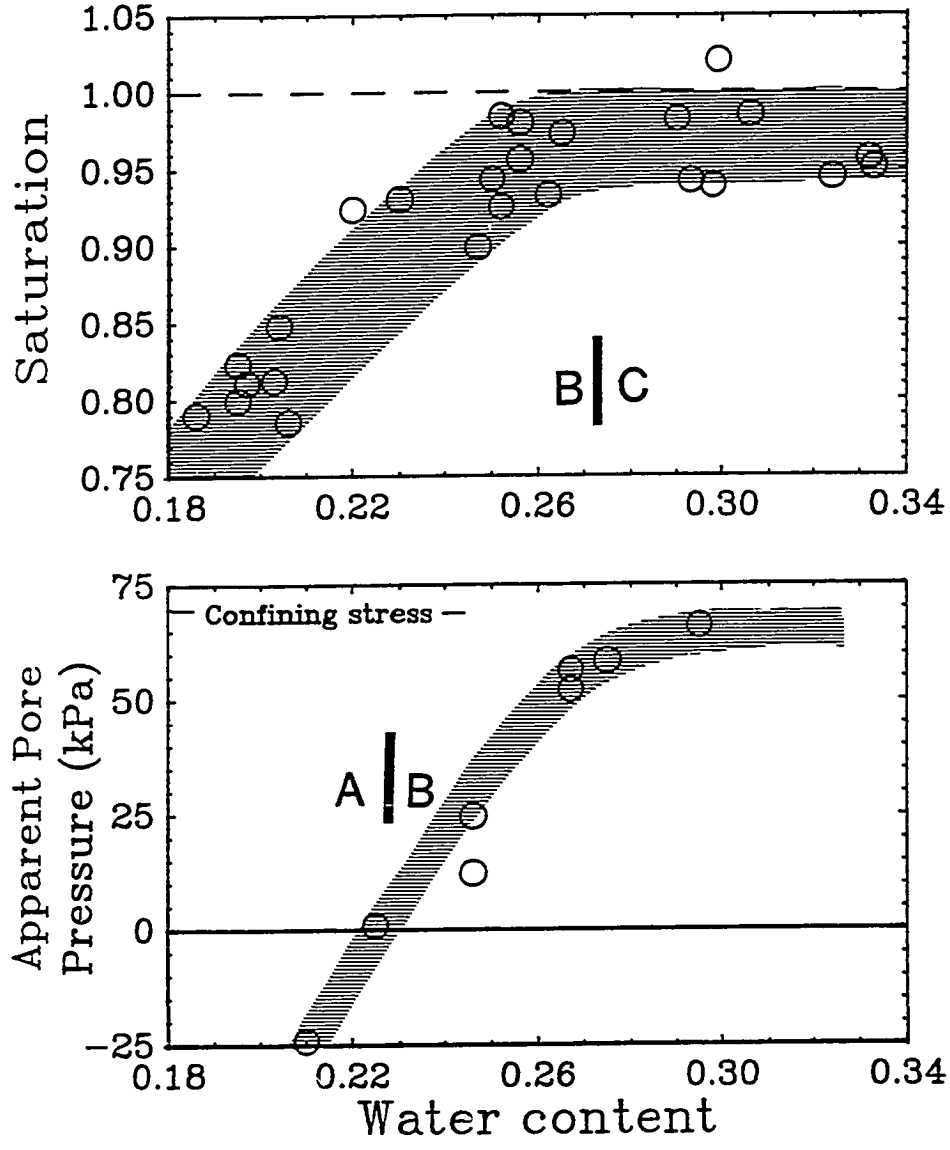

Figure 1.3. Pore pressure (*a.*) and degree of saturation (*b.*) as functions of water content for samples under 69 kPa confining load. Demarcations indicate boundaries of water content Conditions A, B, and C.

where γ_{solid} is the unit weight of solids, γ_w is the unit weight of water, and γ_{dry} is the dry unit weight of a sample, which was determined by calculating the bulk unit weight γ_{bulk} from the weight and volume of a sample block and using

$$\gamma_{dry} = \gamma_{bulk}/(1 + \theta) \tag{1.2}$$

Water content was determined after each test using weights of samples before and after drying in an oven.

Measurements of pore pressure were made in the fracturing cell under 69 kPa of confining stress. A miniature porous cup attached to a vacuum gauge was used to measure negative pore pressure, whereas a tube inserted into a water-filled cavity and attached to a transducer was used to measure positive pore pressures. Both devices were used when samples were in the transition from positive to negative pore pressure. A uniform load of 69 kPa was applied several minutes prior to beginning measurement of pore pressure. A similar loading was used when hydraulic fractures were created, so that the measurements should represent the magnitude of pore pressures at the onset of hydraulic fracturing. The sudden application of a confining load is presumably responsible for the creation of positive pressures in partly-saturated pores in Condition *B*.

Triaxial compression tests were conducted using remolded cylindrical samples of Center Hill clay at various water contents. The samples were 7.3 cm in diameter and 15 cm in height. They were loaded at a constant strain rate of 0.01/min and a confining pressure of 69 kPa was maintained during each test. Axial stress was determined from measurements taken from a load ring, and volumetric deformation of the sample was determined from measurements taken from a burette containing fluid from the triaxial cell.

Axial strains of 0.003 and 0.008, which are the smallest strains that were measured during the triaxial tests, will be used as the best available estimates of elastic behavior. Unloading tests were not conducted at those small strains, so neither the amount of plastic nor the amount of nonlinear elastic deformation could be determined. The elastic properties cited here should thus be considered as apparent values. Elastic modulus E, taken as the ratio of a given pair of axial stress and axial strain measurements, decreases with either increasing strain or increasing water content. It is between 22 and 10 MPa in Condition A, decreases from 10 to 5 MPa in Condition B, and decreases from 5 to 1 MPa in Condition C (Fig. 1.4).

Poisson's ratio ν was estimated to first order by determining volumetric strain V_s and using (Richards, 1961)

$$\nu = 0.5(1 - V_s E / 3\sigma) \tag{1.3}$$

where σ is axial load. Poisson's ratio is between 0.3 and 0.4 at the small values of strain cited above, and a value of 0.35 will be considered representative of conditions during fracturing. As strain increases to between 0.05 and 0.1, ν increases to values of roughly 0.5 according to eq. (1.3). Poisson's ratio at small strain appears to be independent of water content, at least within the resolution of the methods used here.

A suite of geotechnical tests was conducted to identify standard parameters for the Center Hill clay. According to the USCS classification based on Atterburg Limits (Table 1.1), the Center Hill clay is a type CL lean clay soil. It behaves as a plastic material in Atterburg tests over most of the range of water contents used during the fracturing tests, although a few samples had water contents that were drier than the plastic limit. Analysis of grain sizes indicates that the Center Hill clay

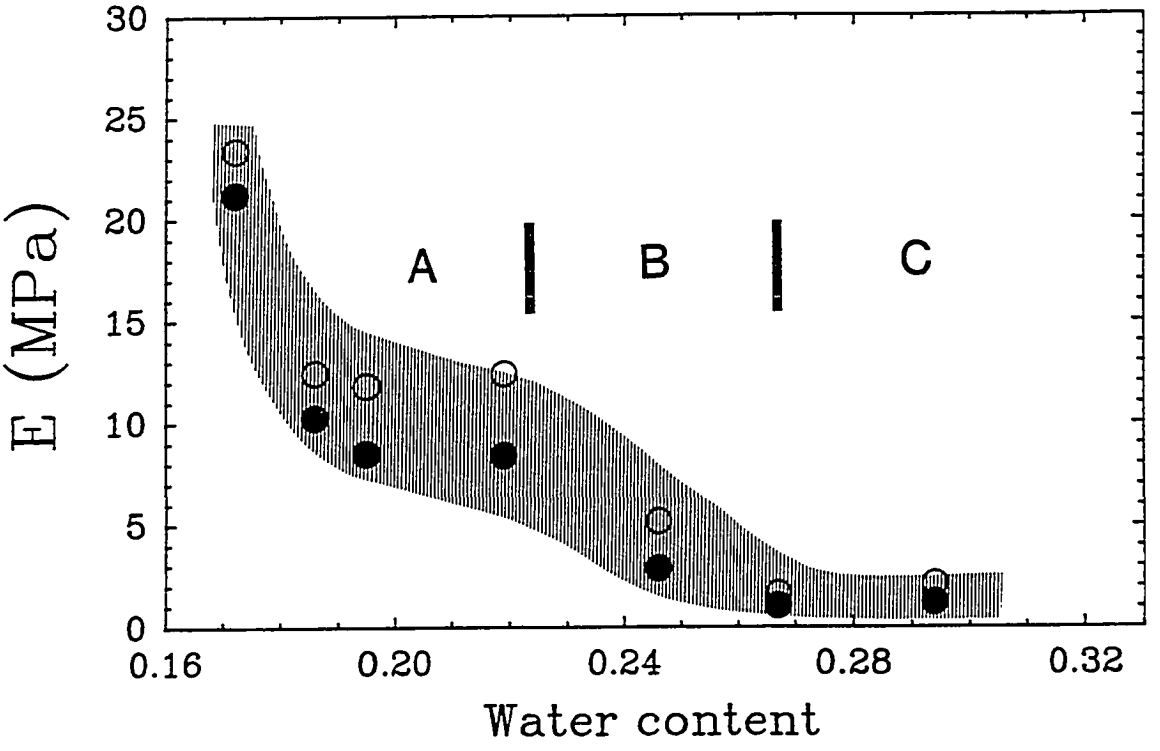

Figure 1.4. Apparent elastic modulus as a function of water content.

is dominantly silt and lesser amounts of clay (Table 1.1; Fig. 1.5). Trace amounts of limestone fragments occur in the soil naturally, but they were removed before the soil was used in the fracturing tests. Results from Proctor Tests (ASTM D698) indicate that the maximum density of the Center Hill clay occurs when the water content is 0.197 (Fig. 1.6). Bulk densities of samples used in the fracturing tests are either equivalent to or slightly greater than densities from the Proctor Tests (Fig. 1.6).

Table 1.1. Characteristics of Center Hill Clay

Atterburg Limits	CH1	CH2	AVE
Liquid Limit	0.429	0.438	0.433
Plastic Limit	0.198	0.200	0.199
Plastic Index	0.231	0.238	0.234
Shrinkage Limit	0.188		
Grain size			
Gravel	0	0	
Sand	0.03	0.03	
Silt	0.61	0.62	
Clay	0.36	0.35	

Proctor Test (ASTM D698)
Water Content of Greatest Density: 0.197
Maximum Dry Density: 1.68 gm/cm^3 (104.7 lb/ft^3)
Maximum Wet Density: 2.01 gm/cm^3 (126.0 lb/ft^3)

Sample Preparation

Techniques of preparing soil samples were developed to yield uniform rectangular blocks of a desired composition, water content and consolidation

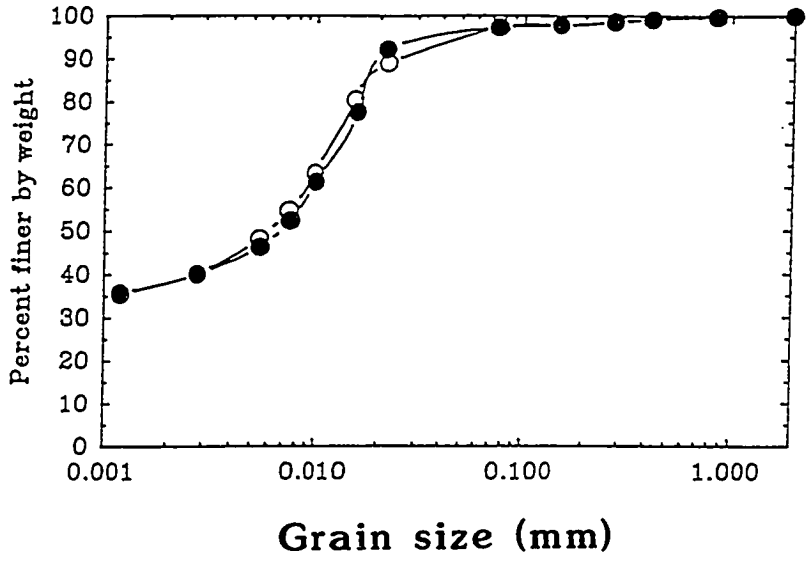

Figure 1.5. Grain-size distribution of Center Hill clay.

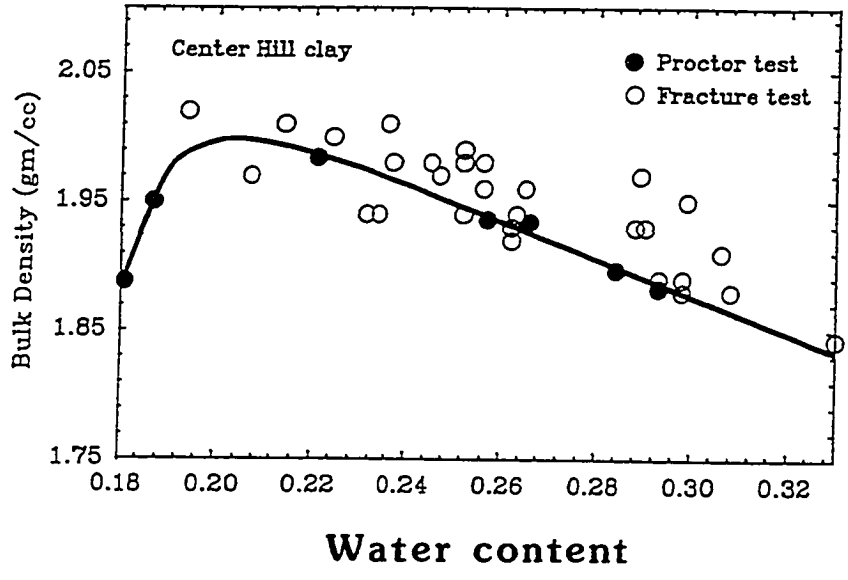

Figure 1.6. Bulk density as a function of water content from Proctor tests and fracture tests.

history. All samples were prepared in rectangular molds the same size as the inside of the fracturing cell. Most samples were formed by compaction, and a few were compacted and consolidated.

A pneumatic press (SoilTest Model CN-425A) was used to load samples that were prepared only by compaction. The press was modified by attaching a rectangular load shoe (5.8 x 9.8 cm), so that the entire width of the sample mold was loaded by each blow. A layer of soil 2 cm thick was compacted by 80 blows from the press, and a pressure of 139 kPa was applied during each blow. The layer was scarified and another layer added and compacted. That process was repeated until the sample mold was filled to a depth of roughly 12 cm. The sample was removed from the mold and trimmed with a wire saw to a height of 10 cm.

The amount of compactive effort was the same for each sample, regardless of its water content. That amount of compactive effort was a compromise between a large enough effort to fuse discrete granules of the drier soil into a continuous block, and a small enough effort so that masses of the wetter soil could be handled without severe disruption.

When samples were to be consolidated, a layer of soil roughly 2 cm thick was compacted with 30 to 40 blows of a drop-weight hammer. The upper surface of the layer was scarified to a depth of 0.5 to 1.0 cm and another layer of similar thickness was added and compacted. That process was repeated until the soil in the mold was 10.5 cm thick. Four sample molds were filled and then placed beneath the corners of a heavy pallet, which exerted a vertical stress of 69 kPa on the samples. Samples were consolidated under that load for as many as 14 days.

A narrow slot (0.04 mm in aperture) was cut through the middle of each sample (Fig. 1.2) using a blade-like tool. The purpose of the slot was to provide a

starting fracture that was much larger than existing flaws (e.g. pores or micro-fractures) in the sample. The slots were rectangular in shape with the long axis of the rectangle spanning the width of the sample. The slot was necessary because measurements of critical stress intensity, a parameter in analyses of linear elastic fracture mechanics, require knowing the length of a fracture when it begins to propagate (Tada and others, 1985). Natural discontinuities resembling fractures several mm long were common in the samples, so a starter slot of at least 12 mm in length was used to nucleate hydraulic fractures. The short axis of the rectangle, or slot length, ranged from 12 to 72 mm depending on the size of the blade used to cut the slot. A hole 3 mm in diameter was cut along the center of the long axis to facilitate distribution of the glycerin.

A film of silicone grease was applied to the surfaces of the soil block to inhibit leaking of the injected fluid where a fracture intersected the sample surface. The grease provided an adequate seal and, because it was nearly transparent, allowed the trace of the fracture on the surface of the sample to be observed through the fracturing cell.

Test Procedure

After a sample was prepared the starter slot was filled with glycerin to ensure that air was expelled from the slot. The loading plate was then secured and the cell positioned so that the starter slot was horizontal, eliminating a static pressure gradient along the slot (Fig. 1.2). The injection tube was fastened to the pressure-tight fitting in the spacer plate, filled with glycerin, and secured to the syringe pump.

A confining load was then applied to the sample by inflating the neoprene bladders. During most tests described here the confining pressure normal to the starter slot was 55 kPa and the confining loads parallel to the slot were both 69 kPa.

This loading configuration was used to promote the growth of a hydraulic fracture in the plane of the starter slot. If all three confining loads were equal or if the minimum compression was in the plane of the starter slot, the hydraulic fracture twisted or curved, yielding complicated forms that were difficult to duplicate. This change in stability with loading is as predicted by Cottrell and Rice (1980).

To conduct a test, the data acquisition device was turned on to begin recording injection pressure as a disk file and to display it as a function of time on a video monitor. The syringe pump was then engaged and the events characterizing the test were noted. After several minutes of injection, the duration of most tests, the pump was turned off and either the pressure was monitored for several more minutes or the pressure was released and the injection fluid drained from the fracture. The sample was then removed from the apparatus and the test was complete.

Typical Events During a Test

Events occurring during the fracturing tests followed a consistent pattern. Pressure within the starter slot, or pupative hydraulic fracture, increased nearly linearly with time early in the test. At some point the slope of the pressure record began to flatten, reaching zero slope as the pressure peaked and then becoming negative as the pressure decreased with continued injection.

A thin (on the order of 0.05 mm) fracture trace typically could be seen on the surface of the sample roughly at the time of maximum injection pressure. Most traces were nearly straight, although in many cases they consisted of a family of straight, sub-parallel segments arranged either en echelon or staggered. The location of the fracture tip was difficult to establish because the aperture tapered gradually until it became undetectable. Thus the tip could be located within

approximately one cm, but the trace was too thin to locate the tip precisely. Fracture tips tapering gradually to extremely fine apertures were described by Segall and Pollard (1983), who studied mineralized joints in granite.

The fracture trace grew at cm-long intervals or segments, initially appearing as lines so thin they could barely be seen and then slowly widening to narrow slits with a recognizable aperture. Growth appeared essentially the same when magnified roughly ten times; greater magnification was impossible using available instruments. Although it was impossible to follow the tip of the fracture trace during propagation, the average rate of propagation could be determined from the total fracture length and the total time of injection; it was on the order of 0.5 to 1.0 mm/sec. For comparison, Medlin and Masse (1984; fig. 9), who used an apparatus similar to the one described above and injected at 0.00833 cm^3/sec in rock, report that the propagation rate decreases with time from 2 mm/sec early in a test to 0.2 mm/sec late in the test.

A fracturing test was terminated by stopping the pump and opening a pressure relief valve, which allowed the injection fluid to flow back into the injection tube as the fracture closed. The dyed glycerin was promptly removed from the fracture in an effort to inhibit staining of the sample by capillary flow unrelated to the process of hydraulic fracturing. The relief valve was not opened after some tests so that the pressure decline following the cessation of pumping could be monitored.

The sample was removed from the fracturing cell and pulled open along the plane of the fracture. A rough, finely-dimpled surface was formed where intact portions of the samples were pulled apart. In contrast, the surface of the hydraulic fracture was relatively flat, or marked by angular steps. In many cases the leading

edge of a hydraulic fracture was undyed, but could be readily distinguished from intact clay by the difference in textures.

APPEARANCE OF A HYDRAULIC FRACTURE IN CENTER HILL CLAY

More than 100 experiments were conducted using the Center Hill clay and a variety of loading conditions, sample preparation techniques, water contents and durations of consolidation. Hydraulic fractures were created during every experiment, except in a few cases when the injection tube was plugged with clay as it was inserted. Examination and description of the appearance of each fracture revealed features of the fractures that occur in virtually every case. Most of those features exhibited slight variations, depending on the conditions of the test, but they were consistently present in some form. The features were described in notes and traced onto transparent mylar.

In gross form most fractures were nearly symmetric with respect to the axis of the starter slot. The half-length of a fracture a (measured from the hole along the axis of the slot to the leading edge) was roughly uniform along the width (measured parallel to the axis of the starter slot), although half-lengths were slightly shorter near the edges than in the center of most fractures.

Some fractures were asymmetric with respect to their width, that is their lengths were several cm greater along one side than along the other. In some cases, the lengths were greater on the side of the injection tube, whereas in other cases the side opposite the injection tube was longer. In virtually all cases, however, the asymmetry was mirrored across the axis of the starter slot. Slight leakage at one side of the sample, either out of the slot or out of the fracture itself, apparently caused this type of asymmetry. Leakage in most instances occurred during

propagation, according to direct observations through the loading plate, so it had little effect on the early stages of nucleation and growth of the fracture.

The typical test revealed a continuous, parent fracture adjacent to the starter slot. The parent fracture broke into discontinuous, lobate planes with increasing distance from the injection hole. At the leading edge, the limit of the fracture was, in many experiments, beyond the zone reached by the dyed glycerin. These features define four distinct zones on a fracture surface, arranged in increasing distance from the injection hole: 1.) starter slot; 2.) parent fracture; 3.) lobes; 4.) and leading edge.

Starter Slot

The starter slot appears on the surface of a cleaved sample as a smooth strip with a shallow trough, which is one half of the injection hole, along the axis of the strip (Fig. 1.7). The width of the strip depends on the length of the blade used to cut the slot.

Parent Fracture

The main, or parent, hydraulic fracture appears as a continuous, dyed surface that lies roughly within the plane defined by the starter slot (Fig. 1.7). Locally, parent fractures are twisted or curved, with most of the distorted regions located near the edges of a sample (e.g. top of Fig. 1.7). Those distortions are minor, however; the fracture rarely deviates by more than 10° from the orientation of the slot.

The surface of a parent fracture is generally flat, but in detail it is marked by irregularities that have as much as one cm of relief. Some of the irregularities are rounded bulges or dimples. More typically the surface is marked by elongate

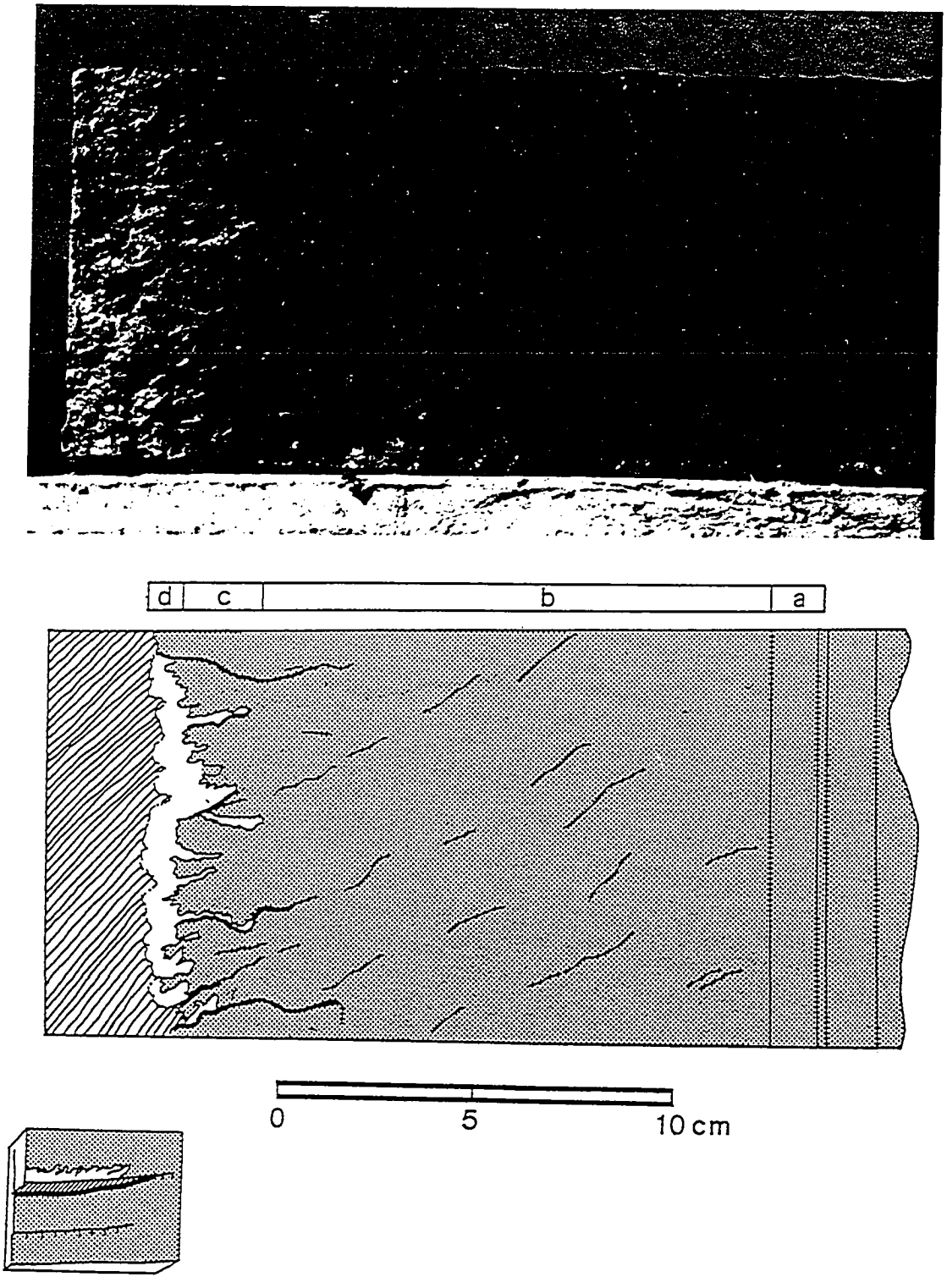

Figure 1.7. Photograph and sketch of the surface of a hydraulic fracture. a.) starter slot; b.) parent fracture; c.) lobes; d.) pristine leading edge. Lines on the sketch are prominent linear features on the fracture surface. Heavy lines represent overlap of fracture lobes (inset).

Black and white copy of photograph in Figure 1.7.

features; narrow ridges, grooves or angular steps (Fig. 1.7). Ridges and grooves typically have one mm or less of relief and the fracture surface on either side of them lies in the same plane. Steps are where the fracture surface abruptly changes height over a narrow interval.

Steps range in size from less than one mm high and several mm long, to 5 mm high and nearly as long as the entire fracture (Fig. 1.8). Lengths of ridges and grooves are on the order of several mm, typically shorter than the steps. The direction of the long axes of the linear features differ, depending on where the feature occurs on the fracture surface. Where they occur near the starter slot, the long axes are perpendicular to the axis of the slot. At the other end of the fracture, near the tip, the steps are perpendicular to a tangent across the leading edge. Within the parent fracture, the axes are sub-parallel to one another and within 20° of the line formed by the edge of the sample. As the edge of the sample is approached, however, the linear features curve outward at increasingly higher angles, and at the edge itself the axes are inclined 45° or more (Fig. 1.8).

Steps, grooves and ridges on fracture surfaces are by no means unique to hydraulic fractures in soil; they have been described on the surfaces of tensile fractures in a variety of materials, ranging from glass to metal, plastic or rock (Degraf and Aydin, 1987; Williams, 1984; Pollard and others, 1982, and references cited therein; Pollard, 1978; Pollard and others, 1975; Daneshy, 1973; Tetelman and McEvily, 1967). A common interpretation is that the steps indicate the direction of propagation when the leading edge of the fracture is at the location of the step (Pollard and others, 1975).

This interpretation is consistent with the patterns of steps on the surfaces of fractures in soil. The typical pattern of steps is shown in Figure (1.9), from which

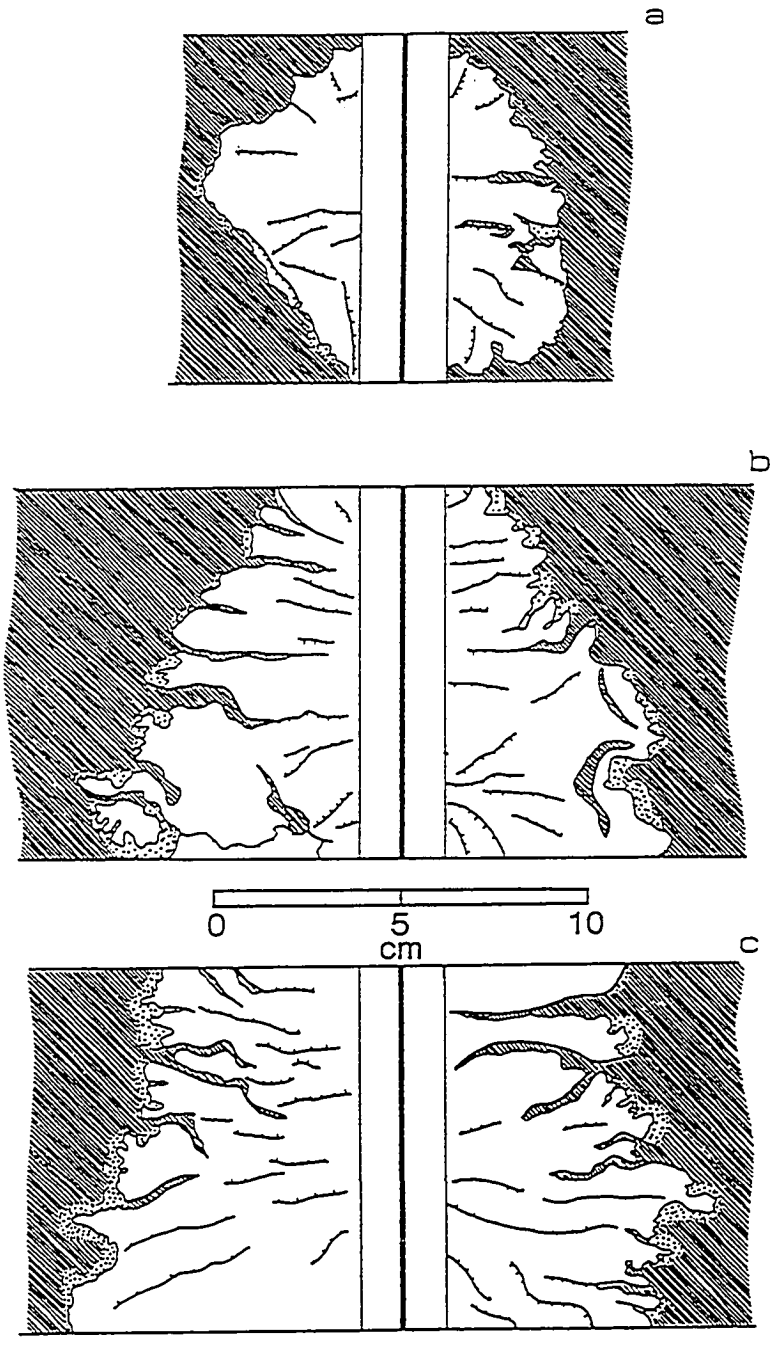

Figure 1.8. Surfaces of three hydraulic fractures of various lengths. Lines on the fracture surfaces are linear features and hatch marks on the lines indicate the lower side of a step. Fracture but undyed areas are stippled. Heavy lines indicate overlap of lobes as in Figure 1.7.

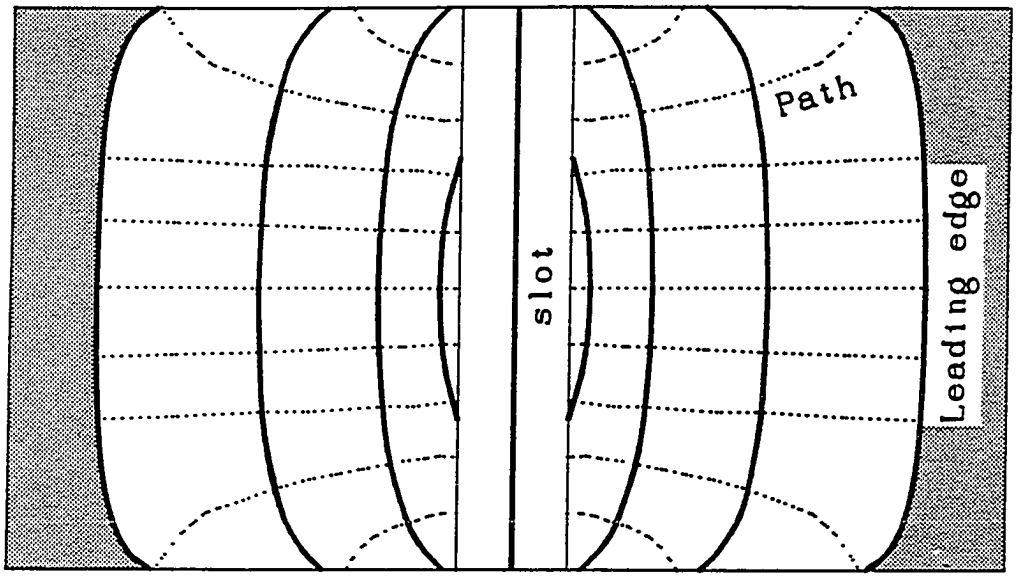

Figure 1.9. Idealized diagram of the position of the leading edge and the path of propagation of a hydraulic fracturing in the laboratory experiments. Inferred from the results of several dozen tests.

the leading edge at several different times during growth is inferred. The inference suggests that propagation began near the center of the slot and the fracture grew toward the edges as it increased in length (Fig. 1.9). Upon reaching the edge of the sample, the fracture grew roughly parallel to it. Propagation at the edges of the sample apparently lagged behind the center because the direction of growth there has an outward component. Thus, the fracture trace on the surface of a sample, viewed through the plexiglass loading plate, was oblique to the direction of propagation of the fracture contained within the sample. In a few cases, as in Figure 1.7, linear features suggest that propagation began near one side of the slot.

Directions of propagation were slightly divergent within the fracture, and strongly divergent near the edges. As a result, all except the center-most of the propagation paths eventually fan outward to intersect the edges of the sample (Fig. 1.9).

A few steps on fracture surfaces were nearly parallel to the axis of the starter fracture -- at a high angle to the steps that indicate propagation direction (Fig. 1.8 *a* and *b*). The axes of the high-angle steps are several cm in length and they are nearly straight to gently arcuate. Their location is variable; some of them occur in the vicinity of the starter slot, whereas others are in the vicinity of the leading edge. In many cases, a high-angle step on a fracture surface is related to a smaller fracture that either overlies or underlies the surface. The origin of the high-angle steps is unknown, but they are similar to rib marks, which were observed by Daneshy (1973), who used them to infer the position of the leading edge of the hydraulic fracture prior to the termination of a test.

Slices were made into several fracture surfaces, exposing sections from the surface into the wall material. In general, dye penetrated 0.01 cm or less into the

clay, according to measurements made with an optical comparitor. Dye penetrated as much as a few mm, however, where macro-pores or small cracks in the clay were intersected by the hydraulic fracture. Those small cracks were spaced between 1 and 2 cm apart along any section, although only a few sections were inspected so the general distribution of the small cracks is unknown.

Lobes

A continuous parent fracture breaks into a family of fracture lobes as the leading edge is approached from the starter slot (Fig. 1.7 and 1.8). The transition from continuous fracture to discontinuous lobes is smooth, marked by slight twisting or curving of lobes with respect to the parent fracture. Lobes occurred in virtually all the tests, although shapes and sizes of the lobes differ markedly between samples.

Lobes range from nearly equant to highly elongate, with aspect ratios from 1:1 to 1:10. In a few cases, fracture lobes originated at the starter slot and the entire fracture consisted of a family of elongate lobes; a continuous parent fracture was absent (upper right side of Fig. 1.8*c*). The major axes of elongate lobes are within a few degrees of parallel to the edges of the sample.

Fine steps or ridges are present on the surfaces of fracture lobes. Axes of steps are parallel to the major axis near the center of a lobe, but curve outward as the leading edge is approached. At the leading edge of a lobe, the steps are nearly perpendicular to the edge. The elongate lobes, therefore, are inferred to have widened as they increased in length.

As many as several dozen lobes are present in any given sample, and they range in size over more than an order of magnitude. The width of the largest lobe is

typically on the order of several cm, roughly one third or more of the width of the sample. Intermediate-sized lobes, whose widths are on the order of several mm, occur along the leading edges of the larger lobes. Other lobes that are even smaller, roughly one mm in width, fringe the edges of the intermediate-sized lobes.

Several of the larger lobes, the ones bounded by unfractured soil, occur in each sample. Each one of these lobes is in close proximity to one or more neighbors. Three types of spatial arrangement between neighboring lobes were identified during the tests. They are as follows (Fig. 1.10):

1. Neighboring: Lobes are coplanar, and their edges are separated by a narrow band of unfractured material.

2. Overlapping: Lobes lie in slightly different planes, and their edges slightly overlap.

3. Superposed: Lobes are roughly parallel. When viewed normal to the plane of the fracture, one lobe entirely overlaps the adjacent lobe.

Neighboring and overlapping lobes are the most common, occurring in nearly all samples. Typically, the wider lobes tend to be overlapping whereas the smaller ones are neighboring. The sense of overlap between lobes was consistent in some samples, so that traces of the lobes would appear en echelon on a surface normal to the long axis of the sample. In other cases, however, the sense of overlapping reversed itself, so that traces of lobes would appear staggered on the normal surface. Typically, the sense of overlap was inconsistent, with some lobes en echelon and others staggered in any given sample (Fig. 1.8).

Superposed lobes, or pairs of lobes with a large amount of overlap, occurred most commonly when the magnitudes of the applied stresses differed by a relatively large amount. Superposed lobes were rare in tests where the applied load normal to the starter slot was 80 percent of the loads parallel to the slot. Highly overlapping

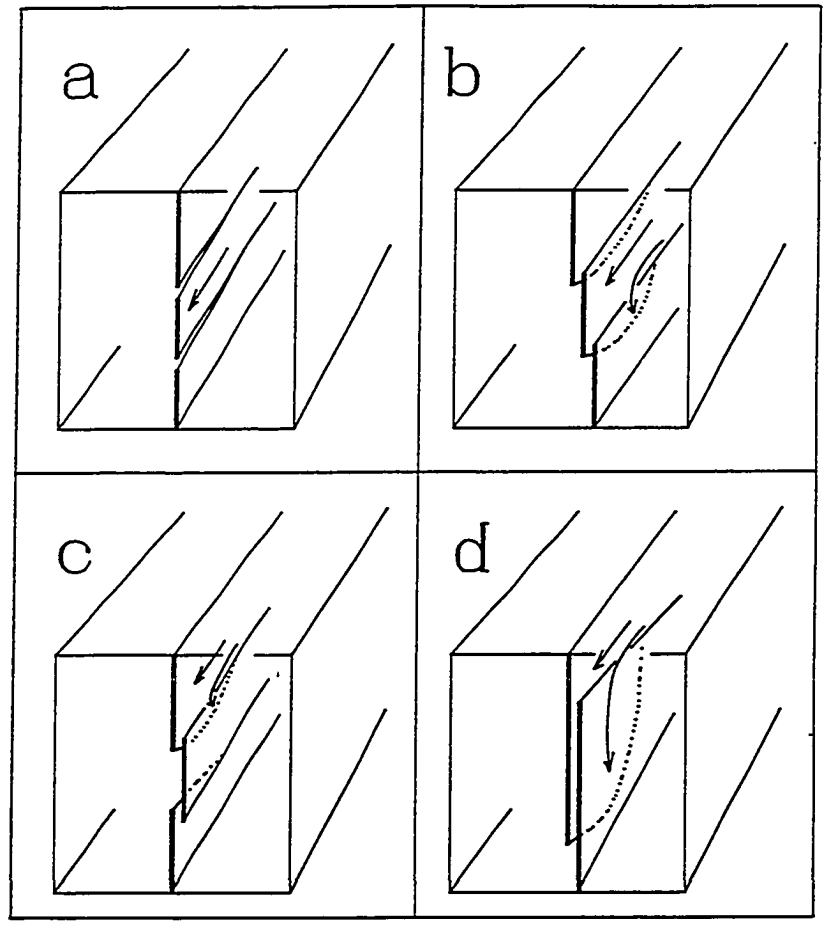

Figure 1.10. Idealized configurations of commonly-occurring fracture lobes. a.) Neighboring lobes; b.) En echelon overlapping lobes; c.) Staggered overlapping lobes; d.) Superposed lobes.

lobes were more common, occurring in roughly half the samples, when the normal load was between 30 and 50 percent of the parallel load.

Steps on the surfaces of superposed lobes were used to infer the path taken by the lobe as it grew, and some of the results are rather surprising. Typically, superposed lobes appear to be overlapping lobes that widen laterally as they grow in length (Fig. 1.10*d*). In some cases, however, the steps indicate that the lobe widened laterally and then propagated back toward the starter slot. In a few cases, superposed lobes are roughly circular features that are nearly isolated from both other lobes and the parent fracture. Small fractures, several mm in length, oriented normal to the lobes are the only connection that could be identified between those superposed lobes and their neighbors. Steps indicate that these isolated fractures grew outward in a radial pattern from the small connecting fractures.

The axes of boundaries between adjacent lobes typically can be traced back toward the starter slot to steps on the surface of a fracture (Fig. 1.8). This was observed on several scales; from boundaries between the larger lobes which can be traced to steps on the surface of the parent fracture, to the boundaries between the smallest lobes which can be traced back to fine steps on a fracture surface.

Pollard (1978) has argued that linear features, such as steps, ridges or grooves, on the surface of a tensile fracture result from the coalescence of lobes during growth of the fracture. The close spatial relationship between the boundaries between lobes and the axes of the linear features in the experiments described above support Pollard's argument. Moreover, Pollard cites the development of lobes, steps, ridges and grooves over a wide range of scales (eight orders of magnitude) and in materials ranging from glass to metal and rock. The

results of this study indicate that the appearance of hydraulic fractures in clay-rich soil is similar to the appearance of hydraulic, or other tensile, fractures in general.

Leading Edge

The appearance of the leading edge depends on the water content of the soil. In relatively dry samples ($\theta < 0.22$), the leading edge of the fracture is a sharply-defined boundary between dyed fracture surface on one side and unfractured clay on the other (Fig. 1.11). It appears that the that dyed glycerin wetted the entire fracture in the relatively dry samples.

As water content increases, however, the appearance changes markedly; the leading edge of the hydraulically-fractured soil is pristine, extending beyond the leading edge of dye staining. The pristine fracture tip was identified based on surface texture and color. The zone lacked dye staining, so it could readily be distinguished from the surface wetted by rhodamine-laced glycerin. The break created when the sample was pulled apart had a rough, dimpled surface and lacked linear features such as steps or ridges (Fig. 1.12). In contrast, the surface of the pristine tip was smooth and nearly planar, marked only by fine steps and resembling the surface texture of the parent fracture. In some cases, a fine step in the unstained region could be traced back into the stained region of the hydraulic fracture (Fig. 1.12).

The similarity in surface textures suggests that the pristine tip represents part of the hydraulic fracture that extends beyond the limit of the injected fluid. The total length of the hydraulic fracture must therefore include this fractured, but undyed zone at the leading edge.

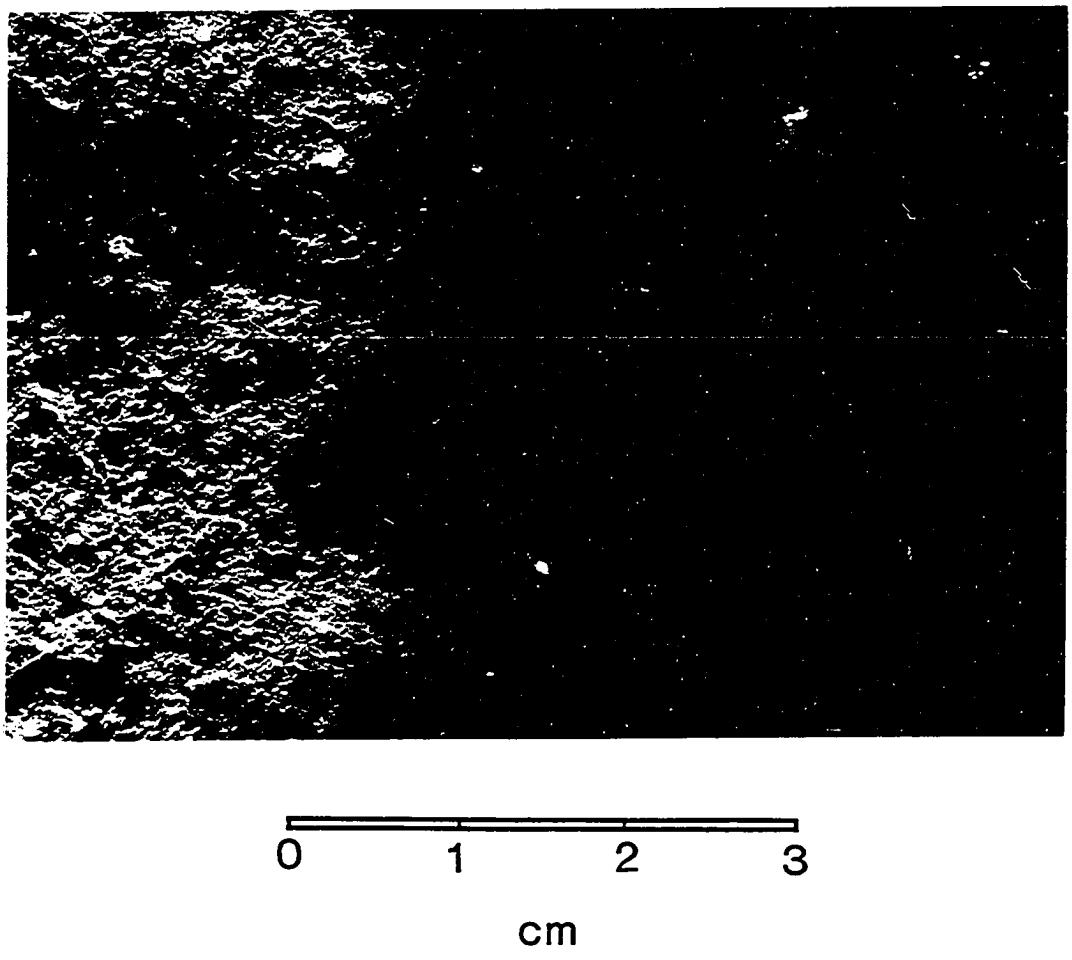

Figure 1.11. Leading edge of a hydraulic fracture in soil of water content Condition *A*.

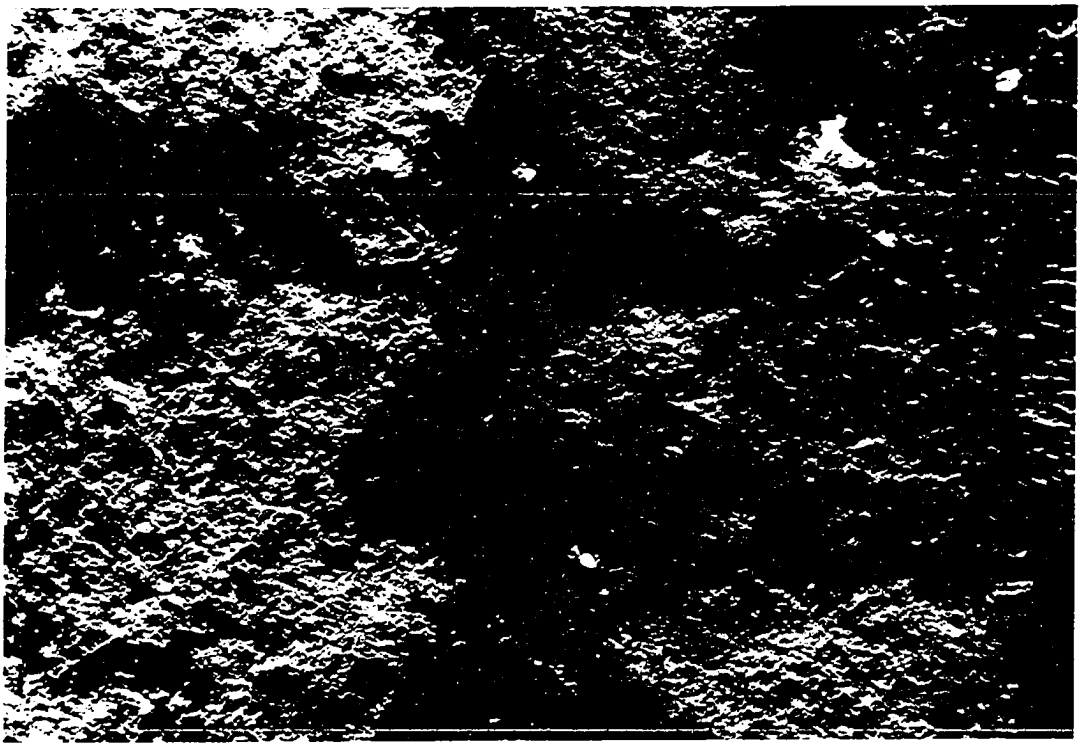

Black and white copy of photograph in Figure 1.11.

Figure 1.12. Leading edge of a hydraulic fracture in soil of water content Condition *B*. Lines on the sketch indicate linear features as in Figures 1.7 and 1.8.

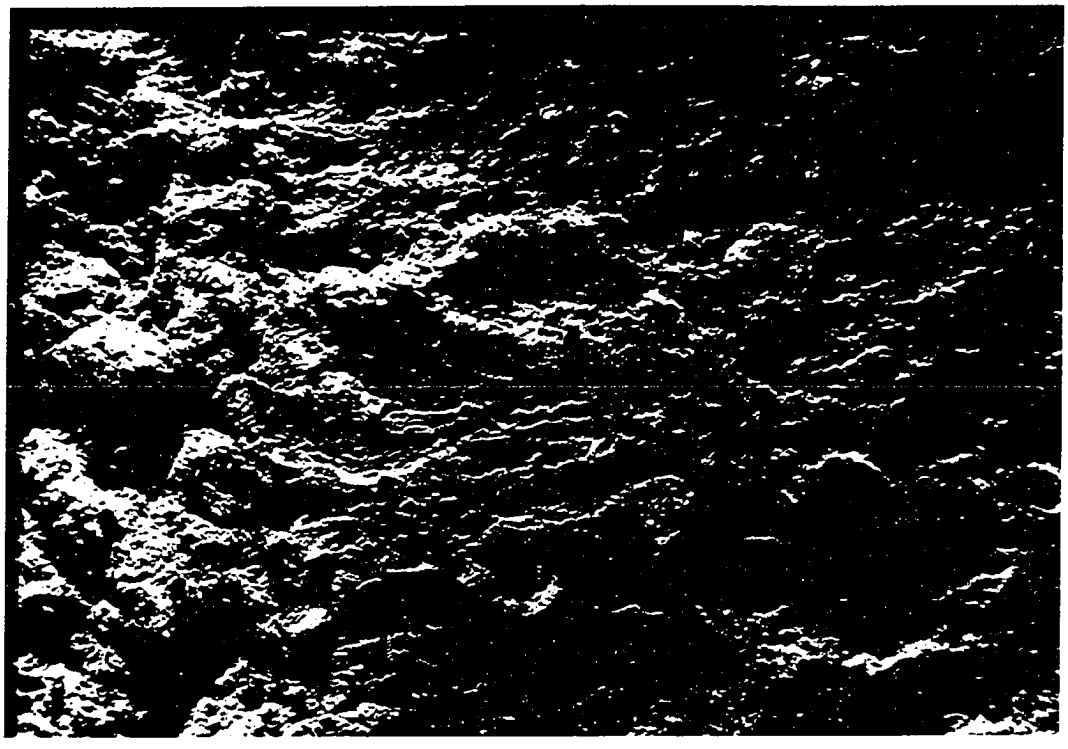

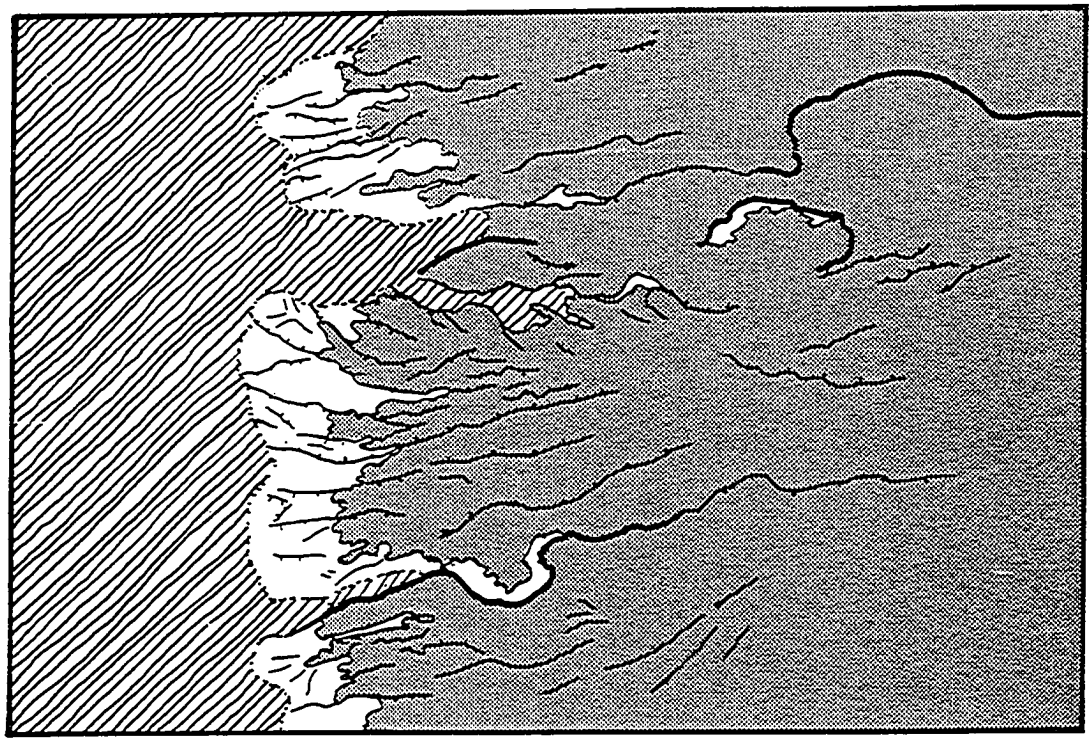

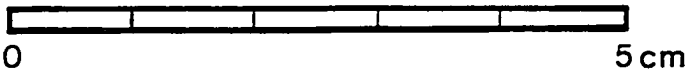

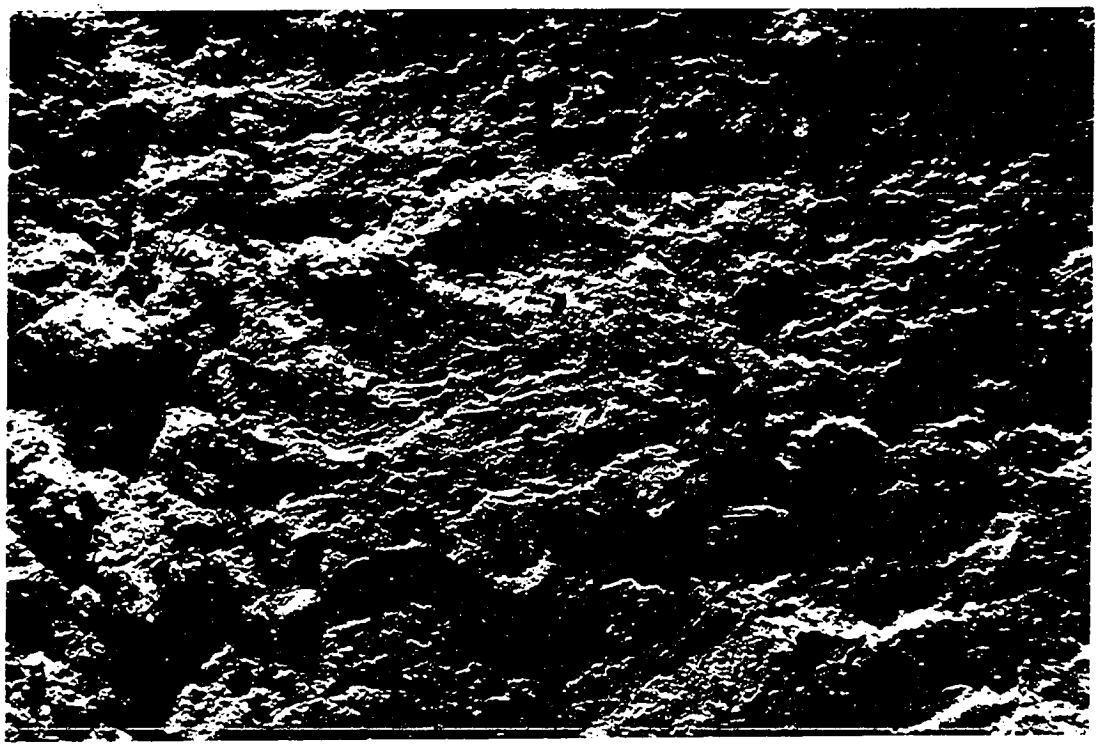

Black and white copy of photograph in Figure 1.12.

The lengths of the pristine tips varied greatly from one sample to another. In general among samples of similar water content, the length of the pristine fracture tip was roughly proportional to the length of the dyed fracture surface. Data shown in Figure 1.13*a* suggest that those lengths are related by

$$a - b = m\,(b - b_i) \tag{1.4}$$

where a is the total fracture half-length, b is the half-length stained by injection fluid, b_i is the intercept (approximately equal to the half-length of the starter slot), and m is a constant relating the length of the pristine tip (a - b) to the half-length of the stained fracture. Symmetry of the fractures about the injection hole will allow the convenient use of half-lengths instead of entire lengths. First order regression lines are shown in Figure 1.13*a* for measurements taken from samples of different water content.

The relation between water content and the relative length of the pristine tip m is summarized in Figure 1.13*b*. Rhodamine stain was present over the entire fracture surface ($m = 0$) for $\theta < 0.22$. The relative length of the pristine tip m increases as water content increases from 0.22 to 0.28. Within that range, m increases with water content and is greatest, roughly 0.25, at water contents between 0.27 and 0.28. At greater water contents, m decreases to values between 0.05 and 0.14. The trend at water contents greater than 0.28 appears to be more erratic, and is based on fewer measurements, than the trend for drier samples.

Diversity in the appearance of the leading edge corresponds to conditions related to water content. The entire fracture is wetted by injection fluid when pore pressure in the sample is negative, Condition *A* (Fig. 13*b*). With increasing water content, a pristine zone at the leading edge develops when pore pressures become

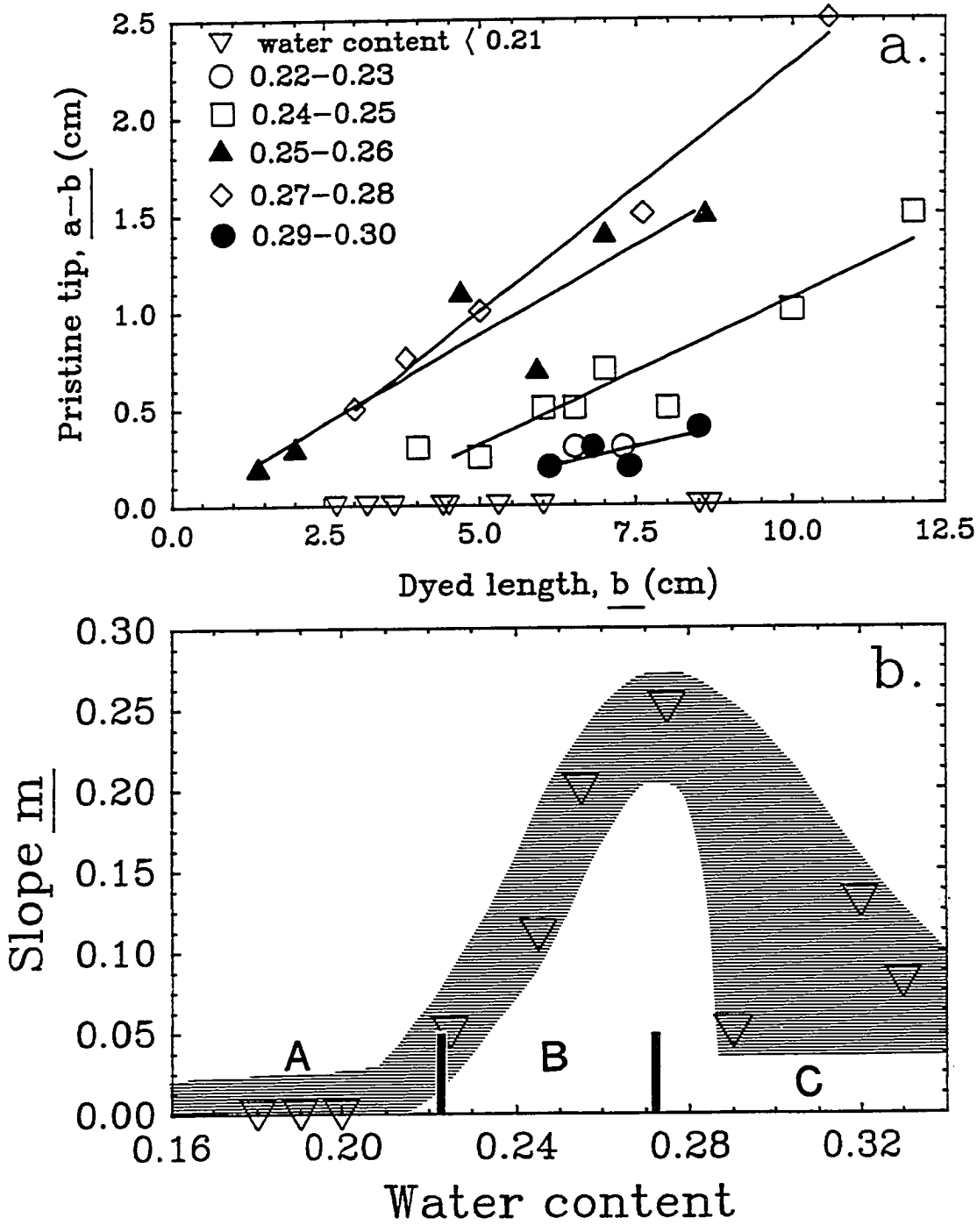

Figure 1.13*a*. Lengths of pristine fracture tips as functions of lengths of stained fractures and water content. 1.13*b*. Relative lengths of the pristine tip, determined from the slopes of lines in 1.13*a*, shown as a function of water content.

positive (i.e. transition from Condition *A* to *B*). The length of the pristine tip increases with water content when pore pressures are positive and pores are partly-saturated (Condition *B*). The length of the pristine leading edge diminishes when water content increases beyond saturation (Condition *C*).

DISCUSSION

What happens at the crack tip? That question has plagued investigators of hydraulic fracturing because of the difficulty in making reliable measurements at the tip. It is of theoretical importance because processes of decohesion, the essence of fracturing, occur at and ahead of the leading edge. The question is of practical importance as well because mathematical models used to predict results of hydraulic fracturing procedures require a boundary condition describing fluid flow at the fracture tip. Crucial details of the theoretical predictions, such as the ratio of aperture to length, depend on assumptions about processes at the fracture tip. We were unable to make direct measurements at the tip of a moving fracture, but the observations of fracture surfaces suggest that the processes there depend on water content, at least for hydraulic fractures in Center Hill clay.

Idealizing the fracture as a straight, narrow cavity viewed in cross-section (Fig. 1.14) we will put forth a conceptual model to explain the appearance of the fracture tip under the different water contents. The conceptual model is based on the conclusion that the fracture can be filled with two fluids; glycerin that was injected from the syringe pump into the body of the fracture, and water that infiltrated from soil pores into the fracture tip. When the pressure of pore water is negative, infiltration cannot occur and the entire fracture appears to be filled with the injected glycerin (Condition *A*; Fig 1.14). When pore pressure becomes positive, however, pore water infiltrates the fracture tip and prevents the tip from

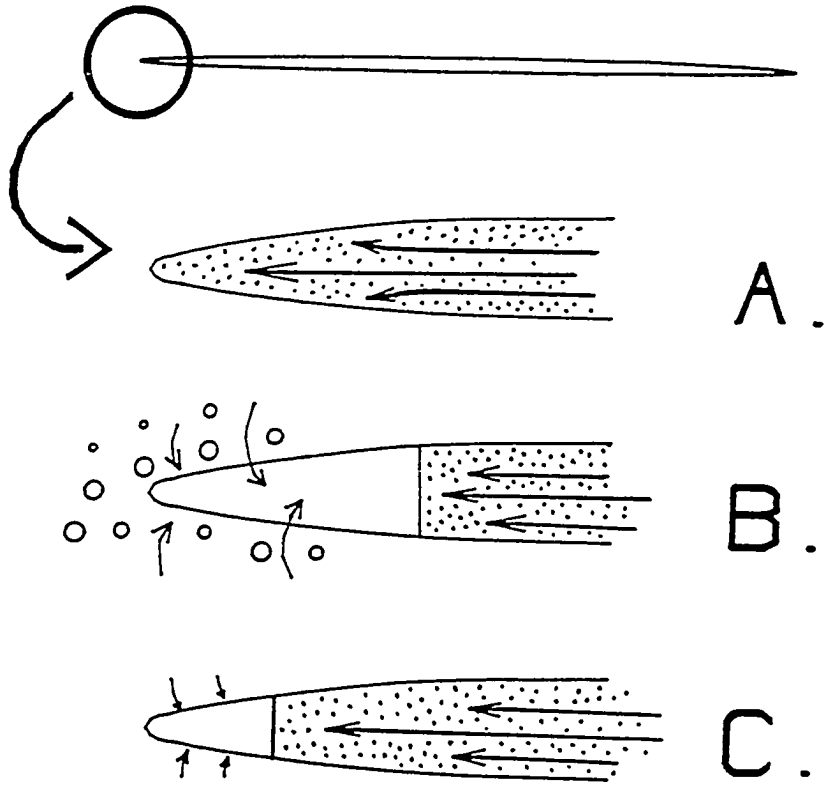

Figure 1.14. Idealized sketch of a fracture in cross-section showing injection fluid wetting the tip in Condition *A*; pore fluid driven into the fracture tip by expanding air in Condition *B*; and pore fluid flowing into the fracture tip in Condition *C*.

becoming stained by the injected glycerin (Condition *B*; Fig. 1.14). The leading edge of the stained fracture surface becomes diffuse as the dyed glycerin is diluted by the pore water filling the tip. The presence of air under positive pressure, a peculiar characteristic of Condition *B*, apparently facilitates the flow of pore water into the fracture. This occurs because the air expands to limit the pressure drop as pores drain into the fracture. Accordingly, the amount of water that enters the tip diminishes when water content increases beyond saturation because under saturated conditions air is unavailable to drive the drainage of pores.

I should point out that the processes at the tip of a fracture propagating in soil at negative pore pressure (Condition *A*) probably cannot by resolved by the present work. The entire fracture surface is stained by injected fluid under Condition *A*, but we are unable to determine that glycerin actually filled the entire fracture during propagation, as inferred in Figure 1.14, Condition *A*. The uncertainty arises from the possibility that during propagation there is an air-filled space ahead of the glycerin front, but that the space is stained as capillary suction pulls glycerin toward the tip after the pump is turned off. To examine the possible effects of capillarity, droplets of dyed glycerin were placed on narrow, flat-lying cracks exposed on surfaces of samples of Center Hill clay. In this simple experiment, glycerin flowed 6 to 12 mm into the open cracks due solely to capillary suction. Thus, it is possible that the injected fluid lags behind the fracture tip *under all Conditions,* but the tip becomes stained by glycerin due to capillarity after the injection pump is turned off.

As a corollary, it follows that the pristine tip observed in Conditions *B* and *C* must have been filled with water because capillary forces would have stained the tip if it was filled with air or vapor.

Pristine zones at the tips of hydraulic fractures are by no means unique to fractures in clay. They have been described at the leading edge of hydraulic fractures in limestone by Medlin and Masse (1984), who created fractures by injecting thick grease using an experimental apparatus similar in dimensions to the one used here. One important difference, however, is that their apparatus was fitted with ultrasonic transducers which yielded data on aperture and fluid content as a fracture was growing. Medlin and Masse observed marked attenuation of the ultrasonic signals near the tip of a growing fracture and inferred that the tip was "liquid-free". Results from one of their experiments (Medlin and Masse, 1984; fig. 6) indicates that the liquid-free zone first formed at the starter slot, grew to roughly 1.5 cm when the fracture was 5 cm long, and then was approximately constant as the length of the fracture increased to 12 cm. Medlin and Masse also noted a fractured zone ahead of staining caused by the injection fluid and inferred this to be a manifestation of the liquid-free zone interpreted from ultrasonic signals.

Similarity between surface textures of the pristine tip and the wetted fracture, as well as the continuity of linear features from the wetted fracture to the pristine tip indicate that the pristine tip is open and a part of the fracture itself. This is in contrast to so-called decohesion zones, or process zones, identified or postulated from studies of fracturing of metal, polymer or rock. The process zone is an interval over which the material becomes separated; the interval where fracturing actually occurs. In tensile fractures, of which hydraulic fractures are a special case, processes of decohesion involve the nucleation and growth of voids or microfractures (Williams, 1984; Tetelman and McEvily, 1967). The process zone is characterized by vestiges of material cohesion resulting from the strength of intact material remaining between voids, and as such it differs from the fracture itself where the material is completely separated and cohesion is absent. Process zones composed of

clusters of voids have been described at the tips of fractures in metals (Shockey and others, 1979; Tetelman and McEvily, 1967; Irwin, 1957) and polymers (Williams, 1984; Weidmann and Doell, 1979). Ouchterlony (1982) postulates a process zone in rock that consists of dilating microfractures, which produce acoustic signals that are commonly used to monitor the fracturing process in rock (Ouchterlony, 1982; Zoback and others, 1977). Time-lapsed sequences of photographs by Knauss (1976) capture the coalescence of voids resulting in the formation of fracture surfaces in polymers.

Phenomena occurring in the process zone of a fracture in clay have received little attention. In normally-consolidated kaolin, micron-sized voids occurring between aggregates of grains were observed to grow by coalescing during the early stages of shear loading (Smart and Dickson, 1979). To my knowledge, descriptions of processes at the tip of a fracture in clay under tensile loading have yet to be published, but it seems reasonable to assume that those processes involve microfracturing or void growth ahead of the fracture itself.

Whatever decohesion phenomena are involved, the zone in which they occur is ahead of, and distinct from, the pristine tip. A model describing growth of a hydraulic fracture in clay should thus be formulated to separately accommodate decohesion at the crack tip, and the distribution of fluid pressure in the fracture.

CONCLUSIONS

Hydraulic fracturing of clay was inevitable in the laboratory experiments; it occurred in all samples that could be properly prepared. Attempts to inhibit fracturing by increasing the water content and softening the clay were unsuccessful. The wettest sample that could be prepared as described above could be hydraulically fractured and the appearance of the fracture in that sample resembled

that of drier samples. Samples of extremely high water contents were too soft to be handled and could not be prepared using the procedures described above.

The general appearance of a hydraulic fracture in the Center Hill clay resembles the appearance of hydraulic fractures, and other tensile fractures, in rock. When hydraulic fractures cut either material they typically consist of a starter fracture, or some flaw or discontinuity that nucleates propagation; a parent fracture, whose surface is marked by steps, grooves, and ridges; and fracture lobes, which range in size over several orders of magnitude and are either staggered or arranged en echelon. There is a zone at the leading edge of some fractures that extends beyond the limit of staining by injected glycerin. Details of the size of that pristine zone at the tip depend on water content of the soil.

Pore water apparently infiltrates into the tips of hydraulic fractures in Center Hill clay if the pore pressure is positive. The infiltrated pore water prevents the injected glycerin from reaching the tips of the hydraulic fractures.

CHAPTER TWO

PROPAGATION OF A HYDRAULIC FRACTURE DURING LABORATORY EXPERIMENTS

The propagation of hydraulic fractures enveloped in natural materials defies direct observation. In the laboratory and in some field cases, hydraulic fractures can be observed directly after they have stopped propagating by excavating the material that envelopes them. But during propagation we typically are unable to make direct observations and so we must infer details of fracture growth from indirect measurements. The pressure of the fluid driving propagation p_f is both essential to the physics of hydraulic fracturing, and can be accurately measured with simple equipment--at least at the point of injection into the fracture. Accordingly, p_f is routinely recorded as a function of time at the point of injection during both laboratory experiments and commercial applications in the field. The records of injection pressure are compared with the results of theoretical analyses (Khristianovich and Zheltov, 1955; Perkins and Kern, 1961; Geerstma and de Klerk, 1969; Nordgren, 1971; Spence and Turcotte, 1985; Nilson, 1986) to infer essential details such as the orientation, shape and the distribution of proppant during growth of a fracture (e.g., Crockett and others, 1989, Nolte, 1988 *a* and *b*; Medlin and Masse, 1984; Nolte and Smith, 1981; Zoback and Pollard, 1978; Zoback and others, 1977; Hubbert and Willis, 1957).

Interpretations of records of injection pressure during hydraulic fracturing of soil are sparse. One problem is that most of the research describing hydraulic fractures in soil emphasize determining a critical pressure when fracturing occurs from a cylindrical borehole (Mori and Tamura, 1987; Bjerrum and others, 1972), or from some other feature (Jaworski and others, 1981; Jaworski and others, 1979). Those tests were conducted by regulating a constant injection pressure and

monitoring rate of flow. Pressure was increased incrementally and the onset of fracturing determined by a marked increase in the rate of flow into the sample. The record of injection pressure from those experiments is, therefore, of limited value because it is controlled by the experimental apparatus.

In contrast, during the experiments conducted for this research and during most hydraulic fracturing experiments conducted using rock, the rate of injection is regulated and the pressure of the injected fluid changes in response to dilation of the wellbore, permeation of the fluid, and the initiation and growth of a fracture. Records of injection pressure were made during this research to examine the effects of parameters, such as slot length and water content, and to compare with similar records from experiments in rock.

Laboratory data will be presented in terms of driving pressure P_d, the difference between the fluid pressure within a fracture and the confining stress acting normal to the fracture σ ,

$$P_d = p_f - \sigma \qquad (2.1)$$

A confining stress of 55.1 kPa (8 psi) was applied normal to the fracture during all experiments unless otherwise noted, so the fluid pressure can be determined from eq. (2.1).

Driving pressure was recorded as a function of time several cm upstream from the point where fluid enters the fracture cell, as described in Chapter One. The records of driving pressure as a function of time, hereafter termed *records*, were obtained for different slot lengths and different water contents. The objective was to examine how those factors affected both the critical driving pressure required to

initiate fracturing P_{df}, and the forms of the records while the fracture was propagating.

The driving pressure at the onset of propagation in the laboratory experiments depended on both the length of the initial slot and the water content of the soil. This dependency can be broadly accommodated within a framework of linear elastic fracture mechanics, which provides a tenable mechanism to predict propagation. According to elastic analyses, stresses in the vicinity of a straight fracture in an infinite elastic medium are concentrated at the fracture tip. In the vicinity of the tip, stresses are proportional to $r^{-1/2}$, where r is the radial distance from the tip. Thus, there is a singularity at the tip itself, where the stresses become infinite when $r = 0$. The strength of the singularity is characterized by the stress intensity factor K which is given by (Irwin, 1957; Tada and others, 1985)

$$K = P_d \sqrt{\pi a}\, f(b) \tag{2.2}$$

where a is the half length of the fracture, and $f(b)$ is some function of the geometry of the fracture and enveloping material.

A basic assumption of linear elastic fracture mechanics is that propagation under dilational, or Mode I, loading occurs when the stress intensity equals a critical value, K_{Ic}. The magnitude of K_{Ic} is commonly regarded as a material property characterizing the resistance of the material to Mode I fracturing, herein termed *fracture toughness*. To my knowledge, fracture toughness has never been applied to predicting the onset of hydraulic fracturing of soil, and one of the purposes of this work is to examine the validity of that application.

DUPLICATING THE RECORDS

Early in the experimental program a suite of four tests was conducted to examine how closely records could be duplicated. Four samples were prepared from a common batch of soil and consolidated together beneath a load of 69 kPa (description of the consolidation procedure in Chapter One). The properties of the samples were similar: densities were within 0.01 gm/cm^3 and water contents differed by less than one percent. Slot lengths, applied loads and other factors were identical.

Forms of the records for the four samples (Fig. 2.1) are similar, characterized by the following time periods:

Period I: Nearly constant positive slope
Period II: Slope diminishes, but remains positive
Period III: Slope is negative

The records are nearly identical during Period I. The boundary between Period I to Period II was identified by marking the location of the break in slope typical of Period I. Three of the records in Figure 2.1 show gradual changes in slope, whereas one of the records shows an abrupt step in the record. Pressures marking the boundaries between periods are indicated by short markers on the records (Fig. 2.1) .

The driving pressures marking the change in slope are within 1.0 kPa for three of the samples, and they range over 4.1 kPa, from 22.8 to 26.8 kPa, for all four samples. The driving pressures average 25.4 kPa and show a standard deviation of 1.86 kPa. The standard deviation normalized by the average value is 0.073.

The forms during Period II are similar for three of the records, showing a gradual decrease in slope. The other record is marked by two short intervals during which the slope changes drastically as the pressure decreases and then increases

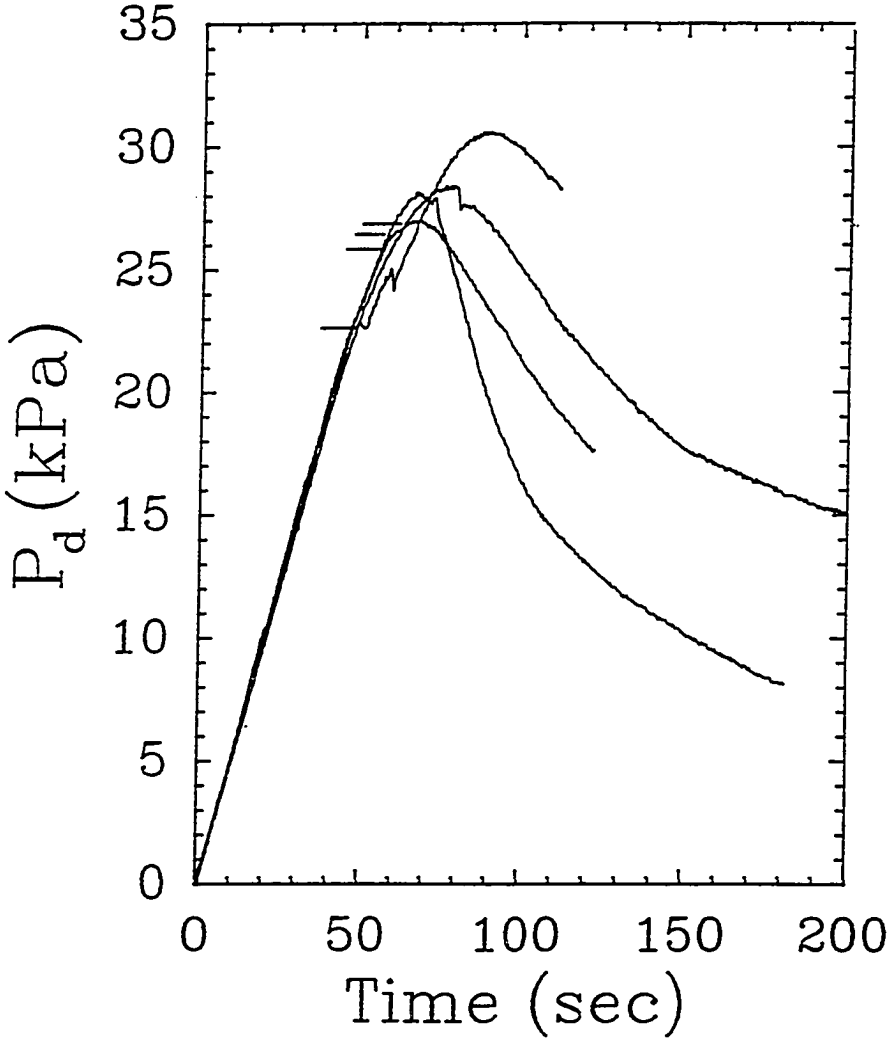

Figure 2.1. Records of injection pressure as a function of time for four similar samples of Center Hill clay. Pressure at the onset of fracturing is marked on each record.

abruptly. That record is similar to the others, however, if the two short intervals are ignored. Slight, abrupt changes in pressure were observed in other records, but their occurrence was unpredictable.

The maximum driving pressure marks the boundary between Periods II and III, and it ranges over 3.7 kPa (from 27.0 to 30.7 kPa), roughly the same range as the boundaries between Period I and II. The record showing the least pressure between Periods I and II yields the greatest pressure between Periods II and III. The average maximum pressure is 28.8 kPa, and the standard deviation is 2.03 kPa.

During Period III, driving pressure decreases and approaches a constant slope that is similar for three of the records. A constant slope is approached by the record of the fourth sample, but it is steeper than the other three. Slopes of two of the records diminish with continued propagation during Period III.

The records can be duplicated in both form and magnitude up to the time of maximum pressure. Variations in the pressures marking the boundaries of the Periods are within 10 percent of the total driving pressure. The records during Period III are similar in form, but their magnitude at any given time ranges over several tens of percent of driving pressure (10 kPa or more). Pairs of duplicate samples tested several months after the suite of four samples described above (and after several slight modifications in sample preparation and testing procedure were made) yielded records that differed by less than 10 percent of the driving pressure during all three Periods.

The forms of the records described above resemble the records presented by Medlin and Masse (1984) and Daneshy (1976a), both of whom used apparatus similar to the one used here but conducted their experiments using limestone or sandstone. The principal difference between the records from tests where rock is

fractured and those in Figure 2.1 is the slope early in Period III; it appears steeper when rock is fractured. However, considerable differences are seen in the forms of records of hydraulic fracturing tests using rock, and some of them are nearly identical to those in Figure 2.1 (e.g. Daneshy, 1976a; fig. 6).

Previous studies of hydraulic fracturing of soil (Mori and Tamura, 1987; Jaworski and others, 1981; Jaworski and others, 1979; Bjerrum and others, 1972) have measured the rate of flow into a sample while keeping pressure constant, and then slightly increasing injection pressure until fracturing occurs. The records of those studies are typically presented as injection pressure plotted with respect to flow rate, and they are difficult to compare to the records from tests presented here where injection rate was constant.

FRACTURE DEVELOPMENT WITH RESPECT TO THE RECORD

When does the fracture begin to propagate? To address this question six tests were terminated during Periods I and II in an effort to correlate the development of a fracture to the form of the record. Samples similar to the ones described in the previous paragraph were prepared so that the pressures marking the boundaries between Periods could be anticipated. The surfaces of fractures terminated at different times are shown in Figure 2.3. The times when each of those tests was terminated are shown on an idealized record (Fig. 2.2).

Most tests terminated during Period I showed a starter slot enveloped by unfractured soil; a hydraulic fracture was absent. In two cases, small hydraulic fractures were observed even though the tests were terminated with the records essentially linear. Those incipient fractures were less than 1.0 cm longer than the starter slot, and short, pristine zones occurred at their leading edge.

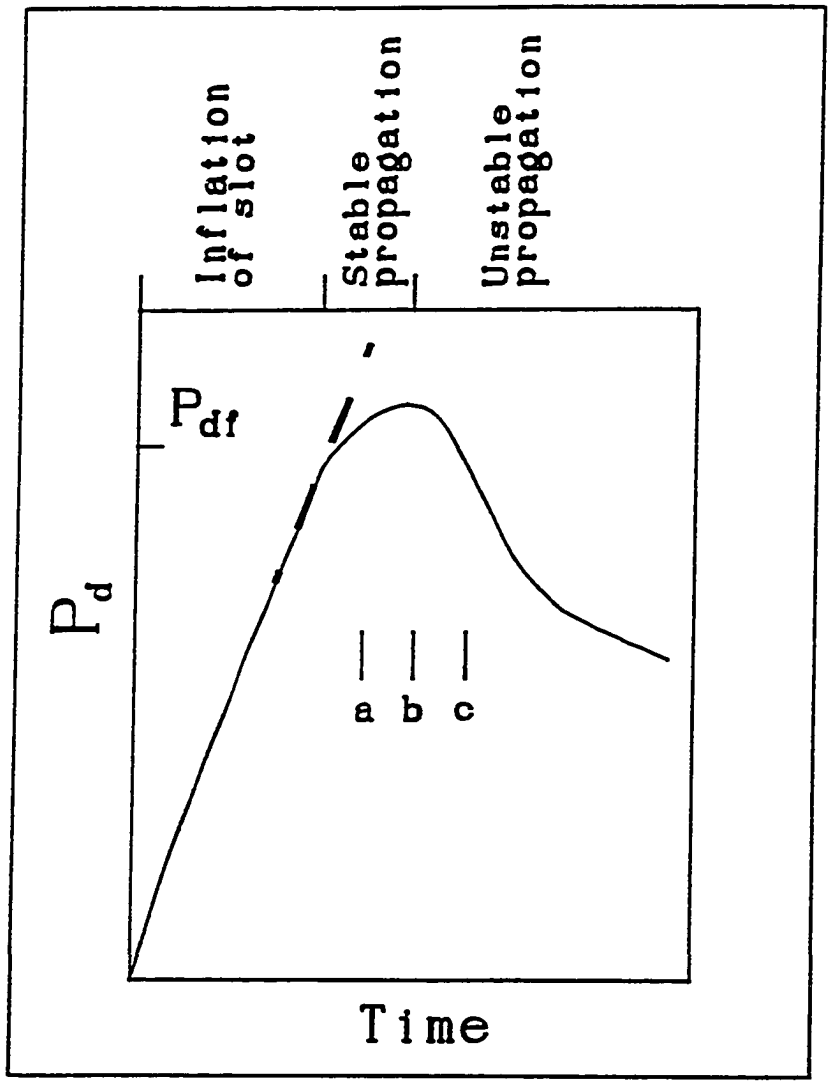

Figure 2.2. Idealized record of driving pressure as a function of time. Letters correspond to times of termination of tests from Figure 2.3.

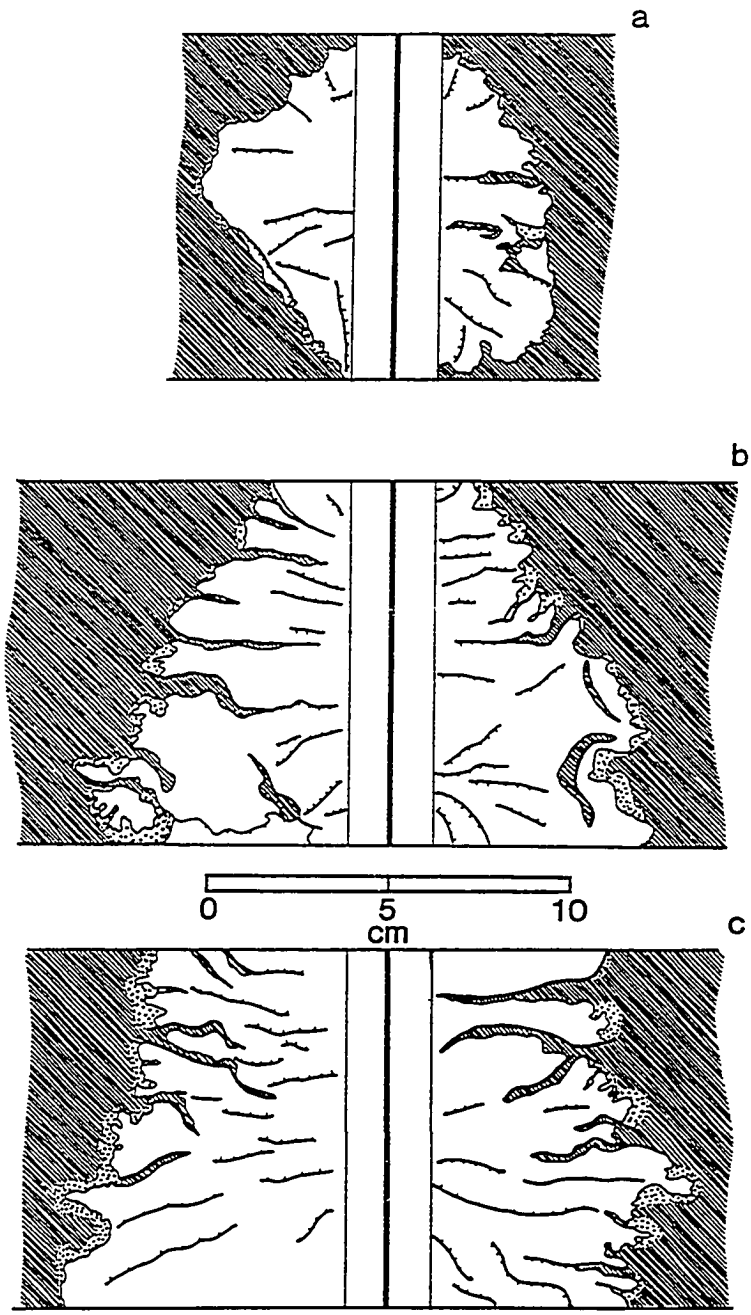

Figure 2.3. Surfaces of three hydraulic fractures created from differing durations of injection. The time of termination of each test is shown one an idealized record in Figure 2.2.

Tests terminated during Period II, however, show well-developed hydraulic fractures several cm in maximum length. The edges of the fracture during Period II are contained within the sample; that is the fracture has not yet reached the edge of the sample (Figs. 2.2 and 2.3a).

Another test was terminated early in Period III, roughly five seconds after the maximum pressure. The sample from this test contains a fracture that is longer than the one terminated during Period II, and it has intersected the edges of the sample (Fig. 2.2 and 2.3b).

The third sample shown in Figure 2.3c was terminated several tens of seconds into Period III and it shows a fully developed fracture cutting from one edge of the sample to another.

Those observations indicate that the onset of hydraulic fracturing occurs when the slope of the record first decreases. In some cases, incipient fracturing apparently occurs prior to the break in slope. Incipient fracturing cannot be detected on the pressure records, at least by the methods of recording pressure used for this work, so I will assume that fully-developed fracturing starts at the break in slope. The driving pressure at the break in slope P_{df} is taken as the critical driving pressure required to initiate fracturing.

Following the onset of fracturing, driving pressure continues to increase during Period II and then decrease during Period III. Increasing driving pressure during propagation indicates a period of *stable* growth of a hydraulic fracture, whereas decreasing pressures indicate *unstable* growth (Tetelman and McEvily, 1967; Zoback and others, 1977; and Zoback Pollard, 1978). These terms are used because if the driving pressure were held constant a stable fracture would be held open but would not propagate, whereas an unstable fracture would continue to

propagate at constant pressure. Thus, the three Periods of the injection record relate to three different processes during a test:

Period I: Inflation of the starter slot
Period II: Stable propagation of a hydraulic fracture
Period III: Unstable propagation

THE ONSET OF PROPAGATION

The pressure at the onset of propagation depends on the length of the initial slot, the water content of the soil, and perhaps other factors. It diminishes markedly as the length of the initial slot increases, according to Figure 2.4, which shows records from four experiments conducted on samples differing only by the lengths of their slots. The pressure P_{df} also depends on water content, θ, decreasing by nearly an order of magnitude as θ increases from 0.20 to 0.25.

Fracture toughness was introduced earlier as a possible material parameter that can be used to indicate the onset of propagation. If it is a material constant, fracture toughness must be independent of slot length. It can depend on water content, however, although we expect that the dependence will follow other properties that also depend on water content (e.g. pore pressure).

Fracture toughness was determined using the pressure P_{df} as the driving pressure, and the half-length of the slot a_i as the half length in eq. (2.2). The function $f(b)$ in eq. (2.2) is equal to unity if the fracture is straight, loaded uniformly, and embedded in a homogeneous, isotropic, linearly elastic material. It is less than unity and can be taken as a correction factor for practical constraints such as finite sample size, and slots intersected by a hole. Tada and others (1985) give expressions for $f(b)$ for a straight slot containing an axial hole, and for a straight slot embedded in a rectangular sample of finite size. Those conditions represent

corrections of less than five percent for the geometries and dimensions used in this work, so $f(b)$ will be set to unity and fracture toughness will be calculated using

$$K_{Ic} = P_{df}\sqrt{a_i \pi} \tag{2.3}$$

Effect of Slot Length

A suite of tests was conducted to investigate the relation between K_{Ic} and a_i. The tests consisted of preparing sets of samples that differed only in slot length. Sixteen sets of samples were prepared; one set consisted of four full-length samples and the records from that set are shown in Fig. 2.4, three sets consisted of three full-length samples, and the other sets consisted of a full--length sample that was cut in half to yield two half-length samples. Slot lengths were typically varied by factors of 2 to 4 within a set of samples. Water content was similar within a set, but varied between sets of samples.

Fracture toughness appears to be independent of the length of the starter slot (Fig. 2.5), under the conditions used here. As the length of the slot increased, the toughness decreased for ten of the sample sets, it increased for four of the sets, and it both increased and decreased for two sets (Fig. 2.5). Although K_{Ic} decreased for more sample sets than it increased, there appears to be no systematic relation between K_{Ic} and a_i.

The standard deviation of toughness was determined for each set of samples and normalized using the average toughness of that set to give the normalized standard deviation s_n resulting from changing the slot length. The mean s_n of all values is 0.18, whereas the median is 0.12. A few sample sets with the K_{Ic} > 10 kPa $m^{1/2}$ tended to be much more variable (larger standard deviations) than the sets K_{Ic}

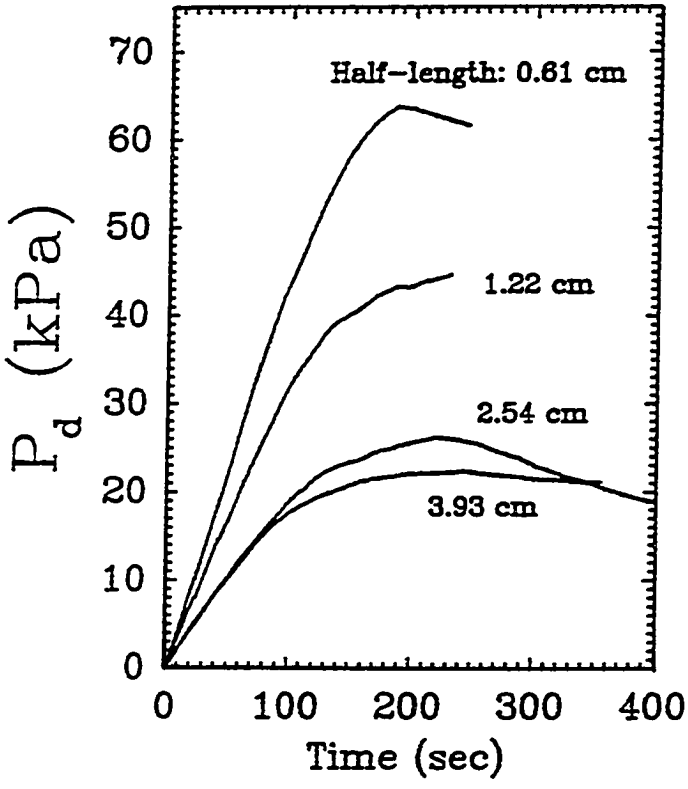

Figure 2.4. Records of injection pressure as a function of time for four samples that were identical except for the lengths of their starter slot, a_i.

< 10 kPa $m^{1/2}$, causing the mean to be larger than the median. The mean is 0.11, for example, if four of the sets for $K_{Ic} > 10$ kPa $m^{1/2}$ are ignored.

For comparison, the samples with similar starter slots shown in Figure 2.1 yield $s_n = 0.07$. Thus, changing a_i between tests introduces somewhat more variability in the determination of K_{Ic} as compared with keeping a_i constant, but the results of either method of testing are acceptable for the purposes of this work.

Effect of Water Content

Fracture toughness and a measure of the length of an initial fracture can be used to predict P_{df} required to propagate a hydraulic fracture in the Center Hill clay, within the variability cited above. It is apparent from Figure 2.5, however, that the value of K_{Ic} varies over more than an order of magnitude, so that some method of anticipating K_{Ic} will be required before it can be a useful predictor of the onset of propagation.

Water content and duration of consolidation varied from one sample set to another, and they both have a marked affect on K_{Ic} (Fig. 2.6*a*). Among samples that were prepared by compaction alone, K_{Ic} is greatest, roughly 20 kPa $m^{1/2}$, in the range $0.17 < \theta < 0.21$.

The fracture toughness decreases abruptly to roughly 3.5 kPa $m^{1/2}$, however, as θ increases from 0.21 to 0.22. The sharp change in K_{Ic} with θ occurs where the pore pressure changes from negative (Condition *A*, as defined in Chapter 1) to positive (Condition *B*). A slight decrease in K_{Ic} occurs with further increase in θ, although the decrease is small and K_{Ic} is practically independent of θ in the range 0.22 to 0.30 (Fig. 2.6*a*).

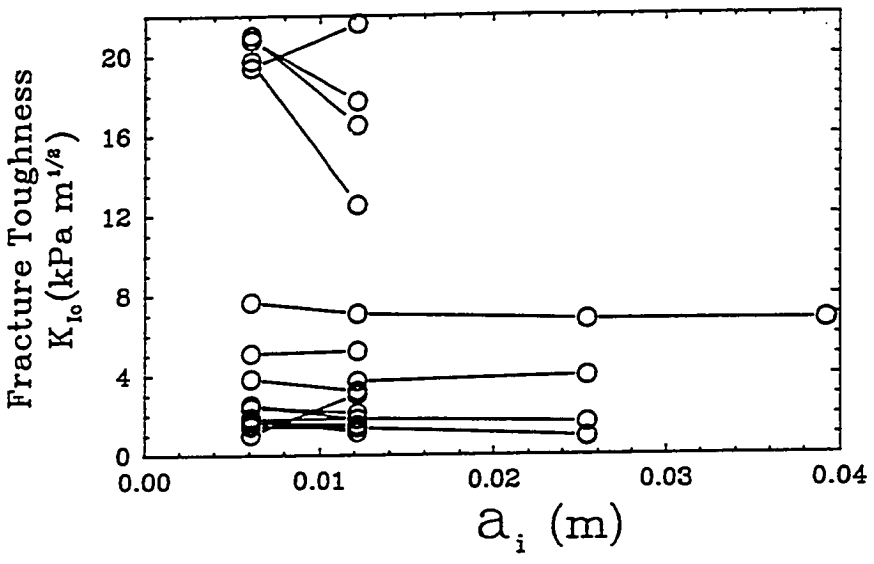

Figure 2.5. Fracture toughness as a function of half-length of starter slot for sets of similar samples of Center Hill clay.

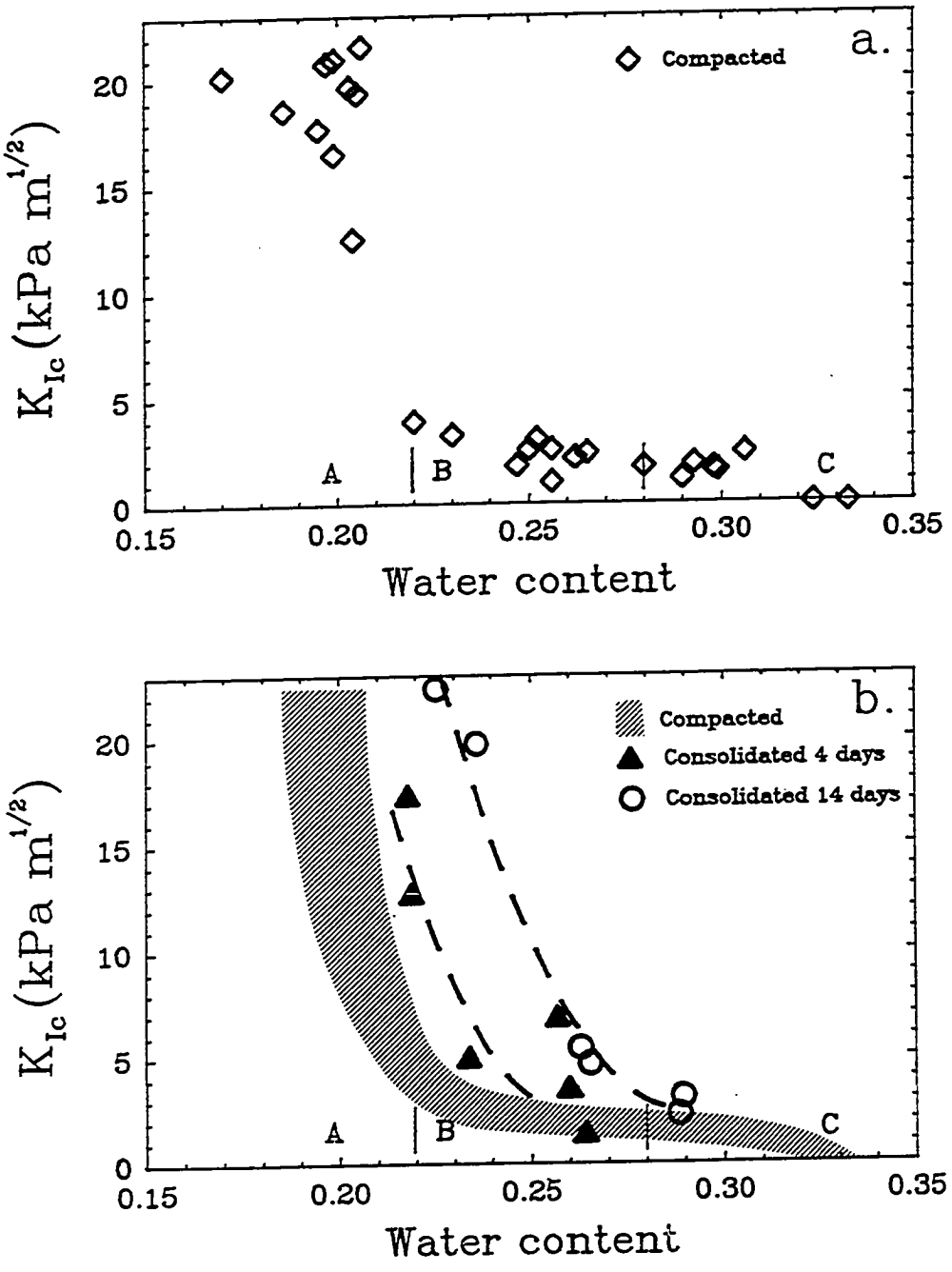

Figure 2.6a. Fracture toughness as a function of water content for compacted soil samples. 2.6b Fracture toughness as a function of water content and duration of consolidation.

Fracture toughness is negligible for samples with $\theta > 0.32$, however. In this case, the break in slope of the pressure record, from which the onset of fracturing is inferred, occurs when the pressure of the injection fluid is equal to the confining stress. Nevertheless, hydraulic fractures produced during these tests are physically similar to other fractures produced when $K_{Ic} > 0$.

Consolidation appears to toughen the Center Hill clay (Fig. 2.5*b*), according to limited results of samples consolidated for 4 to 14 days beneath a static pressure of 69 kPa (details of the procedure are in Chapter One). Fracture toughness of the samples consolidated for 4 days is greater by as much as 7.5 kPa $m^{1/2}$ compared with compacted samples of similar water content. Moreover, increasing the duration of consolidation to 14 days further increases K_{Ic} (Fig. 2.5*b*). The forms of the three curves in Figure. 2.5 are similar, however; they all show K_{Ic} decreasing markedly over a few percent of water content.

The interval where K_{Ic} is independent of θ (Condition *B*) appears to be diminished during consolidation. Condition *B* was defined in Chapter One as having pores that are filled with both air and water (partly saturated), but where the pores are under positive pressure. We surmised that positive pore pressures in Condition *B* result from the sudden application of confining pressure immediately preceding a fracturing test. That condition is expected to be eliminated during consolidation, as pores drain in response to the confining load. Results from Figure 2.5*b* corroborate this expectation because the interval where K_{Ic} is independent of θ in Fig 2.5*a* has apparently been eliminated.

PRESSURE RECORDS DURING PROPAGATION

Decreasing the pressure required to initiate a hydraulic fracture is by no means the only effect of increasing water content; the form of the pressure record is

markedly affected as well (Fig. 2.7). Increasing water content results in a decrease of slope during Period I, as the starter slot inflates but before the onset of propagation. The most striking effects, however, are seen during Periods II and III while propagation is occurring.

Increasing water content causes the pressure record during propagation to flatten, with the duration of stable propagation (Period II) increasing, and the magnitude of pressure changes during both stable and unstable propagation diminishing. For example, the form of the record of the driest sample (θ = 0.20) in Figure 2.7 is characterized by a break in slope at roughly P_{df} = 62 kPa, indicating the onset of propagation. A short period (roughly 2 seconds) of increasing pressure, which indicates stable propagation, is followed by an abrupt decrease in driving pressure. Driving pressure decreases by 25 kPa during 48 seconds of propagation, and the form of the record indicates a generally positive curvature. A sharp drop in pressure of roughly 8 kPa at 28 seconds is recovered at 34 seconds. Similar sharp fluctuations in pressure were fairly common, but impossible to predict. They apparently occur when the propagating fracture intersects a large pore or cavity created inadvertently during molding of the sample.

In the sample with θ = 0.25, stable propagation occurs for 4 seconds and is followed by unstable propagation where the driving pressure diminishes by only 8 kPa. The curvature of that record is generally positive, but it is much less than that of the record of the θ = 0.20 sample. Those trends continue with the θ = 0.30 sample, where stable propagation persists for 8 seconds (roughly), and is followed by a slight decrease of only 3 to 4 kPa during unstable propagation.

The break in slope of the record for the sample with θ = 0.33 occurs at negligible driving pressure. The linear part of the record for that sample occurs

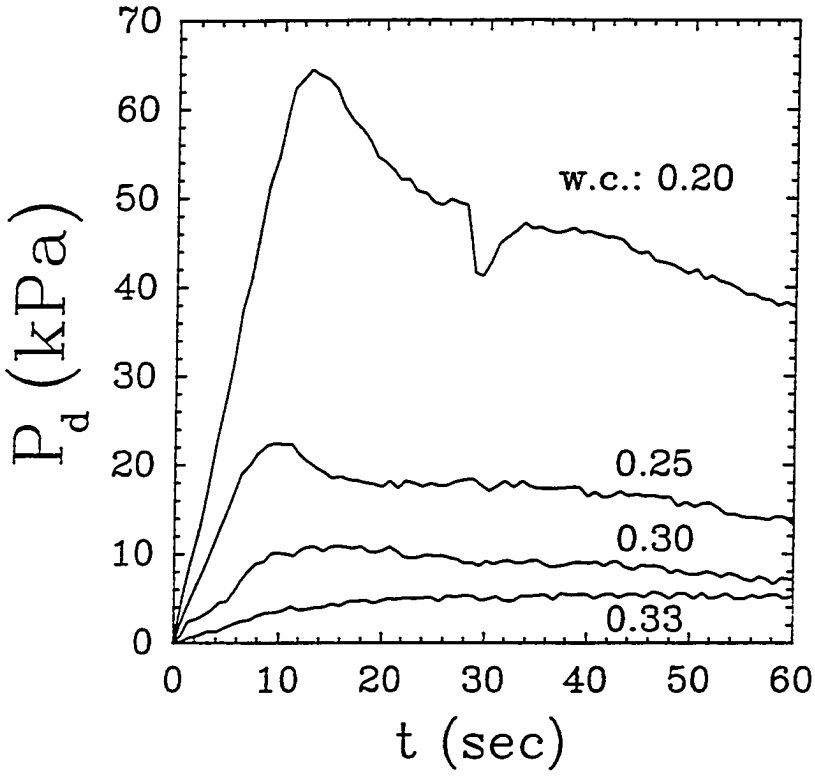

Figure 2.7. Pressure records from four samples of differing water content (a_i = 1.22).

where driving pressure is negative, so the break in slope is difficult to determine from Figure 2.7. The break in slope is assumed to indicate the onset of fracture propagation, as for drier samples, although with $\theta = 0.33$ the sample is extremely soft and plastic deformation of soil enveloping the starter slot may affect the form of the record.

Propagation of the fracture in the sample with $\theta = 0.33$ is essentially entirely stable. Driving pressure increases to 4 kPa after 10 seconds, and it continues to slowly increase until it reaches 5 kPa after roughly 35 seconds. Driving pressure is essentially constant after 35 seconds, except for minor pressure fluctuations 0.25 kPa in amplitude which occur on all records throughout propagation.

DISCUSSION

Injecting glycerin at constant rate into a block of silty clay containing an incipient fracture initially causes the pressure of the glycerin to increase. The slope of the pressure record is positive and roughly constant as the incipient fracture inflates. The intensity of stresses at the tip of the fracture exceed the fracture toughness of the clay at some time during injection and a hydraulic fracture is nucleated. The onset of propagation diminishes the rate of increase of pressure, so that a break in slope of the record serves as an indicator that propagation has begun. In some cases, incipient hydraulic fracturing of clay may occur slightly prior to the break in slope.

Early growth of the fracture is stable, characterized by a positive slope that diminishes with time. The duration of the period of stable growth depends on the water content; as water content increases the duration of stable propagation increases. Early stable propagation of hydraulic fractures in rock was described by Zoback and Pollard (1978), who attributed the stability to high losses in driving

pressure along the length of the fracture. The losses in pressure could be due to viscous dissipation during flow in a narrow incipient fracture (Zoback and Pollard, 1978), but observations described in Chapter One suggest an alternative. Those observations suggest that the injected fluid lags behind the tip of the fracture, and the amount of lag depends on water content. The implication of fluid lagging behind the tip is demonstrated by Clifton and others (1976), who performed experiments where they prevented fluid from entering a hydraulic fracture by lining a starter hole with a flexible membrane. Stable propagation was observed when the membrane was in place, and unstable propagation when the membrane was omitted. Their study, which is supported by theoretical analyses, shows that lack of fluid penetration to the fracture tip favors stable propagation. Those results suggest a relation between the form of the pressure record and features of the fractures themselves. That relation was the motivation behind the theoretical analysis presented in Chapter Three.

In this work, fracture toughness was tested empirically as an indicator of the onset of propagation in the Center Hill clay. In linear elastic fracture mechanics, the use of K_{Ic} as a failure criterion generally requires that the fracture process zone, where inelastic behavior such as microcracking or void coalescence occurs, is small compared with the dimensions of the fracture and the specimen (Tada and others, 1985; Williams, 1984; Ouchterlony, 1982; Rice, 1968). Schmidt (1980) describes a method of estimating the size of the process zone based on a maximum normal stress criterion. That method tacitly assumes that dilation of microcracks is the dominant phenomenon occurring in the process zone, an assumption that is accepted for rocks (Ouchterlony, 1982) and seems reasonable for clayey soil as well. The maximum length of the process zone L_p is given by

$$L_p = 0.269\,[K_{Ic}/(\sigma_y + \sigma_c)]^2 \qquad (2.4)$$

where σ_c is the mean confining stress, and σ_y is the tensile yield stress required to open microcracks. The tension of porewater (e.g. Fig. 1.3) will be taken as a tensile yield strength because the dilation of microcracks presumably must overcome that tension. Methods of measuring tensile yield strength of soil, such as those described by Snyder and Miller (1985), Snyder (1980), Vomocil and Chancellor (1967), and Farrell and others (1967), require special equipment that was unavailable during this study.

The maximum dimension of the process zone decreases with increasing water content, according to eq (2.4) and data in Figure 1.3. For example, L_p = 0.47 cm for θ = 0.20 (using σ_y = 60 kPa), and L_p = 0.13 cm for θ = 0.27. Ouchterlony (1982) suggests that the starter slot be 9.3 times longer than the maximum dimension of the process zone to ensure small-scale yielding. Slot lengths used in this work ranged from 1.22 to 5.05 cm. Thus, Ouchterlony's criterion is satisfied for samples whose water contents exceed 0.22 (Condition *B* and *C*) for all slot lengths, and it is satisfied for drier material when using the longer slot.

The small-scale yielding criterion of linear elastic fracture mechanics appears to support the use of K_{Ic} to predict hydraulic fracturing in the Center Hill clay. A loss of accuracy in K_{Ic} is an expected consequence if the size of the process zone exceeds that required for small-scale yielding (Tada and others, 1985; Williams, 1984). The increase in size of the process zone with decreasing water content is a possible explanation of the observation that the drier samples exhibit a greater variability in K_{Ic} (Figs. 2.5 and 2.6a). Increasing the length of the starter slot when testing drier soil samples should improve accuracy according the theoretical arguments presented above. However, there are practical limitations. Attempts to

cut slots 3 to 5 cm long in relatively dry samples either resulted in damage to the cutting tool, or damage to the sample itself.

CONCLUSIONS

Fracture toughness can be used as a material property to predict the driving pressure of a hydraulic fracture in soil when both K_{Ic} and the length of the hydraulic fracture are known. It may be difficult to know K_{Ic} precisely without testing, however, because it depends strongly on water content, duration of consolidation and other factors. Fracture toughness of the Center Hill clay decreases markedly (from 20 to 2.5 kPa $m^{1/2}$) in the range $0.20 < \theta < 0.23$, is roughly constant in the range $0.23 < \theta < 0.31$, and decreases to negligible values when $\theta > 0.31$. Duration of consolidation increases K_{Ic} for a given water content, although only preliminary values of the effects of consolidation are presented here. Increasing compactive effort increases P_{df} according to the laboratory experiments of Jaworski and others (1979), presumably because compactive effort affects fracture toughness.

When soil is completely saturated, K_{Ic} is essentially zero. Nevertheless, well-developed hydraulic fractures were created in soils of negligible toughness. Presumably there is an upper limit of water content (with increasing θ the soil will eventually become a slurry), above which injection of the glycerin will form a bubble-like feature rather than a fracture. Inasmuch as K_{Ic} appears to be a useful indicator of the onset of propagation, it is unable to predict conditions when a hydraulic fracture will not form.

Early propagation is commonly stable, characterized by driving pressure that increases with time. At some time, propagation changes from stable to unstable and P_d begins to decrease. The details of a pressure record depend strongly on the water content of soil in the following ways:

a.) Increasing θ decreases the slope during inflation of the starter fracture.

b.) Increasing θ decreases the driving pressure required to initiate and propagate a fracture (and also K_{Ic}).

c.) Increasing θ increases the duration of stable propagation.

d.) Increasing θ decreases the pressure change during propagation (both pressure increase during stable and pressure decrease during unstable propagation).

CHAPTER THREE

ANALYSIS OF FRACTURE PROPAGATION

Essential details of the laboratory experiments described in the previous two chapters cannot be predicted using published analyses of hydraulic fracturing of soil. This is because many published analyses focus on methods of predicting the onset of propagation (Mori and Tamura, 1987; Horsrud and others, 1982; Bjerrum and others, 1972; Morgenstern and Vaughn; 1963) in order to safeguard various geotechnical practices, such as dam construction, permeability testing, or injection grouting, and so they are incapable of predicting aspects of propagation. Analyses have been developed, however, to describe propagation of a hydraulic fracture in rock under a wide range of geometries and boundary conditions, including those resembling the laboratory experiments. Those analyses typically describe the deformation of the material enveloping a hydraulic fracture using linear elastic fracture mechanics (LEFM). The purpose of this chapter is to use methods of LEFM to formulate an analysis of hydraulic fracture propagation during the laboratory experiments and compare the predictions of the analysis to the observations from the laboratory.

The analysis used here will only consider linear elastic deformation; however, a hydraulic fracture cutting through silty clay clearly will cause some plastic deformation, particularly in the vicinity of the fracture tip. The linear elastic methods remain valid, however, so long as the zone of plastic deformation remains small compared with the length of the fracture. Rough estimates presented in Chapter Two suggest that the size of the plastic zone near the tip of a hydraulic fracture in remolded silty clay is on the order of several mm. This suggests that the zone of plastic deformation during the laboratory experiments is small enough to

ignore if the fracture is a few cm in length. Moreover, we saw in Chapter Two that the critical stress intensity K_{Ic}, a fundamental parameter of LEFM, predicts the onset of fracturing in silty clay. This observation further supports the application of LEFM to the experiments. Ultimately, the justification for applying a LEFM model to hydraulic fractures in soil will come from the similarities between analytical results and experimental observations.

The geometry and boundary conditions used in the theoretical analysis will be closely tied to the descriptions of the fractures in Chapter One, and the analyses will be formulated to predict pressures as a function of time as reported in Chapter Two. Once derived, the analysis will be used to show how slight variations in essential parameters, such as K_{Ic}, affect the shape of the pressure record. The validity of the analysis will then be tested by comparing pressure records generated theoretically to records from the experiments.

DERIVATION OF THE SOLUTION

A hydraulic fracture in the laboratory experiments will be idealized in the following derivation by making a variety of assumptions which are intended to simplify the problem to a tractable form while preserving essential features. The lengths of fractures created in the laboratory were roughly uniform with respect to their width, so that the fracture cross-section is nearly independent of location along the width. A hydraulic fracture will thus be idealized as a two-dimensional feature viewed in cross-section; effects due to the edge of the sample, as well as effects of fracture lobes will be ignored. The experimental apparatus was designed to restrict deformation parallel to the long axis of the starter slot, so an assumption of plane strain conditions at the leading edge of the fracture will be adopted. Interaction between the growing fracture and the edges of the sample is minor while the

fracture is small compared with the sample dimensions, so we will simply ignore any such interaction and assume that the idealized fracture is embedded in a medium of infinite extent.

The hydraulic fracture lies in the x-z plane, with the z-axis trending along the fracture mid-line, and the direction of growth is parallel to the x -axis (Fig. 3.1). Fracture width w is measured along the z-axis and is constant. Symmetry about the z -axis is assumed, so that we will only treat the positive x part of the fracture. Accordingly, fracture length will hereafter be described using the half-length a.

Observations from the laboratory suggest that the fracture is filled with two fluids, one that is injected at constant rate Q along the mid-line, and another that infiltrates out of the soil pores and into the fracture tip. I will assume that the driving pressure of the injected fluid, P_d, is uniform along the fracture but that it varies with time. The injected fluid flows toward the fracture tip, so there must be a pressure gradient in that direction. A numerical analysis of the fluid pressure due to flow in a hydraulic fracture created under conditions of the laboratory experiments (Murdoch and others, 1990), however, indicates that the pressure gradient is small and that the distribution of pressure is nearly uniform. Analyses of pressure within a fluid flowing in a two-dimensional fracture are also presented by Nilson and Griffiths (1986; fig.2), Nilson (1986; figs. 6 and 7), Geertsma and DeKlerk (1969; fig. 8), Khristianovich and Zheltov (1955; fig. 5). Those analyses indicate that the pressure can be nearly uniform within most of the fracture, particularly when the flow rate is low and the driving pressure is small, as in the laboratory experiments.

Driving pressure of the infiltrated pore fluid P_{dtip} will be taken to be constant and uniformly distributed over a zone at the tip. That P_{dtip} is constant seems to be a reasonable preliminary assumption because the pressure of the infiltrated fluid

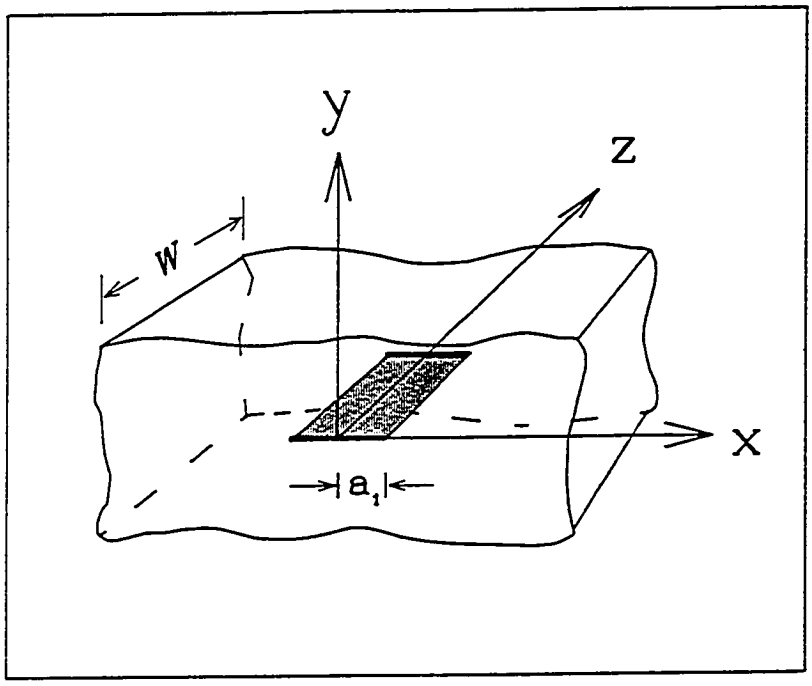

Figure 3.1. Geometry of idealized fracture used in the analysis

should be related to the pressure of pore fluid ahead of the fracture, which itself is constant.

To accommodate those assumptions we require that the fracture is filled with injected fluid to a point b along the x-axis, and P_d is uniform over $0 < x < b$ (Fig. 3.2). The tip of the fracture is filled with fluid at driving pressure P_{dtip} over the interval $b < x < a$.

The driving pressure P_d changes as the fracture lengthens to maintain static equilibrium. The magnitude of the P_d is constrained because for equilibrium we require that $K_I = K_{Ic}$ throughout propagation (Nilson, 1986; Spence and Turcotte, 1985).

A solution can be obtained by superposition of two loading conditions (Fig. 3.2).

Loading 1: $P = p_1$; $0 < x < b$; and $P_d = 0$; $b < x < a$.

Loading 2: $P = P_{dtip}$; $0 < x < a$

where by inspection it is apparent that the superposition yields

$$P_d = p_1 + P_{dtip} \tag{3.1}$$

For Loading 1, the Mode I stress intensity K_I, volume V, and aperture at the origin δ_o of a fracture is (Tada, 1985)

$$K_{I1} = p_1\sqrt{\pi a}\,[(2/\pi)\ \sin^{-1} b/a] \tag{3.2a}$$

$$V_1 = 4p_1a^2w/E\,[\sin^{-1} b/a + b/a\sqrt{1 - (b/a)^2}] \tag{3.2b}$$

$$\delta_{o\,1} = 8\,p_1\,a/\pi E\,[\sin^{-1} b/a + b/a\,\cosh^{-1} a/b] \tag{3.2c}$$

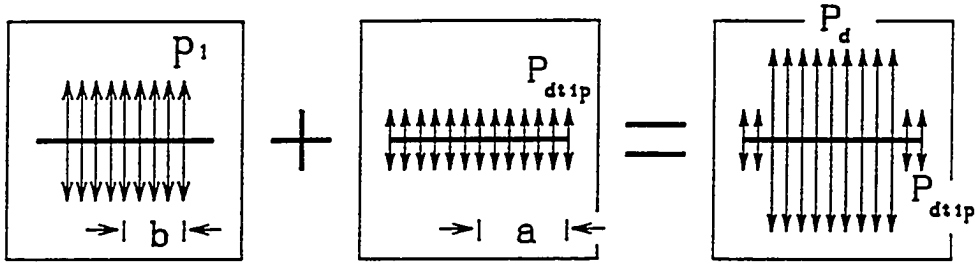

Figure 3.2. Loading conditions used to develop the analytical model.

and for Loading 2

$$K_{I2} = P_{dtip}\sqrt{\pi a} \tag{3.3a}$$

$$V_2 = 2\,\pi P_{dtip} a^2 w/E \tag{3.3b}$$

$$\delta_{o\,2} = 4\,P_{dtip}\,a/E \tag{3.3c}$$

Adding the solutions and using eq (3.1) yields

$$K_I = \sqrt{\pi a}\,[P_d\,\theta + P_{dtip}\,(1 - \theta)] \tag{3.4a}$$

$$V = 2\,\pi a^2 w/E\ [P_d\,\psi + P_{dtip}\,(1 - \psi)] \tag{3.4b}$$

$$\delta_o = 4\,a/E\,[P_d\,\phi + P_{dtip}\,(1 - \phi)] \tag{3.4c}$$

where the terms θ, ψ, and ϕ depend only on b/a, the geometry of loading at the tip

$$\theta = (2/\pi)\,\sin^{-1} b/a \tag{3.4d}$$

$$\psi = (2/\pi)\,[\sin^{-1} b/a + b/a\sqrt{1 - (b/a)^2}] \tag{3.4e}$$

$$\phi = (2/\pi)\ [\sin^{-1} b/a + b/a\,\cosh^{-1} a/b] \tag{3.4f}$$

An estimate of b/a will be obtained from the laboratory measurements by rearranging eq. (1.4)

$$b/a = [a + ma_i]/[a(m+1)] \tag{3.5}$$

where m is the rate of growth of the tip zone, as described in Chapter One. Hereafter eq. (3.5) will be used to determine b/a as a function of m and fracture length.

Rearranging eq.(3.4a)

$$P_d = [K_I/\sqrt{\pi a} - P_{dtip}(1 - \theta)]/\theta \tag{3.6}$$

yields the driving pressure required to propagate a fracture of half-length a.

Equation (3.6) is made a function of time by introducing a mass balance expression containing the rate and duration of injection. This approach tacitly ignores dynamic effects during propagation, but, as Nilson (1986) points out, viscous effects in the fluid filling a hydraulic fracture will limit propagation velocity and dynamic effects will be negligible. Assuming that fluid filling the fracture is incompressible, we have the balance

$$Qt = V_{frx} + V_{pump} + V_{leak} \tag{3.7}$$

where Q is the flow rate of the pump, t is time of injection, V_{frx} is the volume of injected fluid in the fracture, V_{pump} is the volume of fluid stored by elastic distortion of the injection system and V_{leak} is the volume of fluid that has flowed through the wall of the fracture into the soil. The latter process is termed *leakoff* by Howard and Fast (1970) and other investigators of hydraulic fracturing of rock.

We will ignore the second and third terms on the right hand side of eq. (3.7) to obtain a preliminary solution. During inflation of the starter slot, $b/a = 1.0$ and the pressure record is obtained from eq. (3.4*b*)

$$P_d = [QE/2\pi a_i^2 w]\, t \tag{3.8}$$

During propagation, we solve for fracture length and substitute into eq. (3.6) to obtain P_d as a function of time. Assuming that eq. (3.4b) is an adequate expression for the injected volume, then

$$t = \{2\,\pi a^2 w/QE\}\,[P_d\,\psi + P_{dtip}\,(1 - \psi)] \qquad (3.9a)$$

Substituting eq.(3.6) into eq. (3.9*a*) and rearranging

$$a = \sqrt{2\,\pi w/tQE\;\;[\psi\,K_I/\sqrt{\pi a} - P_{dtip}\;\;\psi(1-\theta)(\psi-1)/\theta\,]} \qquad (3.9b)$$

This expression for fracture length as an implicit function of time was solved using a commercially-available Newton-Raphson algorithm. Driving pressure and aperture as functions of time were obtained using eqs. (3.9*b*), (3.6) and (3.4*c*).

Now we will return to eq. (3.7) and include all storage terms. The volume of fluid stored by elastic dilation of the injection equipment depends on fluid pressure $p_f = (P_d + \sigma)$. The stored volume was determined as a function of fluid pressure by plugging the injection tube on the pumping system and recording pressure as a function of volume displaced by the pump. The following expression was obtained by regression

$$V_{equip} = c_o + c_1 p_f + c_2 p_f^2 + c_3 p_f^3 \qquad (3.10)$$

where p_f is measured in kPa and

$$c_o = 1.757 \times 10^{-2}\ cm^3$$

$$c_1 = 7.262 \times 10^{-3}\ cm^3/kPa$$

$$c_2 = -2.868 \times 10^{-5}\ cm^3/kPa^2$$

$$c_3 = 4.652 \times 10^{-8}\ \mathrm{cm^3/kPa^3}$$

The correlation coefficient is 0.9995 for the regression.

The volume of fluid that has leaked out of an incremental area dA on the fracture wall during an incremental time dt after an elapsed time t since the onset of injection is

$$V_{leak}(dA, dt) = 2\,C\,dA dt/\sqrt{t - \tau(A)} \qquad (3.11)$$

where we assume that the pressure difference between the fluid in the fracture and the pore fluid remains constant throughout the test (Carter, in Howard and Fast, 1957). The parameter C is the fluid-loss, or leakoff coefficient, and $\tau(A)$ is the time when dA was created.

Integrating with respect to time and with respect to area, and recognizing that for a rectangular fracture

$$dA = 2wda$$

where a is the half-length

$$V_{leak}(a_1, t) = 8\,C\,w \int_0^{a_1} \sqrt{t - \tau(a)}\,da \qquad (3.12)$$

For small values of leakoff C and values of b/a that are essentially unity then $\tau(a)$ can be estimated by rearranging eq. (3.4a)

$$P_d = K_I/\sqrt{\pi a} \qquad (3.13)$$

using $V_{frx} = Qt$ and substituting into eq. 3.4b

$$\tau(a) = [2w\sqrt{\pi}K_I/QE]\, a^{3/2} \tag{3.14}$$

A more general evaluation of $\tau(a)$, where large leakoff and the growth of the tip zone were possible, was obtained by assuming a power law form

$$\tau(a) = C_1 a^n \tag{3.15}$$

The constants C_1 and n where estimated using eq (3.14). The estimate was adjusted by obtaining t for several values of a, using an expression similar to eq. (3.9*a*), and recalculating C_1 and n by curve fitting for each new pair of t and a. Values of n would increase and C_1 would decrease as leakoff or the growth of the tip zone increased ($C>0$, or $m>0$). During analyses conducted to check the approach described above, fracture lengths predicted by inverting eq. (3.9*b*) were typically within a few percent of lengths determined using eq. (3.15).

Substituting eq.(3.14) or eq. (3.15) and eq.(3.10) into eq. (3.7) yields an implicit expression that is similar to eq. (3.9*b*), but which contains expressions for elastic distortion of the pumping system as well as leakoff from of the fracture. As with eq. (3.9*b*), the expression is readily inverted using a computer.

EFFECTS OF CRITICAL PARAMETERS

The theory outlined above predicts that driving pressure during propagation depends on these parameters: initial fracture length, elastic modulus, pressure in the fracture tip, growth of the infiltrated region at the tip, fracture toughness, and the rate of leakoff. A sensitivity analysis was conducted to highlight the effects of each of those parameters individually. The analysis consists of determining driving pressure as a function of time using a set of baseline values of parameters (Table

3.1) selected to represent conditions during hydraulic fracturing of Center Hill clay with a water content of roughly $\theta = 0.26$. Additional driving pressure records were determined by slightly increasing or decreasing the value of each parameter.

Table 3.1: Baseline values of parameters used in sensitivity analysis.

E	6 MPa	C	0.007 cm/min$^{1/2}$
K_{Ic}	2.5 kPa m$^{1/2}$	m	0.1
a_i	1.22 cm	P_{dtip}	0
Q	2.01 cm^3/min	σ_{min}	55 kPa

The pressure record (Fig. 3.3) resulting from the baseline values shows a form that qualitatively resembles records from the laboratory experiments. It is characterized by a period of linear increase in pressure during inflation of the starter slot. The onset of propagation is marked by a decrease in the slope of the record, indicating that the initial propagation is stable. This occurs because the low pressure zone at the tip, characterized by P_{dtip} and m, tends to stabilize propagation while the fracture is short. Eventually, the fracture becomes long enough that the effects at the tip are unable to stabilize it, and P_d decreases during unstable propagation.

Modulus

Each parameter affects different aspects of the pressure record. Two parameters, elastic modulus E and leakoff C, affect the record only by changing the time scale through eq. (3.7). Increasing the modulus reduces the time until the onset of propagation (Fig. 3.3*a*). This occurs because stiffening the material enveloping a fracture will cause the fracture to be smaller in volume when the

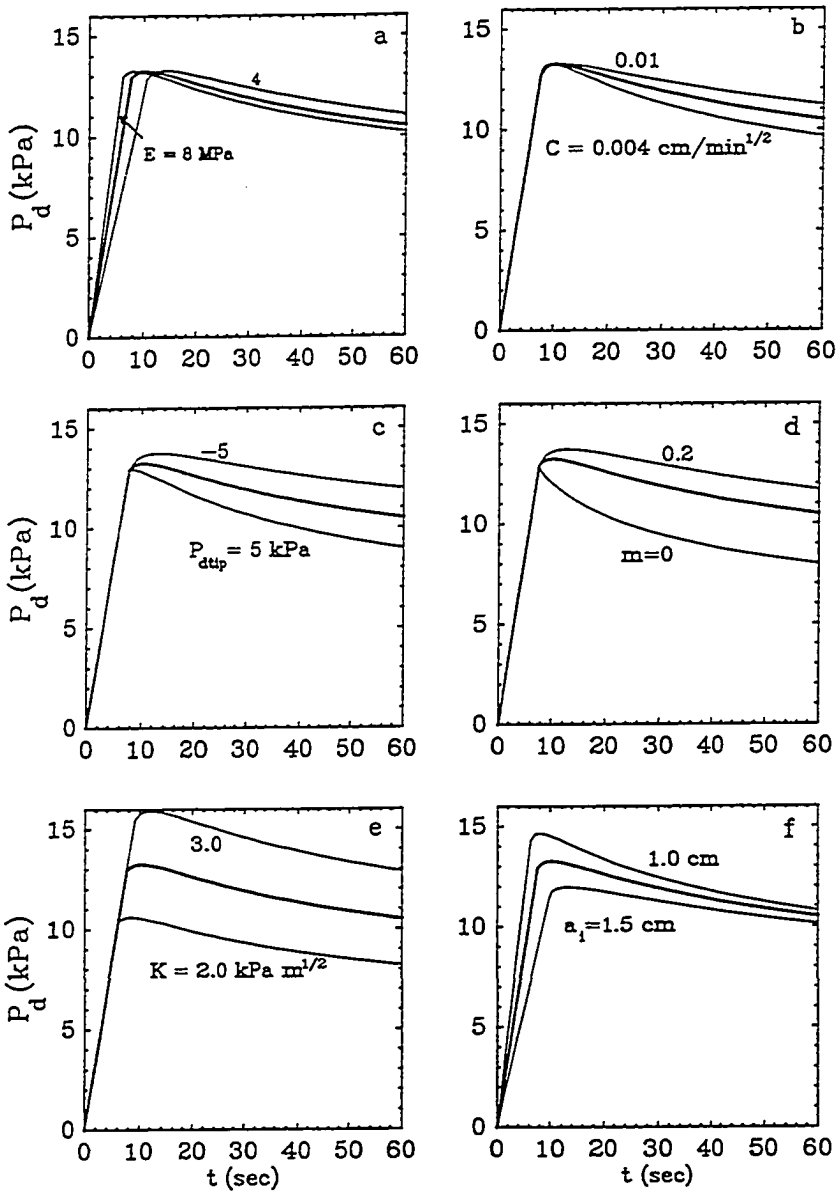

Figure 3.3. Pressure records predicted for various values of parameters in the analysis. The heavy solid line is the same on each panel and was obtained using parameters in Table 3.1.

pressure required to initiate propagation is achieved. Reducing the volume at the onset of propagation reduces the time of injection required for propagation. According to the analysis, the time until the onset of propagation is determined from eq. (3.6a) as

$$t_{\text{onset}} = 2\,\pi a^{3/2} w K_{\text{Ic}} / \pi^{1/2} Q E \qquad (3.16)$$

if we ignore leakoff during inflation of starter slot. Time is related to the inverse of the modulus in eq. (3.16), so changing the modulus results in a translation of the record parallel to the abscissa. An equal amount of translation is present throughout the record, so the shape of the record during propagation is unaffected by a change in E (Fig. 3.3*a*).

Leakoff

The effect of leakoff increases with time and results in a flattening of the record with increasing C (Fig. 3.3*b*). The physical explanation behind this behavior is that the rate of fracture growth decreases as C increases, simply because increasing amounts of fluid are lost from the fracture. Thus, the rate of decrease in P_d diminishes (and appears as a flattening of the record) because the rate of fracture growth decreases. In the analysis, leakoff only affects the expression for time (entering eq. 3.7 through eq. 3.12), so changing C results in a translation of points parallel to the abscissa. Unlike the effect due to E, however, the amount of translation increases with time. This is because the value of the integral in eq. (3.12) increases with time for $\tau(t)$ represented by eq.(3.14) or (3.15).

The Fracture Tip

Driving pressure in the fracture tip, P_{dtip}, and the relative length of the infiltrated tip, m, affect the record in a similar fashion (Fig. 3.3*c* and *d*). The

fracture is stabilized when the pressure of fluid at the fracture tip is less than the driving pressure of the injected fluid. This stabilizing effect is manifested as an increase in P_d at early times, and a flattening of the record at later times (Fig. 3.3*c*). The magnitude of the stabilizing effect depends on both the length of the infiltrated zone (a - b) and the pressure in the zone. Accordingly, increasing m has much the same effect, qualitatively, on the form of the record as decreasing P_{dtip}. Comparing the records for P_{dtip} = -5 kPa to the one for m = 0.2 illustrates the similarity. Moreover, the magnitude of the effect of a change in either P_{dtip} or m depends strongly on the magnitude of the other variable. For example, the stabilizing effect of changing P_{dtip} from 0 to -5 kPa for m = 0.1 (Fig. 3.3*c*) is much greater when m = 0.2.

The effect of the infiltrated tip is removed completely when m = 0 (Fig. 3.3*d*). In this case, the fracture is completely filled with injected fluid and propagation is always unstable. The pressure record during propagation then reduces to the power law form

$$P_d = [\, 2wK_{Ic}^4/QE\pi]^{1/3}\ t^{-1/3} \qquad (3.17)$$

for C = 0.

Fracture Toughness

Fracture toughness increases the driving pressure and time required to initiate propagation, but neither the slope of the record during inflation nor the form of the record during propagation are affected (Fig. 3.3*e*). Physically, this occurs because K_{Ic} dictates the driving pressure required for propagation of a fracture of given length. That effect results in the linear relation between t_{onset} and K_{Ic} (eq. 3.16), and a linear relation between P_d and K_{Ic} (eq. 3.6).

Slot Length

The length of the initial fracture or starter slot, a_i, has a marked effect early in the record, but the effect diminishes with time. Shortening a_i causes the onset of propagation to occur at earlier times and greater pressures. Moreover, it also affects the form of the record by increasing the curvature during early stable propagation. After propagating for several tens of seconds to a minute, however, the records converge and appear to become independent of a_i.

The physical interpretation is that the increase in pressure accompanies a decrease in leverage that attends a reduction in a_i. A shorter slot will require more pressure to propagate, but it will inflate more rapidly than a longer slot. The effect of a difference in a_i, however, diminishes with propagation as the difference becomes an increasingly smaller proportion of the entire fracture length.

A starter slot was cut into samples during the laboratory experiments and so a_i is obviously not a property of the fracturing process, as are the other parameters whose effects are described above. In a few of our experiments, and in experiments by Mori and Tamura (1987) and Jaworski and others (1979), the starter slot was omitted and fluid injected into an open cylindrical hole. We found that the pressure records from those experiments were difficult to duplicate. Similar difficulties were reported by Jaworski and others. Presumably, small pre-existing cracks or pores intersected by the cylindrical hole acted as starter slots during those experiments. Thus, a_i was unknown and probably varied both within a single sample and among different samples, so the effects shown in Figure 3.3*f* could not be separated from effects of the other parameters. Cutting the starter slot allowed us to replace an unknown and possibly variable a_i with a known constant value. In light of the marked effects that a_i has on the pressure record, the procedure of cutting a starter

slot is considered to be essential to obtaining meaningful results during the laboratory experiments.

COMPARISON WITH LABORATORY RESULTS

The validity of the theoretical analysis was tested by comparing results of the analysis to records from the laboratory. The comparison was done by first using estimation techniques to determine values of the critical parameters that yielded the best fit between the theoretical curves and the experimental pressure records. Then the values of the parameters estimated by curve fitting were matched against values measured in the laboratory.

Estimation of Parameters

Elastic modulus was estimated from the slope of the pressure record during inflation of the starter slot, essentially by differentiating eq. (3.8) with respect to time. Fracture toughness was obtained from the driving pressure at the onset of propagation and initial half length, according to eq. (3.4*a*) with $b/a = 1.0$.

Initial estimates of P_{dtip} and m were made using a curve-fitting procedure based on the Levenberg-Marquardt method of nonlinear parameter estimation (Press and others, 1986). In some cases, this approach yielded ambiguous results because, as explained above, slight variations in those two parameters affected the pressure record in similar ways. As a result of this non-uniqueness, the Levenberg-Marquardt routine was slow to converge and presented values of P_{dtip} and m which differed only slightly in χ^2 (e.g. the goodness of fit was similar for a variety of pairs of P_{dtip} and m). Moreover, some of the values obtained by unconstrained parameter estimation were nonsensical; for example, $P_{dtip} > P_d$ or m approaching 1.0. To resolve this difficulty, we selected the pair of P_{dtip} and m that yielded the best fit of

the experimental data, but we required that the fluid pressure in the tip p_t was positive but less than the maximum confining stress; $0 < p_t < \sigma_{max}$ (69 kPa).

The leakoff coefficient C was obtained by estimating the so-called fluid efficiency e_f (Gidley and others, 1990) from the pressure records. Fluid efficiency is the ratio of the volume of the injected fluid to the volume of fluid in the fracture. In general, e_f decreases with increasing C, but it also decreases with duration of injection. Nolte (1986) presents a graphical technique, which is based on a numerical analysis, for determining e_f, from the ratio t_c/t_o, where t_c is the time elapsed between shutting off the pump and when P_d diminishes to 0, and t_o is the duration of injection. During the laboratory experiments, pressure was typically recorded for several minutes after the pump was turned off, so that both t_c and t_o were known.

To estimate C, e_f was determined from t_c/t_o using laboratory data and Nolte (1986; fig. 5). Then e_f was calculated using the theoretical analysis described above and C adjusted until the calculated efficiency approached the one estimated from laboratory data. Values of e_f from the theoretical analyses were within 0.2 of values determined using the experimental procedures described above; typically the theoretically derived values overestimated the values determined experimentally.

Pressure Records

The theoretical analysis is able to capture details of the pressure records at various water contents. An example of four laboratory records, which include water contents that range from 0.20 to 0.33, is given in Figure 3.4. The similarity between the laboratory records and the theoretical analysis in Figure 3.4 is remarkable. The analysis is able to accommodate the decrease in slope during inflation of the slot,

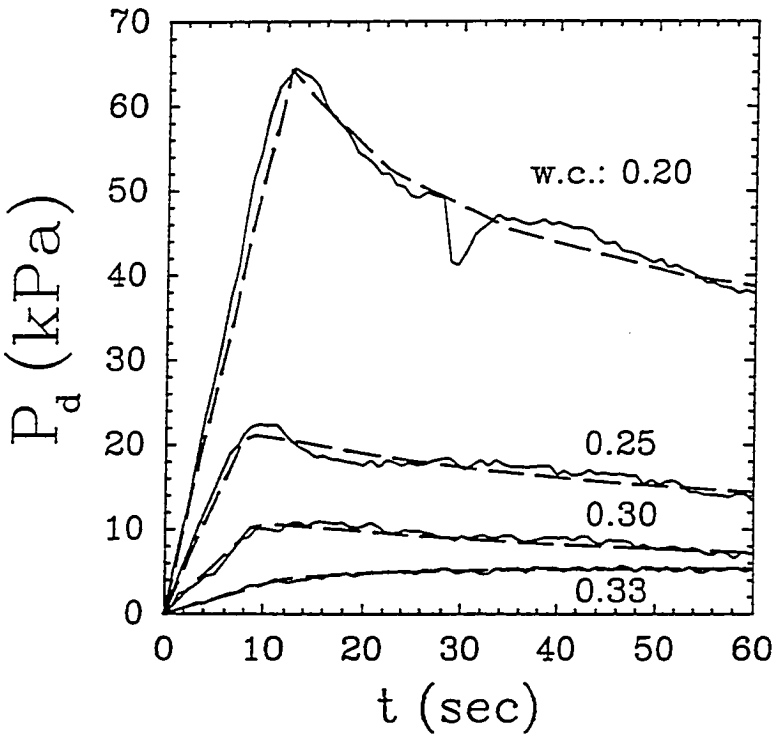

Figure 3.4. Pressure records from the laboratory (solid line) and from theoretical analysis (dashed line). Water contents of the four curves are indicated. Parameters used in the theoretical analysis are given in Table 3.2.

the decrease in pressure during the onset of propagation, and the change in curvature of the record observed as the water content of the samples increases.

Some aspects of the records cannot be predicted. All the laboratory records show short-term pressure fluctuations of 0.5 to several kPa throughout propagation, whereas the theory predicts only long-term changes in pressure. The short-term fluctuations in pressure result from both the laboratory apparatus (the syringe pump is advanced incrementally with a stepper motor), and probably from the creation of fracture lobes or other details of the fracturing process. Those effects are ignored by the analysis. Larger fluctuations in pressure, such as the momentary drop in pressure of the curve for $\theta = 0.20$ at roughly 30 seconds (Fig. 3.4), probably occur when the fracture intersects a cavity or large pore in the sample, and this behavior was omitted during formulation of the analysis.

Other discrepancies between the theoretical and observed pressure records were typically encountered either shortly after the onset of propagation or after a minute or more of propagation. The analysis predicts an early period of stable propagation if $m > 0$. It is unable to predict early stable propagation when m = 0, however, although such an early period commonly occurred (e.g. curve for $\theta = 0.20$ in Fig. 3.5) when laboratory observations indicated that $m = 0$. In general, the analysis underpredicts the duration and magnitude of pressure change as compared with duration and magnitude during the period of stable propagation in the laboratory.

The agreement between laboratory and theory in some records was good during the first several tens of seconds, but then the laboratory data would decrease to values less than predicted theoretically. This behavior could have been caused by venting of the fluid filling the fracture out one of the sides of the sample. For those

experiments where venting was suspected, the parameters were estimated using only the early part of the record.

Parameters

We have information on most parameters used in the analysis that is independent of the values obtained by curve fitting. Elastic modulus, for example, was determined for samples of different water contents using a triaxial loading apparatus (e.g. Chapter One). The modulii determined by parameter estimation are similar to those determined with the triaxial device at water contents greater than 0.22; they indicate that E diminishes from 5 to 10 MPa when θ = 0.23 to 1 MPa or less when θ <0.3 (Table 3.2; Fig. 3.5). Both methods indicate an abrupt increase in E as samples become drier than θ = 0.22, although the values obtained by the two methods are different for the relatively dry soil (Fig. 3.5).

The fluid pressure in the infiltrated tip, p_{tip}, ($p_{tip} = P_{dtip} + \sigma_{min}$) increases from 0 for $\theta < 0.22$, to between 45 and 65 kPa for $\theta > 0.22$ (Table 3.2; Fig. 3.6*a*). That water content marks the boundary between negative and positive pore pressure under conditions of the laboratory experiments. Indeed, values of p_{tip} are similar to values of pore pressure for $\theta > 0.22$. One reason for this is that we did not allow p_{tip} to exceed σ_{max} during the parameter estimation procedure. Nevertheless, the results shown in Figure 3.6*a* indicate that the pressure records can be predicted if p_{tip} is roughly equal to the pore pressure.

Parameter estimation indicates that the tip growth factor, m, is zero when $\theta < 0.22$, increases from 0 to 0.25 over $0.22 < \theta < 0.27$ and decreases from 0.25 when $\theta > 0.27$. Values of m determined from laboratory experiments are similar to those from parameter estimation (Fig 3.6*b*). Unlike the determination of p_{tip}, values of m

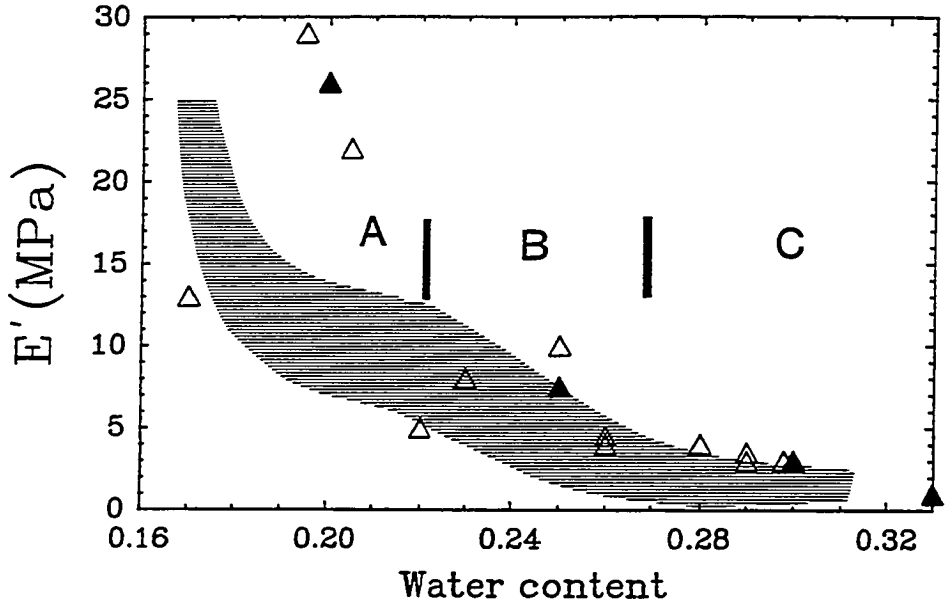

Figure 3.5. Elastic modulus as a function of water content from triaxial loading (shaded) and from parameter estimation techniques (triangles). Filled symbols indicate values used to create curves shown in Figure 3.4.

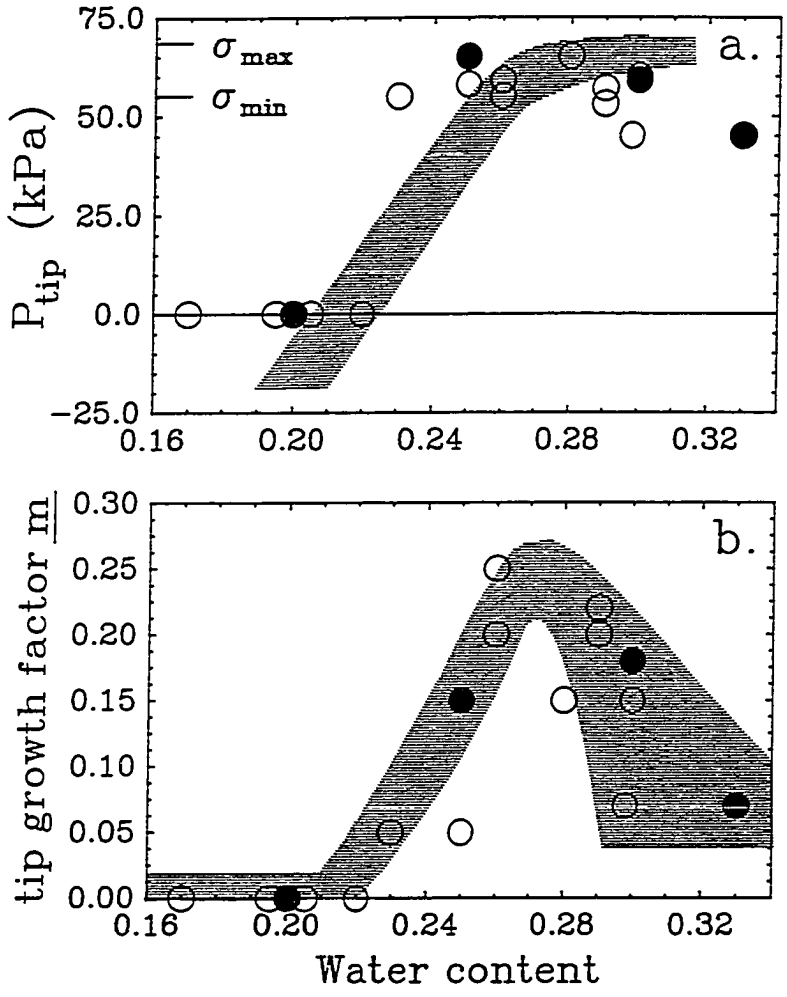

Figure 3.6a. Pressure of pore fluid (shaded) and fluid pressure in the tip of the fracture from parameter estimation as a function of water content. 3.6b.) Values of *m* from laboratory observations (shaded) and from parameter estimation. Filled symbols indicate values used to create curves shown in Figure 3.4.

were allowed to vary to give the best agreement between laboratory data and theory.

Table 3.2. Values of parameters determined by fitting laboratory pressure records with curves generated theoretically.

θ	E	C	p_t	m	K_{Ic}	a_i
	MPa	cm/min$^{1/2}$	kPa		kPa m$^{1/2}$	cm
0.17	13.0	0.020	0	0	19.8	1.22
0.195	29.0	0.025	0	0	17.7	1.22
0.20	26.0	0.020	0	0	12.4	1.22*
0.205	22.0	0.022	0	0	19.6	0.61
0.22	5.0	0.008	0	0	3.8	0.61
0.23	8.0	0.005	55.12	0.05	4.5	1.22
0.25	7.5	0.007	65.12	0.15	4.0	1.22*
0.25	10.0	0.005	58.12	0.05	3.5	1.22
0.26	4.0	0.008	55.12	0.25	2.2	1.22
0.26	4.5	0.005	59.12	0.20	2.2	1.22
0.28	4.0	0.005	65.12	0.15	3.5	1.22
0.29	3.5	0.008	53.12	0.22	1.2	1.22
0.29	3.0	0.007	57.12	0.20	1.8	0.61
0.298	3.0	0.008	45.12	0.07	1.4	0.61
0.30	3.0	0.010	59.12	0.18	2.0	1.22*
0.30	3.0	0.008	60.12	0.15	2.4	0.61
0.33	1.0	0.010	45.12	0.07	0.8	1.22*

* Results shown in Figure 4.

Values of the leakoff coefficient C range from 0.005 to 0.025 cm/min$^{1/2}$ based on the parameter estimation results. I was unable to conduct an independent assessment of C; for example, using laboratory methods developed by petroleum engineers and reviewed in Gidley and others (1989). In general, C depends on

permeability of the medium enveloping the fracture, the rheology of the injected fluid, and the pressure difference between the injected fluid and pore fluid. Values of C determined by petroleum engineers for reservoir conditions span a wide range, and the values measured for this work are near the lower limit of that range.

It is noteworthy that values of C determined from the theoretical analysis decrease by a factor of three to four as θ increases from 0.22 to 0.23. This decrease in C occurs in the range of θ where pore pressure changes from negative to positive. Most of the other parameters affecting hydraulic fracturing also show marked changes in value as water contents vary in that range.

DISCUSSION

Investigators who model hydraulic fracture propagation have long recognized the importance of processes at the fracture tip. Khristianovich and Zheltov (1955), who published the first analysis of hydraulic fracture propagation, postulated that the injected fluid would be unable to reach the fracture tip. They argued that an unwetted zone at the tip of the fracture was required to maintain mechanical equilibrium because a stress singularity at the tip would result if pressurized fluid filled the entire fracture. This reasoning was later used by Geerstma and DeKlerk (1969), Daneshy (1973), Abe and others (1976), and Rogiers and others (1982), who typically assume zero driving pressure within the tip zone and ignore interactions with pore fluid.

The reasoning used here is slightly different. We assume that the stress singularity is dissipated by plastic deformation within a small region at the fracture tip and that the strength of the singularity during propagation is characterized through K_{Ic}. Equilibrium propagation is satisfied by requiring $K = K_{Ic}$ during propagation, and we place no additional requirements on the distribution of loads

on the fracture. This reasoning has the intuitive appeal of separating processes of the flow of fluid in the vicinity of the fracture tip from the requirements for mechanical equilibrium.

Cleary (1978, 1979) recognized that pore fluid could flow toward the fracture near its tip while at the same time flowing away from the major portion of the fracture due to leakoff of the injected fluid. He anticipated that the fluid pressure in the fracture tip would equilibrate with the pore fluid pressure under conditions of slow propagation. The results of this study support Cleary's conclusions by showing that the pressure records from the laboratory experiments can be produced theoretically by a fracture whose tip is filled with a fluid at a pressure roughly equivalent to the pore pressure. Moreover, the laboratory observations indicate that pore water actually fills the tip of the fracture if the pressure of the pore water is positive.

There are several implications that this work has on field applications of hydraulic fracturing to increase the yields of wells. The analyses indicate that the infiltration of pore fluid into the fracture tip can markedly affect the pressure record. Similarly, fracture length and width as functions of time are affected by infiltration at the tip (e.g. through eq. 3.3*c* and 3.9*b*), although results of those calculations are not presented here. Field applications commonly rely on models both to estimate fracture geometries from pressure records, and to estimate fracture width and length for a particular injection scenario. Those models range from simple analytical expressions that provide rough estimates of fracturing results, to sophisticated numerical codes that are capable of estimating effects of a wide range of processes. Models that allow the infiltration of pore water into the fracture tip will more accurately represent the physics of hydraulic fracturing than models that assume pore fluid cannot enter the fracture. Cleary (1978, 1979) formulates a

sophisticated analysis that accounts for the flow of pore water toward the tip of a fracture. An implementation of Cleary's solution was inaccessible during this study.

We have shown how tip infiltration can be represented in an analytical model, without actually including flow processes. The representation is based on an empirical characterization of b/a, through eq. (3.5), and a tip growth factor, m. An application of the approach of this chapter to field conditions would require some empirical function, akin to eq. (3.5), to represent b/a under field conditions. One method of obtaining such a function is to adapt the parameter estimation approach described above. Whereas the method of obtaining eq. (3.5) for field conditions has yet to be evaluated, it seems reasonable to expect that the pressure in the tip will be equal to the pore pressure when the fracture cuts through saturated material.

CONCLUSIONS

Pressure records from hydraulic fracturing experiments in silty clay can be predicted using a simple analytical model based on LEFM. A key to the model is the assumption that one fluid is injected along the axis of the fracture and another fluid infiltrates into the fracture tip. This assumption is based on observations made in the laboratory. Growth of the infiltrated zone at the fracture tip during the onset of propagation causes an early period of stable propagation according to the model. Early stable propagation was commonly observed during the experiments.

Water content of soil is a fundamental control of hydraulic fracturing in silty clay. The analytical model is able to accommodate the effect of water content by including five parameters E, C, P_{tip}, m, K_{Ic}, the values of which depend on θ. Values of those parameters at various water contents were estimated by analyzing pressure records from fracturing experiments conducted on samples of various water contents. Those estimates are similar to values measured independently in the

laboratory. The pressure in the tip of the fracture is one parameter that could not be measured independently in the laboratory. However, tip pressures determined from the analysis are similar to pressures of pore fluid in the soil. This suggests that water entering the tip of the fracture is roughly in equilibrium with pore fluid.

The water content marking the boundary between positive and negative pore pressure marks a significant difference in the results of hydraulic fracturing. The change in pore pressure is reflected in major changes in values E, C, P_{tip}, m, K_{Ic}, and it results in correspondingly major changes in the form of the pressure record predicted by the analysis. This result could be significant when applying the results of this work, which is based only on tests using the Center Hill clay, to hydraulic fracturing in other soil materials.

CHAPTER FOUR

A FIELD TEST OF HYDRAULIC FRACTURING OF SOIL

Hydraulic fractures of remarkable size were created at shallow depths during field tests at a site underlain by Pleistocene glacial drift, an unlithified material composed of clay, silt, sand and gravel. The fractures were as much as 10 or more meters in maximum dimension and were created from boreholes roughly 2 m deep. Sand was injected into some of the fractures, resulting in layers that were much more permeable than the enveloping drift. These tests are, to my knowledge, the first demonstration that hydraulic fractures with potential environmental engineering applications can be created at shallow depth in soil.

The field test was conducted at a site 10 km north of downtown Cincinnati, on the western side of the valley of Mill Creek, a southerly-flowing tributary of the Ohio River. The site is on the southeastern side of property owned by the ELDA Company and used as a municipal landfill.

Investigation and preparation of the test site took place during several months in spring, 1988. The actual test, however, only required 12 hours and was completed on 15 June 1988. Ten hydraulic fractures were created during the test. Field evaluation of the results of the test took place during the six weeks following the test.

These two observations, 1.) an abrupt decrease in the pressure of the injection fluid, and 2.) venting of the fluid several m from the point of injection were strong evidence that hydraulic fracturing of soil occurred during the field test. There was little information at the time of the test, however, about fracture geometry, that is the size, shape, orientation, location, and thickness of the fractures.

Those parameters largely control how the fracture will affect the recovery of groundwater, and are a primary focus of this research. As a result, the vicinity of each fracture was excavated and the resulting exposures mapped in detail to provide us with an exceptionally detailed image of the fracture form.

SETTING OF THE TEST

The vicinity of the test site is gently sloping ground bounded on the northwest by a vertical face and on the southwest by moderate slopes into an excavated trough (Fig. 4.1). The southern side of the trough is bounded by a north-facing vertical cut, the eastern end of which is shown on the southwestern corner of Figure 4.1. The ground surface at the time of the test had been excavated during operations at the landfill to several meters below the natural ground surface.

The site itself is an elongate strip trending N20E and roughly 80 m long. The northern end of the site is on a gentle, south-facing slope, whereas the southern end of the site is on level ground (Fig. 4.1). The slope of the ground surface is important because it apparently affected forms of the fractures.

Eleven boreholes were hydraulically fractured during the field test. Most borings are approximately 10 m from their neighbors (Fig. 4.1), except at the southern end of the site where a cluster of four borings are each 2.5 m from their nearest neighbor.

Depths to the bottom of casing ranged between 1.64 m and 1.95 m at 9 of 11 boreholes. The other two boreholes were deeper; 2.72 m and 3.81 m.

Geology

Glacial drift, probably of Illinoian age, underlies the test site. Three stratigraphic units were identified in the drift based on exposures of cliff faces near

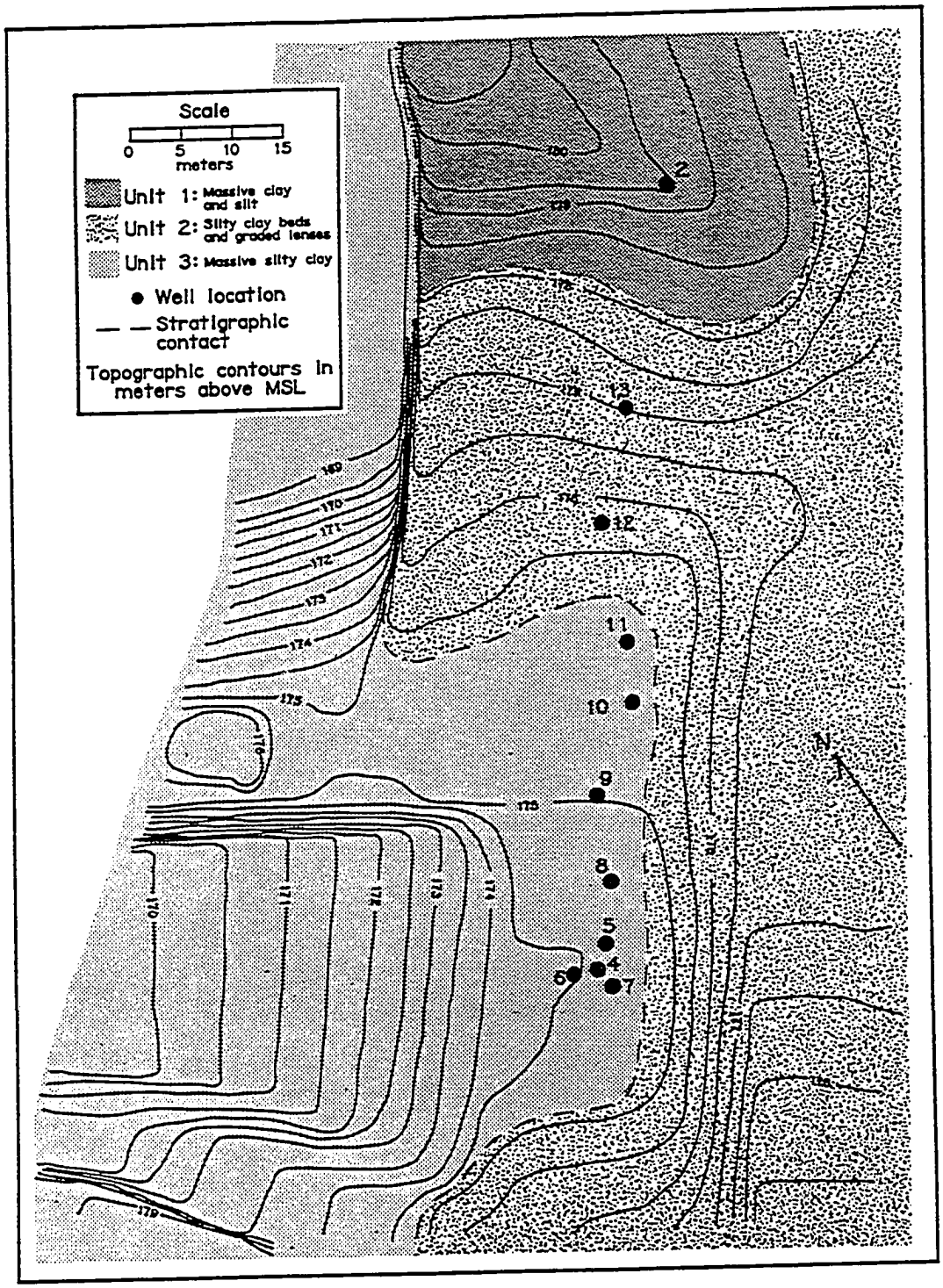

Figure 4.1. Geology, topography and locations of boreholes at the ELDA site.

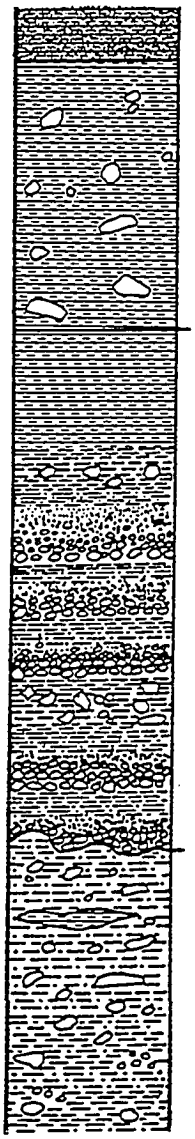

Weathered till topsoil, 0 to 0.3 m thick.

UNIT 1

Light brown to grey, massive clay and silt containing 5 to 15 percent disseminated gravel, cobbles and rock fragments. Roots common. One half to 2 m thick.

Sharp, planar contact.

UNIT 2

Light brownish-grey, massive silt. One m thick, thins south of site.

Upwardly-grading beds and lenses of gravel, sand silt and clay that range from 0.1 to 0.4 m thick; and massive to laminated beds of grey silty-clay 0.2 to 1.0 m thick. Irregular, contorted bed-forms common. Total thickness 4 to 7 m.

Irregular contact.

UNIT 3

Light grey, massive, silty-clay containing 5 to 20 percent disseminated gravel, cobbles and rock fragments. Irregular lenses of silt, or yellow-brown sand present locally. Lower contact not exposed, at least 8 m thick.

Figure 4.2. Stratigraphic column of the units in the vicinity of the test site.

the site, on boring logs, and on exposures in trenches cut in the test site (Fig. 4.2). The upper unit is 0.5 to 2 meters thick and consists of massive light brown-grey clay and silt containing coarse gravel, cobbles, fragments of limestone and organic matter disseminated throughout. The middle unit is 3 to 7 m of dominantly flat-lying beds that fine upward from coarse gravel to clay. A typical bed consists of orange-brown cobbles and gravel at the base that grades upward to orange-brown coarse and fine sand, to light brown silt, and to light brown clay at the top. The graded beds range in thickness from 0.1 to 0.4 m, and in most exposures they are several m to several tens of m in lateral extent. Locally, the beds are irregular and highly contorted with large changes in thickness occurring over several m. (An example of the irregular bed forms is shown in Fig. 4.9) Massive beds of grey clay and silt are locally intercalated with graded beds.

The upper surface of a light brown, massive silt bed, several dm to one m in thickness, marks the contact between units 1 and 2. The contact is planar and nearly flat-lying, differing in elevation by roughly 1 dm over the study area.

The lower unit consists of massive, grey silty-clay containing 5 to 20 percent disseminated rock fragments. It contains pods and beds of light grey silt, or brown sandy-gravel. The lower contact is unexposed, so the thickness of unit 3 is unknown. The upper surface of the massive grey clay marks the contact between Units 2 and 3 (Fig. 4.2). The contact varies in elevation by several meters in the vicinity of the site.

Hydraulic fractures were created in units 2 and 3. Fractures at boreholes 2 and 13 were in unit 2, the one at borehole 12 propagated upward from unit 3 into unit 2, and the others were contained within unit 3.

Eleven of the 14 boreholes drilled during exploration of the site were dry when the hydraulic fractures were created. In those boreholes that did contain

water, the depths were less than 20 cm at the time of fracturing. Some other boreholes contained water several days prior to fracturing, but the day before fracturing they contained soft mud, but no standing water.

The silty clay that comprises most of the subsurface was unsaturated during testing (ratio of volume of water to volume of pores of 0.29). Water that was observed in boreholes apparently drained from perched zones within sand and gravel lenses in the till.

Effects of hydrologic conditions on the results of hydraulic fractures were undetectable. A regional water table is present several tens or more meters below the level of the boreholes and is insignificant to the test.

We adapted methods of estimating lateral confining stress in rock to estimate lateral confining stress in the silty clay of unit 3 at the ELDA site (details in Murdoch and others, 1990). The methods used at the ELDA site have since been refined, however, we consider them to be rough estimates of the in-situ stress. They indicated that the lateral stress is several times to as much as an order of magnitude more than the vertical stress at a depth of 1.2 m. That relative magnitude of the vertical and lateral stresses was expected to favor the creation of sub-horizontal hydraulic fractures.

Physical Characteristics of the Soil

Laboratory tests were conducted on samples obtained from four Shelby tubes pushed into exposures of silty clay from unit 3 at the test site. Standard laboratory measurements described in the ASTM Handbook on Soil Testing were used to obtain the basic characteristics. A Guelph permeameter, a device designed to measure flow rate while holding a constant head in a borehole, was used to

determine in-situ saturated hydraulic conductivity, K_s, using methods described by Elrick and others (1988). Details of the measurements of K_s are described in Murdoch and others (1990).

In general, the saturated hydraulic conductivity of silty clay is between 1.5 x 10^{-8} m/sec and 1.9 x 10^{-9} m/sec, whereas those measured in silty sands and gravels of unit 2 are an order of magnitude or more greater; between 1.0 x 10^{-7} m/sec and 3.5 x 10^{-7} m/sec. Measurements of K_s were made at five locations, and the values are in Table 4.1.

Table 4.1. Saturated in-situ hydraulic conductivities of glacial drift at the ELDA Site

Location	Depth (m)	Material	K_s (m/sec)
1	0.40	silty clay	7.5 x 10^{-9} to 1.5 x 10^{-8}
2	0.45	silty clay	1.0 x 10^{-8} to 1.4 x 10^{-8}
3	1.50	silty clay	1.9 x 10^{-9} to 8.9 x 10^{-9}
4	0.30	silty sand and gravel	1.0 x 10^{-7} to 2.4 x 10^{-7}
5	0.42	silty sand and gravel	3.0 x 10^{-7} to 3.5 x 10^{-7}

The characteristics of the ELDA till are similar to those of other tills in the vicinity of Cincinnati. It is a *hard* soil, requiring more than 30 blows during a standard penetration test (Navfac, 1982), and it is relatively dense (bulk unit weight of 22.24 kN/m^3 or 141.6 lb/ft^3) compared with colluvial soil or alluvium.

The till is well-graded from particles of clay size to sand size or larger. Cobble- to boulder-sized rock fragments are common in field exposures, although

they were absent from the sample used for the grain size analysis (Table 4.1; Fig. 4.3).

Table: 4.2 Physical characteristics of silty-clay till (unit 3).

	ET1	ET2	ET3	ET4	AVE
Atterburg Limits					
Liquid	22.6	22.9	24.8	25.0	23.8
Plastic	12.5	10.5	11.4	15.7	12.5
Shrinkage	19.8	15.5	15.3		16.8
P. I.	10.1	12.4	13.4	9.3	11.3
Grain sizes (by wt.)					
Gravel	0.13	0.18	0.10	0.11	
Sand	0.29	0.28	0.34	0.33	
Silt	0.36	0.31	0.34	0.37	
Clay	0.22	0.23	0.22	0.19	
Void Ratio:	0.34				
Porosity:	0.25				
Moisture:	11.6	13.5			
Degree of Saturation:	0.29				
Bulk Unit Weight:	22.24 kN/m^3 (141.6 lb/ft^3)				
Bulk S.G.:		2.2			
Dry Unit Weight:		19.92 kN/m^3 (126.8 lb/ft^3)			
Specific gravity, solids:	2.68				

Results from tests of the Atterburg Limits (Table 4.2) plot above the *A* line and indicate that the till is a CL type soil, in the nomenclature of the Unified Soil Classification System (ASTM D2487).

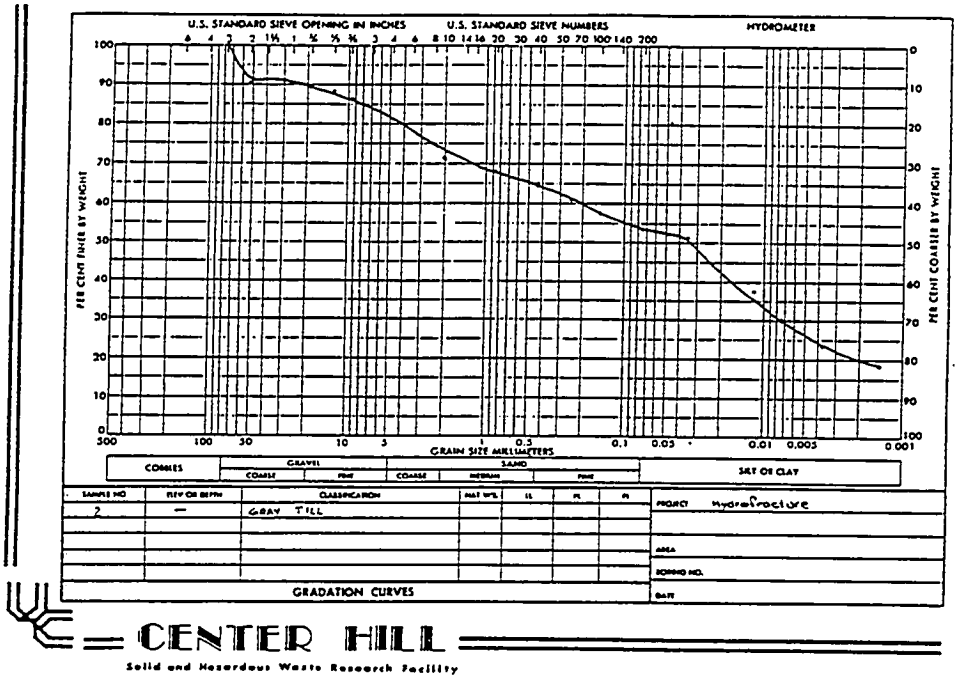

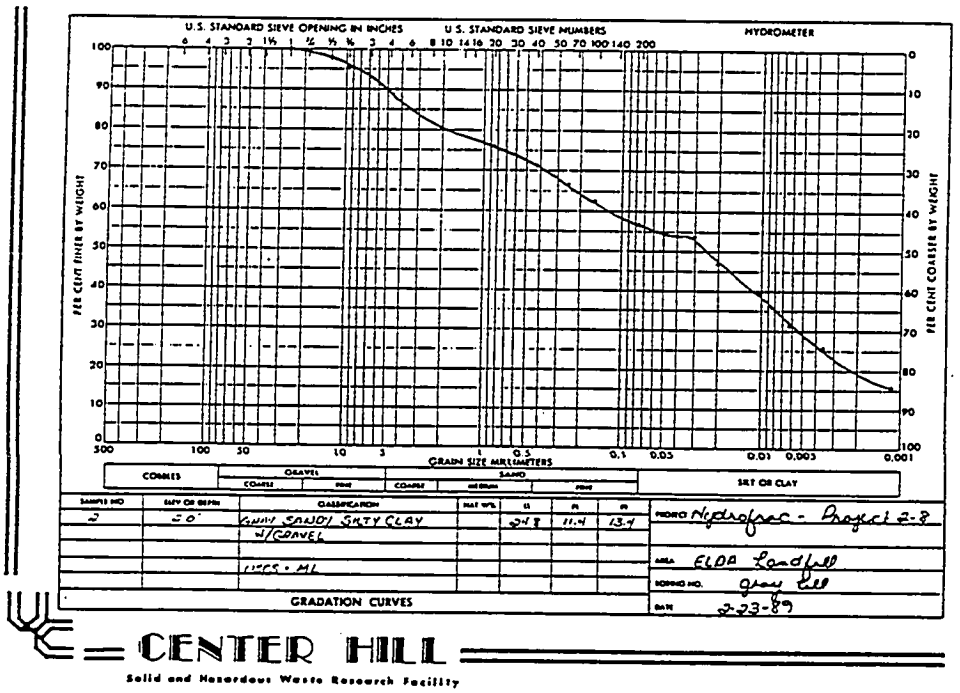

Figure 4.3. Distribution of grain sizes in samples from unit 3.

EQUIPMENT AND METHODS

There were three key components of the hydraulic fracturing process: 1.) a fluid to suspend proppant grains during injection; 2.) an above-ground system to mix and inject slurry; and 3.) a below-ground system to isolate the zone where the fracture was to be created. The fluid and above-ground equipment used during this test were obtained from and operated by Halliburton Services, a contractor who specializes in hydraulic fracturing of oil wells. The design of the below-ground system, the borehole, however, was developed for the project.

Borehole Design

The borehole design consists of a steel tube cemented into a boring, and open at both ends (Fig. 4.4). A *basket* is fixed to the lower end of the casing to prevent cement from plugging the bottom of the borehole. The open boring extends several dm below the basket and is partly filled with fragments (cuttings) of till. A narrow *notch*, oriented normal to the axis of the borehole, is cut in the wall of the boring several cm below the bottom of the casing. The inside diameter of a boring was 7.6 cm (3 in) and the notch extended 3.75 cm (1.5 in) into the wall of the bore. Specifications and other details of the boreholes are in Murdoch and others (1990).

The notches were intended to nucleate horizontal fractures at a predetermined location along the borehole. Although roughly horizontal hydraulic fractures were created, most of the fractures initiated at or above the basket, not at the notch.

Above-Ground Equipment

The above-ground fracturing equipment was mounted on five vehicles: a truck containing a blender and a positive displacement pump, two trucks containing

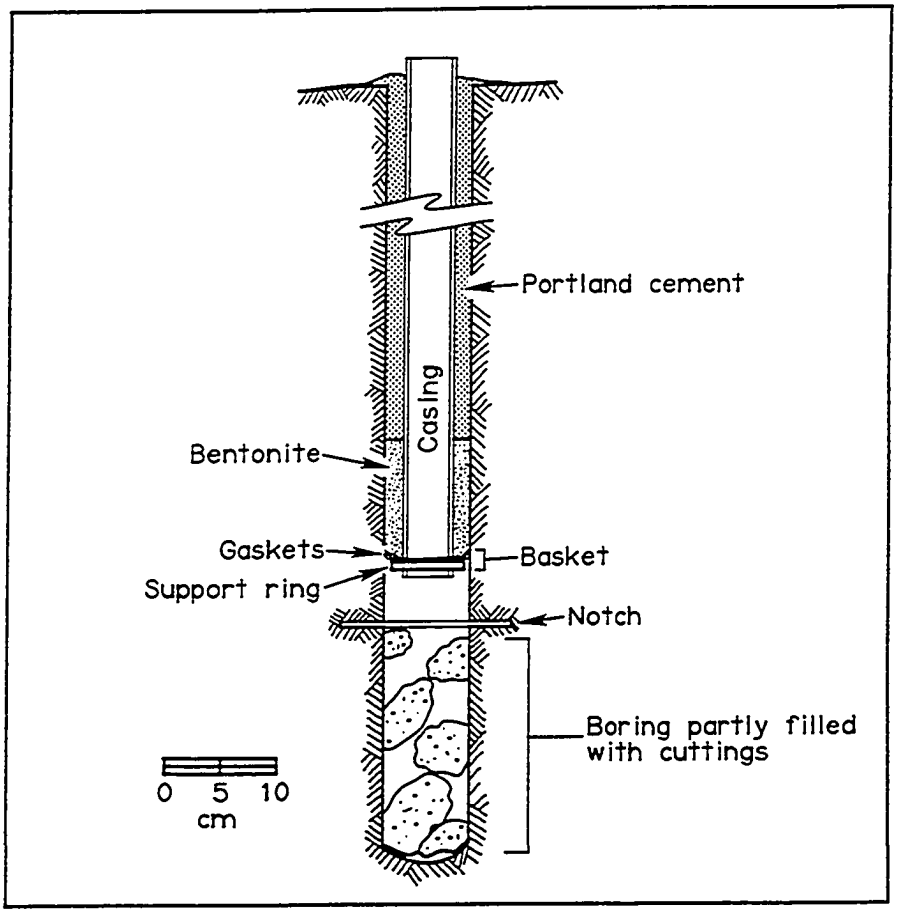

Figure 4.4. A borehole used to create hydraulic fractures.

sand, a truck containing water, and a van containing monitoring and control equipment.

Three pumps were used in the operation: a Triplex positive displacement pump, and two centrifugal pumps, one upstream and one downstream from the blender. The positive displacement pump can generate a maximum of 41,000 kPa (6000 psi), whereas the centrifugal pumps can produce a maximum of between 400 and 550 kPa (60 and 80 psi) and flow rates of 2.4 to 2.8 m^3/min (630 to 750 gpm).

The Injection Fluid

The injection fluid is a slurry of Ottawa sand and crosslinked, guar gum-based gel. The gel is a stiff fluid (apparent viscosity of 100 to 200 cp; apparent shear strength of roughly 25 Pa) designed to suspend sand grains during injection into the fracture. An enzyme is blended with the gel to break it down several hours after injection. The breaking enzyme improves removal of gel, greatly increasing the permeability of the sand-filled fracture. Chemicals used to create the gel were developed by Halliburton Services. Potassium chloride was added (three percent by weight) to increase the electrical conductivity of the injection fluid, thereby improving the resolution of fractures by electrical geophysical techniques (Murdoch and others, 1990; and Wang and others, 1990). Dye was added to the fluid to stain the fracture surfaces and make them easier to identify during excavation. Three types of dye were tested during the experiment: rhodamine, fluorecene, and fluorescent orange paint pigment. Dye was mixed at a concentration of 1:500 in the first few fractures but it was more dilute (1:1000 to 1:2000) in the last few fractures.

Ottawa sand was mixed with the fracturing fluid to prop open the fractures. Two different sizes of sand, very coarse-grained, 12/20 mesh, and medium-grained,

20/40 mesh, were used. Concentrations of sand ranged from 0.09 to 0.18 by volume (2 to 4 lbs. sand/gal. fluid).

The Fracturing Procedure

The fracturing procedure began by filling the casing with water, so the initial fracture would be created with water rather than gel. Pipes were connected from the borehole to the trucks containing the fracturing equipment, which were parked on the northeastern edge of the site (Fig. 4.1).

Injection using a centrifugal pump caused pressures measured at the borehole to increase to between 400 and 550 kPa (60 and 80 psi). In some cases, a fracture was created soon after the pressure reached 60 to 80 psi, but in other cases 5 to 10 minutes were required before a fracture was created. Injection pressure was increased using the positive displacement pump if a fracture was not created after approximately 10 minutes. Injection pressures of as great as 820 kPa (120 psi) were required to initiate fracturing at some boreholes (Table. 4.3).

The onset of fracturing was determined by an abrupt decrease in the injection pressure and increase in the injection rate. During propagation, injection pressures decreased to between 69 and 275 kPa (Table 4.3). Records of the pressures and volumes as functions of time are in Murdoch and others (1990).

Injection was terminated at the shallow boreholes when fluid vented to the ground surface, and at the deeper boreholes injection was terminated after a predetermined volume of injection. Each fracture was created in less then ten minutes. The pipes extending from the pump truck to the borehole were uncoupled at the borehole immediately after termination of injection. Roughly 0.1 m^3 (several

tens of gallons) of injection fluid flowed back out of the fracture into the borehole and onto the ground following uncoupling.

Flow rates of between 0.075 and 0.42 m^3/min (20 and 90 gal/min) were used to create the fractures (Table 4.3). In general, the flow rate was low during peak pressure and increased as the pressure decreased and the fracture began to grow.

Table: 4.3. Summary of Data From Field Tests

Id	FLUID			SAND		PRESSURE		
	Volume		Dye	Volume	Gr.Size	Max.		Propagation
	m^3	(gal)		m^3		kPa	(psi)	kPa
13	1.51	(400)	rh	0.28-0.42	20/40	620	(90)	140-340
11	0.11	(30)	rh	0.057	20/40	340	(50)	140
12	0.45	(120)	rh	0.08-0.14	20/40	410	(60)	140
2	0.46	(110)	rh	0.85	12/20	410	(60)	140-280
10	0.57	(150)	rh	0.22-0.24	12/20	410	(60)	340
4	0.57	(150)	fo+fl	0.17-0.22	12/20	760	(110)	480
9	0.76	(200)	fo+fl	0.08-0.14	20/40	820	(120)	200-275
5	0.76	(20)	fo	0.03-0.08	20/40	410	(60)	410
8	0	(0)	fo	0	20/40	3700	(540)	--
7	0.38	(10)	fo	0.03-0.08	20/40	550	(80)	550
6	0.57	(150)	fo+fl	0.14	20/40	550	(80)	200

rh: rhodamine red
fo: fluorescent orange pigment
fl: fluorecene

Shown in the order in which the fractures were created.

Details of the history of flow rates, however, are poorly known because the flow meter used by Halliburton Services was often clogged with sand and non-functional.

Clogging apparently occurred because the flow rates that were used were less than those designed to be measured by the meter.

The total volumes of fluid and sand pumped out of the blender were estimated by the operator of the pump truck. Typically the fractures required 0.38 to 0.76 m^3 (100 to 200 gals) of fluid, but the volume ranged from as little as 0.076 m^3 to as much as 1.51 m^3 (Table 4.3).

The volume of sand pumped to the fractures was typically 0.056 to 0.14 m^3 (2 to 5 ft^3), but it ranged from less than 0.03 to as much as 0.85 m^3 (30 ft^3). These estimates are greater than the volume contained in fractures because they do not account for material that remained in the pipes after fracturing, or that flowed out during venting.

Hydraulic fracturing was attempted at eleven boreholes and fractures were successfully created at ten of those boreholes. Hydraulic fracturing did not occur at borehole 8. Two attempts were made to fracture borehole 8; during the first injection pressures reached 1720 kPa (250 psi), and during the second injection pressures reached a maximum of 3700 kPa (540 psi). Following both attempts, plugs of sand were discovered several dm from the bottom of the casing that presumably blocked the injection fluid. The cause of the sand blockage is unclear. One explanation is that the gel in the injection fluid broke down and was unable to adequately transport sand. The rheology of the gel is sensitive to heat and could have been affected by the ambient temperature (which was 38 °C (100 °F) on the day of the test), according to Mark Roberts, field engineer with Halliburton Services.

RESULTS

The day after the fractures were created, the locations of the vents were mapped and the vicinity of each borehole prepared for excavation. The strategy used during excavation was to first cut a trench from the vent to the parent borehole. The fracture was identified at the vent and traced along the trench during excavation. The trench was extended beyond the borehole until the fracture could no longer be identified in the trench walls. Then another trench was cut perpendicular to the first one. Subsequent trenches were placed to intercept the fracture at critical locations based on existing exposures.

Traces of fractures on the walls of the trenches were identified and marked with brightly-colored flagging. Many of the fractures lacked sand and could be identified only after detailed excavation revealed traces of dye staining.

Form of an Idealized Fracture

Forms of hydraulic fractures created during the field test differ in detail, but there are certain characteristics that are common to nearly all the fractures. The common traits were used to infer an idealized form that characterizes the fractures created beneath level ground.

The form of the idealized fracture consists of four zones, which are arranged in increasing distance from the parent borehole (Fig. 4.5):

Zone One: a sub-vertical orientation adjacent to the borehole.

Zone Two: a flat-lying orientation in the vicinity of the borehole (within several m). This Zone is absent in some cases.

Zone Three: a planar to trough-like fracture dipping gently toward the borehole. This zone composes most of each hydraulic fracture.

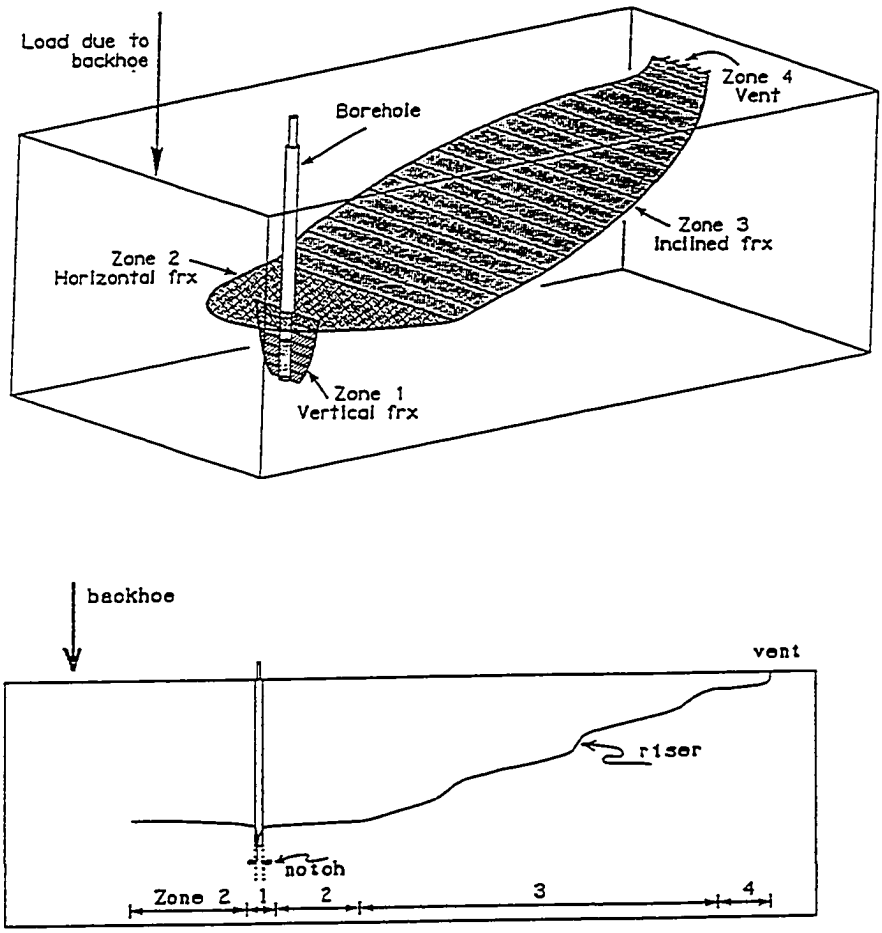

Figure 4.5. Idealized hydraulic fracture created at the ELDA test site. Inferred from exposures of fractures created beneath level ground. *a.*) Oblique view. *b.*) Section along major axis.

Zone Four: a steeply dipping orientation occurring within several dm of the ground surface.

Details of Fracture Form

One or more vertical fractures containing the axis of the borehole and initiating along the open interval below the casing characterize Zone One of the idealized hydraulic fracture. Vertical fractures were observed at all boreholes except HF12 (designation for hydraulic fracture at borehole 12), where the bottom of the borehole was poorly exposed during initial excavation and the trench was flooded before we could complete excavation.

Several examples of fractures in Zone One are shown in Figure 4.6. Vertical fractures that extend from the borehole notch a few dm upward to the contact between open hole and bentonite are shown in Figures 4.6 *a* and *b*. In those cases, the orientation of the fracture changes abruptly, or *rolls over*, from vertical to gently-dipping as the fracture climbs above the open hole. The change in orientation occurs with a radius of curvature of a few cm in both cases. The vicinities of borehole 5 and 11 were similar to those shown in Figure 4.6 *a* and *b*.

The other examples show vertical fractures that climb above the bentonite and roll over adjacent to the grouted portion of the borehole. A single vertical fracture occurring at borehole 10 (Fig. 4.6c), for example, rolls over to one gently dipping fracture roughly 0.6 m and another roughly 0.8 m above the notch. The lower part of the vertical fracture at borehole 10 was poorly exposed; presumably it extended downward at least to the open interval of the borehole.

In another case (Fig. 4.6 *d*), a vertical fracture at borehole 7 extends along the entire open interval of the borehole, even below the notch. The fracture climbed above the open interval and rolls over relatively gradually. The radius of

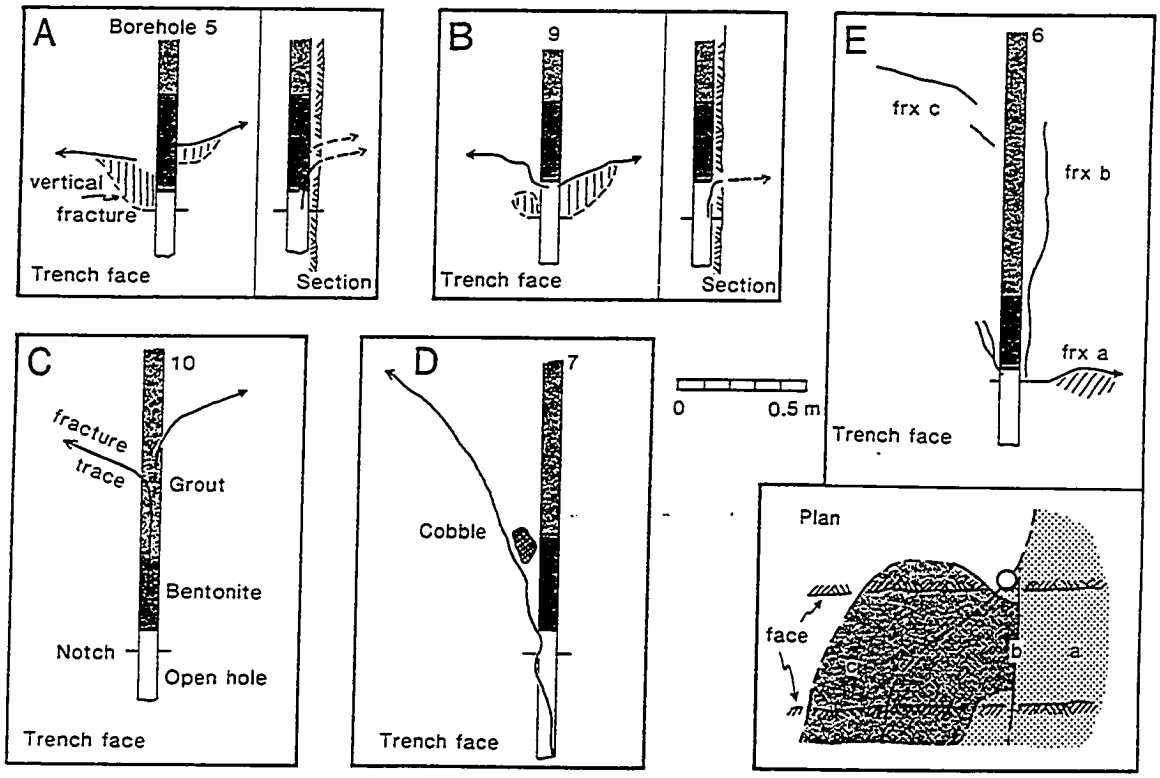

Figure 4.6. Hydraulic fractures in the vicinities of boreholes (Zone 1). Scale is the same for all. Fracture traces exposed on trench walls shown as solid lines, dashed where located approximately. Arrows indicate the traces extends further in that direction.

curvature of the fracture surface is more than a meter where it rolls over, much greater than at any of the other fractures. A vertical fracture cut the entire open interval of borehole 2, and thus resembles Figure 4.6 *d*. Poor exposures limited the mapping of fracture 2 to the vicinity of the borehole and no roll over was discovered.

There are two major fractures created at borehole 6; a lower one that begins at the notch and is designated *frx a* in Figure 4.6 *e*, and an upper one that begins at a vertical fracture and is designated *frx c*. The lower fracture is the only one created during the tests that nucleated at a notch cut in the borehole. That fracture twisted and was dipping 20° a few dm from the borehole. The twisting was local, however, because the fracture flattened within a few more dm (it was flat-lying in exposures on neighboring trench walls).

A vertical fracture climbed from the notch at borehole 6 upward roughly 1 m, where its trace on the trench wall terminated. That fracture was also exposed on an adjacent trench wall, so its strike length was at least 0.5 m. It was roughly tangential to the grouted hole, cutting host till without actually cutting the grout. Traces of the upper, gently dipping fracture (*frx c* Fig. 4.6e) are separated from the vertical fracture by unbroken ground, even though the vertical fracture appears to have fed the upper fracture. In this case, the vertical fracture appears to have broken into several segments as it rolled over.

Two vertical fractures whose strikes differed by 125° were identified at borehole 13. The two fractures extended up to the bentonite where they rolled over, so they resembled fractures shown in Figure 4.6 *a* and *b*.

I have presented several examples of Zone 1 because the details of that area reflect the mechanism of nucleation of the hydraulic fractures. It is clear from those

examples that the notch was insufficient to nucleate a hydraulic fracture in all but one case (HF6). Instead of using the notch, the hydraulic fractures nucleated in the wall of the open hole and the plane of the incipient fracture contained the axis of the borehole. This occurred despite a rather strong tendency for the fractures to be sub-horizontal once they grew away from the open hole.

The major portion of the idealized hydraulic fracture is composed of Zones Two and Three. The gross form of the fractures is slightly elongate in plan with aspect ratios of 1.5:1 to 2:1 (Fig. 4.7). The fractures are markedly asymmetric with respect to their parent boreholes. Typically, the radial dimension from the borehole is 5 to 10 times more in one direction than it is in the opposite direction, and in some cases, the boreholes occur at an extreme end of a fracture (e.g. Fig. 4.8*a*). In every case, the greatest radial length of a fracture (as measured from the borehole) occurred between the borehole and the vent.

The distinction between the flat-lying fracture of Zone Two and the gently dipping fracture of Zone Three is apparent in the cross-sections of Figure 4.7. HF9, for example, is flat-lying on the southeastern and southwestern sides of the borehole (the left side of the cross-section in Fig. 4.7a). To the north, however, HF9 climbs gently toward the ground surface at a dip of 20°.

Hydraulic fractures within a few meters of boreholes 6 and 12 are roughly flat-lying, and this is the form represented as Zone Two in the idealized case. HF12 steepens gradually, whereas at HF6, the fracture steepens abruptly in the transition from Zone Two to Zone Three.

The fracture in Zone Three is generally planar to slightly trough-like and dips toward the borehole at roughly 20° (dips range between 12° and 25°). In the

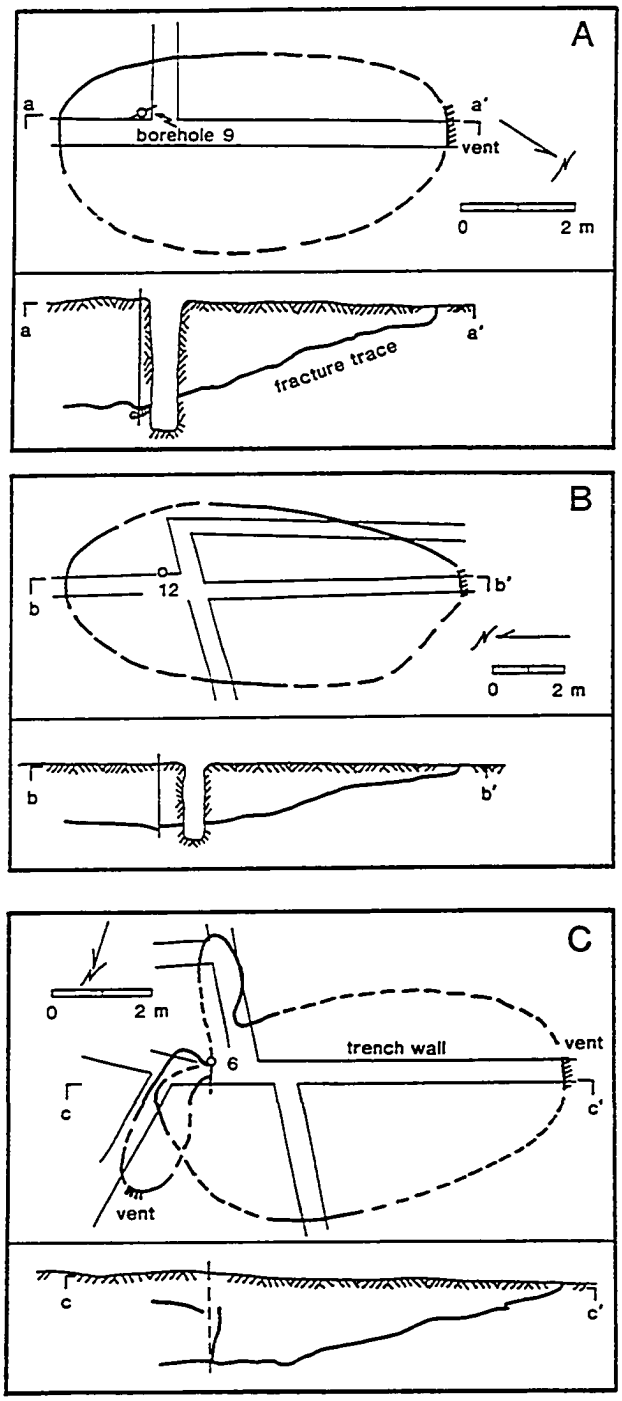

Figure 4.7. Field exposures of hydraulic fractures. Leading edge of fracture dashed where located approximately. Straight, narrow lines are trench walls.

field, this Zone is commonly composed of several distinct lobes, which taken together result in the idealized form.

Traces of the fracture in Zone Three are remarkably straight over the length of the zone. In detail, however, the traces are slightly stepped, consisting of straight segments of approximately one meter connected by risers of roughly 0.1 m. The form is evident in the section of Figure 4.7a, and in the detailed descriptions given in Murdoch and others (1990)

In Zone Four the hydraulic fractures approach the ground surface and vent. In cross-section most of the hydraulic fractures flatten slightly a few dm below the ground surface then curve upward abruptly and become subvertical (e.g. Fig. 4.7a). They vent as nearly vertical fractures roughly 0.5 to 1.5 m long. The strike of the vertical fracture at the vent is perpendicular to the major axis of the hydraulic fracture, and is commonly parallel to the vertical fracture adjacent to the borehole.

Variations

There are several notable features of hydraulic fractures that differ from the idealized form in Figure 4.5. Hydraulic fractures created from boreholes 9 and 10 (Fig. 4.8a), for example, are inclined adjacent to the borehole; there is no evidence of the flat-lying Zone Two. There are two hydraulic fractures adjacent to borehole 10, one on the southwestern, the other on the northeastern side of the borehole. Both fractures are roughly planar and gently dipping; one dips 22° and the other 25° toward the borehole. The fracture created from borehole 9 is also inclined adjacent to the borehole. It propagated to the southwest and cut across the northeastern lobe of HF10. In other cases, such as HF7 (described in Murdoch and others, 1990), Zone Two is also absent. All of those cases resemble the idealized fracture if we

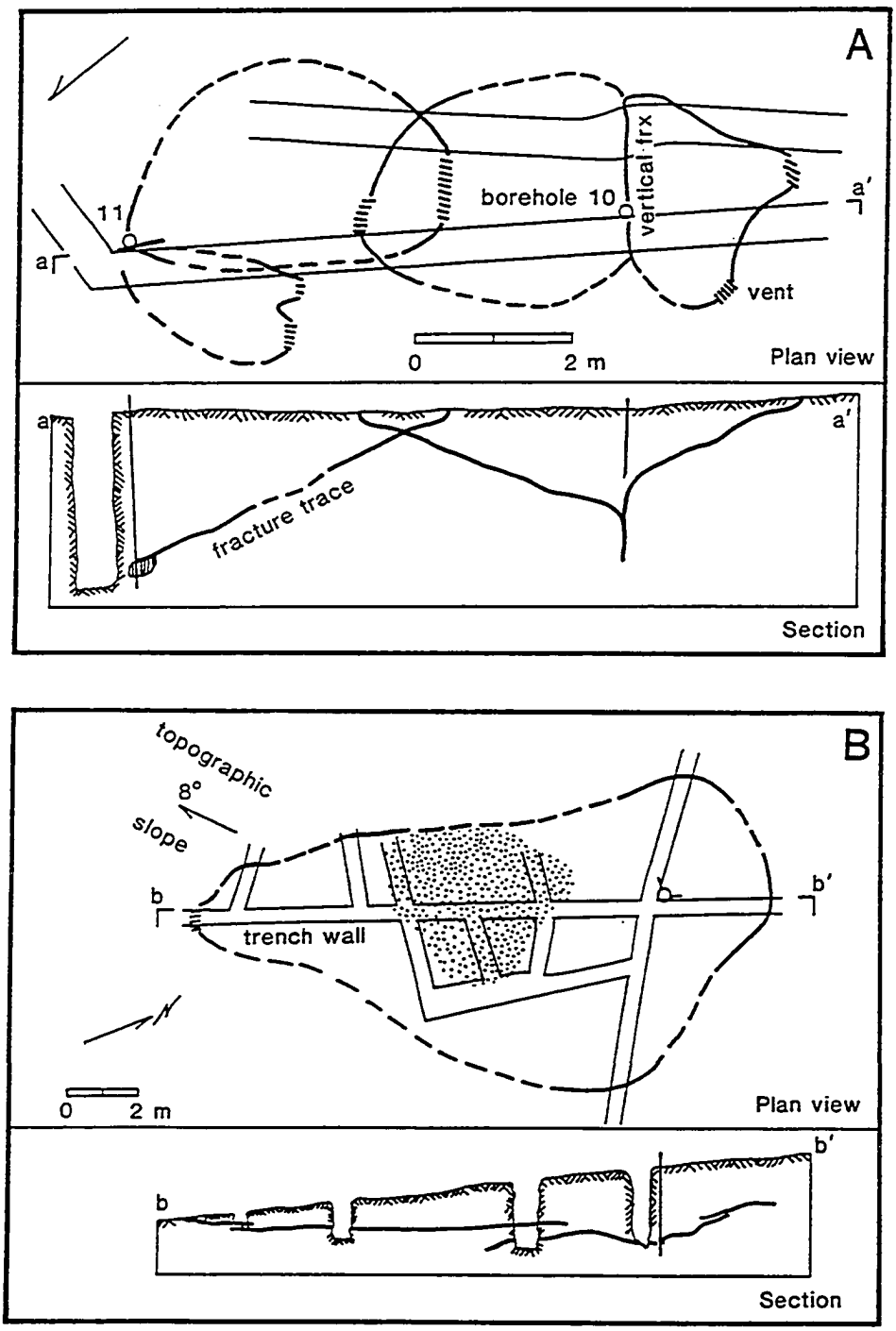

Figure 4.8. Exceptions to the idealized form. *a.*) Hydraulic fractures created at boreholes 10 and 11 showing a lack of Zone 2. *b.*) Hydraulic fracture created at borehole 13 showing a roughly flat-lying feature beneath sloping ground. Stiple indicates where the fractures cuts through a flat-lying, graded bed of sand and silt.

simply omit Zone Two (Figure 4.5), with Zone Three beginning adjacent to the borehole.

The fracture created adjacent to borehole 13 is exceptional in both form and size. It is essentially flat-lying and is the largest fracture created during the tests. There are at least two factors that could have affected the form HF13; the slope of the overlying ground and the density of the injected fluid. In contrast to the other fractures, the ground slopes markedly over HF13. The fracture grew predominantly in the downslope direction and venting occurred when it intersected the sloping ground (Figs. 4.9 and 4.8b). The fracture only climbed 0.75 m above the elevation of the bottom of the casing at the point of venting.

Sand was successfully pumped into HF13, whereas most of the other fractures lacked sand. The sand filling reaches a maximum thickness of 9 mm roughly 4 m south of the borehole at HF13, and the total volume of sand in the fracture is approximately 0.12 m^3 (4.3 ft^3). The sand-laden slurry injected into HF13 was denser than the slurry injected into other fractures, which typically contained sparse concentrations of sand. Abou-Sayed and others (1984) have shown that the density contrast between injection fluid and host material results in a buoyant force that causes a hydraulic fracture to climb. It is feasible that the relatively dense slurry injected into HF13 contributed to the relatively flat-lying orientation.

Bedding and local heterogeneities in the glacial drift affected both the form and the distribution of sand in the fractures. Most of the hydraulic fractures cut massive till ranging from clay to cobble-size fragments. Bedding was essentially absent in that material, so the development of the idealized fracture in Figure 4.5 is independent of bedding. One fracture, HF12, cut through a contorted bed of gravelly-sand embedded in silty-clay till 1 m below the ground surface. The fracture

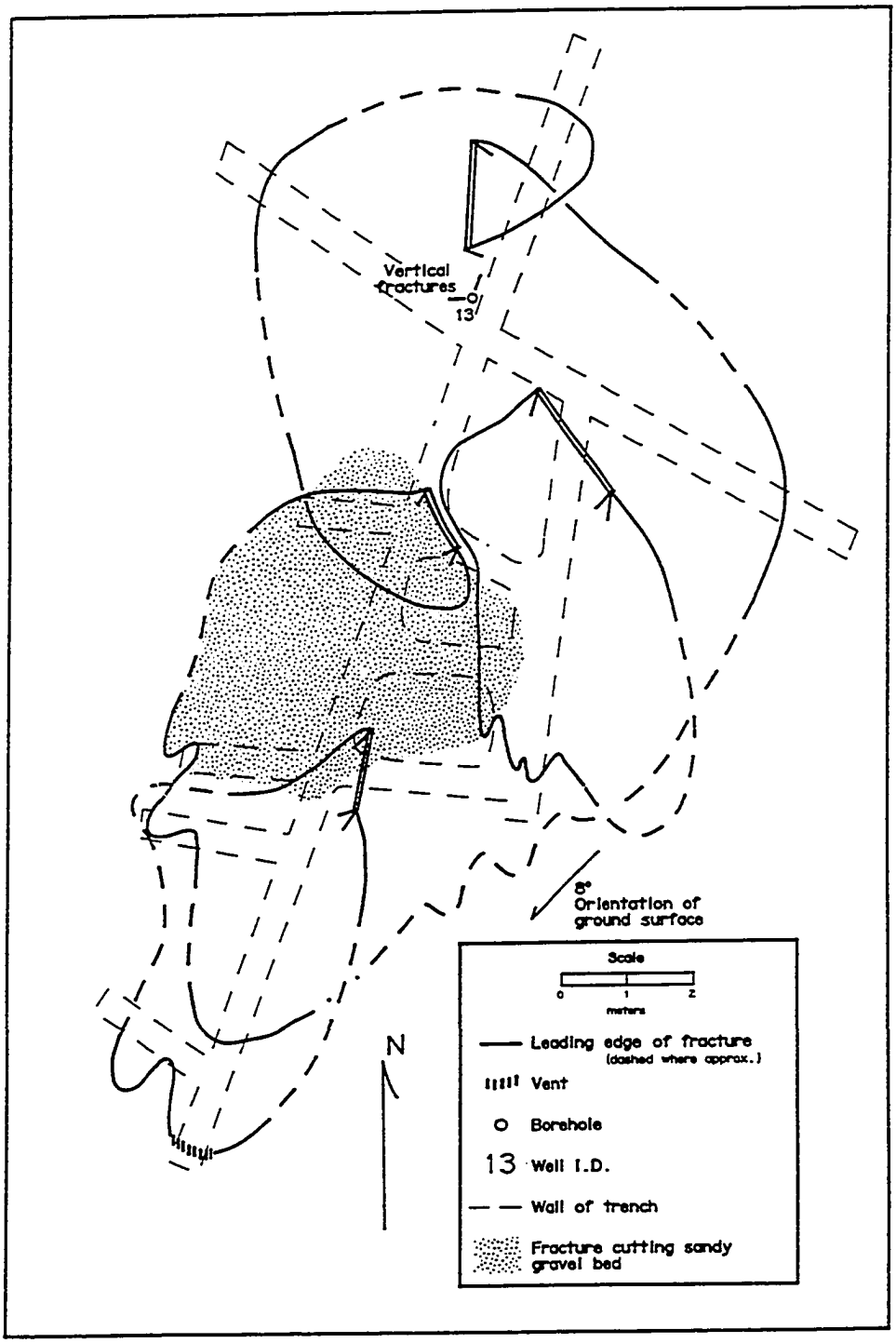

Figure 4.9 Map of HF13 showing several lobes that split from the main fracture plane. Double lines mark the intersections of fracture lobes. Fracture cuts graded lens of gravel, sand, and silt in stipled area, it cuts silty clay elswhere.

dips 20° as it approaches the bed, cuts through a sandy stringer with little change in orientation, then flattens to approximately 10° where it cuts along the upper surface of the gravel and sand bed. The upper surface of that bed is irregular, however, but the fracture trace remains straight, cutting both sand and silty-clay on either side of the contact (Figure 4.10). The fracture climbs upward away from the contact after one m, and it cuts through another bed of sand and gravel, through a pod of grey silt and then it curves upward and vents. Comparing the form of HF12 to the other fractures suggests that the dip of HF12 diminished by 8° where it encountered a bed of sand and gravel. In general, however, the form of HF12 resembles that of the other fractures, so the effect of bedding on fracture form appears to be minor.

In another example, the form of HF13 appears to only slightly affected by bedding, but the distribution of sand in that fracture is markedly affected. HF13 intersects a flat-lying lens that grades from gravel at its base upward to silt at its top. The lens is several dm at its thickest and the fracture cuts along the top of the lens in an area that is roughly 5 m in diameter a few m south of the borehole (Figs. 4.11, 4.9, and 4.8*b*). The fracture toughness of silt is less than clay, so it is possible that the fracture was mechanically contained within the lens. However, most of HF13 cuts massive silty clay (Fig. 4.9), and it has the same orientation in the clay as it does in the silt. The orientation of HF13 appears to result from factors other than bedding.

The distribution of sand within HF13 is known in detail from measurements of fracture thickness made along the walls of the trenches. A noteworthy example occurs where a fracture lobe underlies the main fracture near the center of the cross-section of Figure 4.8*b*. The lobe was mapped in detail and the results plotted on a section (Fig. 4.11) whose northernmost point is 1.5 m south of the borehole. Thickness measurements were made every 1.25 cm along the section using drafting

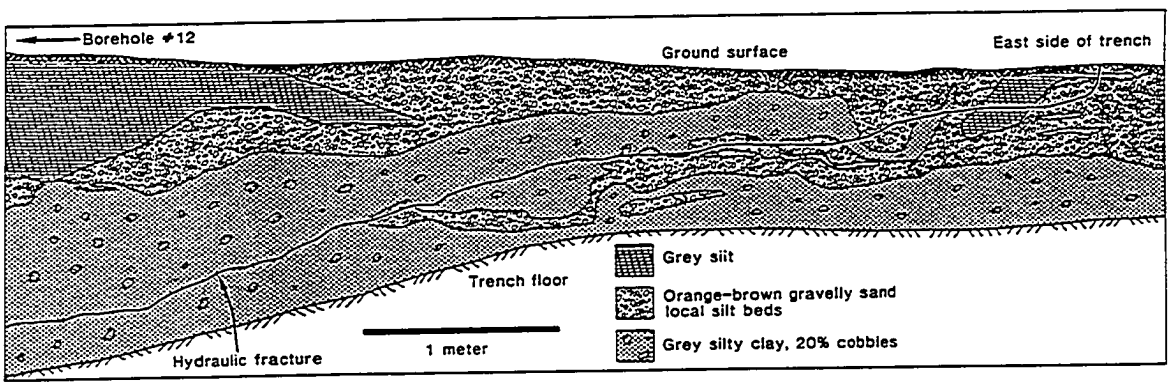

Figure 4.10. Geology and trace of a hydraulic fracture on the eastern wall of the trench cutting the major axis of HF12. Detail of the section shown in Figure 4.7*b*.

dividers and a fine scale. The solid line in Figure 4.11*b* is a regression fit of the thickness data, where the solid dots have been omitted from the regression because they apparently represent local thickness variations associated with pebbles in the walls of the fractures. Injection fluid flowed from right to left, roughly parallel to the plane of the section in Figure 4.11a.

The thickness of the sand is variable over short distances, but it follows a general pattern, shown by the regression line, as the graded lens is approached. Thicknesses are 0.1 cm between 60 and 110 cm upstream from the edge of the sand lens. They increase as the lens is approached and are 0.3 cm where the fracture intersects the lens. Sand thickness continues to increase within the lens and reaches a maximum of 0.5 cm between 20 and 25 cm downstream of the leading edge of the lens. Thickness decreases markedly in the downstream direction, and sand is virtually absent 70 cm from the leading edge of the lens (Fig. 4.11).

Areas where the fracture cuts around pebbles or cobbles in the till also show concentrations of sand. Two examples of local concentrations are pods of sand shown by filled circles 15 cm and 75 cm upstream of the leading edge of the lens (Fig. 4.11). In both cases, the pods occur on the upstream sides of the pebbles. The pods are 5 to 10 cm long and reach maximum thicknesses of 0.5 cm, which is more than double the thickness of the fracture in the vicinity of the pebbles. Sand in most of the other fractures occurred as small pods associated with pebbles or rock fragments protruding from the fracture wall.

Dimensions

The plan areas of most of the fractures were between 10 m^2 and 30 m^2 (Table 4.4). One fracture, HF13, was much larger, covering an area of 90 m^2, and another fracture, HF7, was smaller (2.2 m^2) than most of the others.

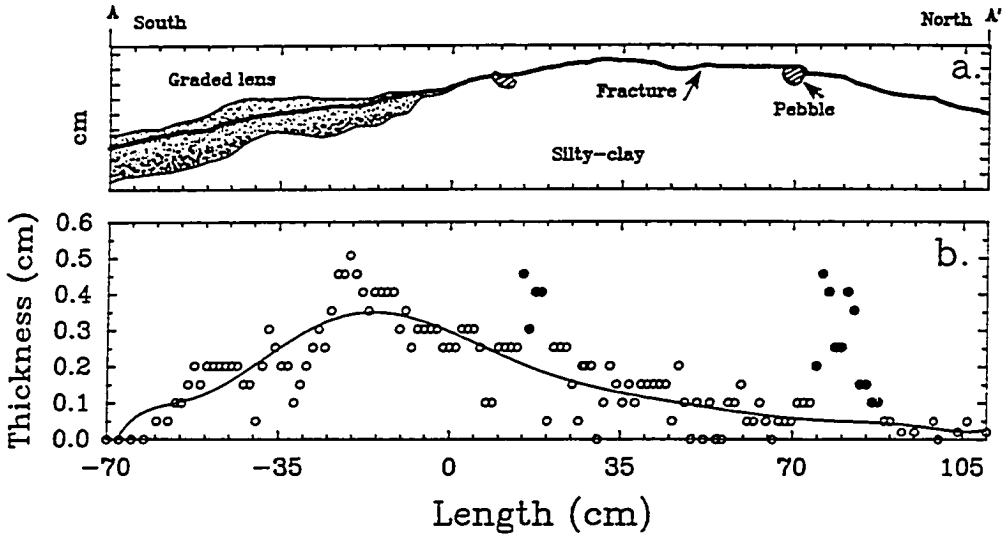

Figure 4.11. Trace of HF13 in the vicinity of a graded lens. *a.*) Geologic cross-section of the fracture trace and the lens (enlarged from Figure 4.8*b*). *b.*) Thickness of sand in the fracture. Solid line is a high-order regression of the thickness neglecting areas in the vicinity of pebbles.

The greatest length, where length is measured from the injection well to the leading edge, of all exposed fractures occurred between the well and the vent. The maximum length of most of the fractures was between 3 and 8 m. The longest fracture was 13.5 m, and the shortest one was 1.8 m (Table 4.4).

Ratios of maximum length to depth of initiation typically range between 1.5 and 4, with a maximum of 7.4 and a minimum of 1.0. HF2 and HF4 did not vent and were too deep to excavate completely, so their lengths are unknown.

Table: 4.4. Dimensions And Dips Of Hydraulic Fractures

Frx	Depth (m)	Plan Area (m^2)	Max. Length (m)	Ave. Dip
HF2	2.77	unknown	unknown	shallow
HF4	3.84	unknown	unknown	shallow
HF5	1.64	13	3.6	25°
HF6	1.85	28	6.4	15°
HF7	1.83	2.2	1.8	variable
HF9	1.75	20	5.5	20°
HF10	1.83	12	3.3	22°,25°
HF11	1.67	9	4.1	24°
HF12	1.98	30	8.2	14°
HF13	1.83	90	13.5	sub-horiz.

Many of the hydraulic fractures are approximately planar between the borehole and the vent. The average dips of the fractures are similar; all except HF13 are within 5° of a 20° dip. HF13 is sub-horizontal.

Directions of Propagation

All the hydraulic fractures were asymmetric with respect to their parent borehole. Thus, the fractures acquire a preferred, or dominant direction of propagation as they grow away from their parent boreholes. The dominant direction of propagation, the azimuth of the line between the borehole and a vent, ranges from northeast to west to southeast (Table 4.5). The direction of propagation of HF13 is nearly parallel to the direction of maximum slope of the overlying ground surface, which is 225° (Fig. 4.12 and Table 4.5). At the other fractures, however, the direction of propagation is unrelated to geologic or topographic features.

Table 4.5. Azimuths Of Features Of Hydraulic Fractures.

	Propagation Direction	Vent Frx	Borehole Frx
HF5	325, 282	60	62
HF6	225, 10	165	157
HF7	150	62	58
HF9	326	35	117
HF10	206, 39	124	128
HF11	205, 240	130	18
HF12	175	75	--
HF13	200	105	265, 20

The direction of propagation is related to the location of the backhoe used to prevent movement of the casing during fracturing. In most cases, the fractures propagated away from the backhoe. The two exceptions, HF7 and the southwestern lobe of HF10, are small fractures that propagated toward the backhoe, venting near

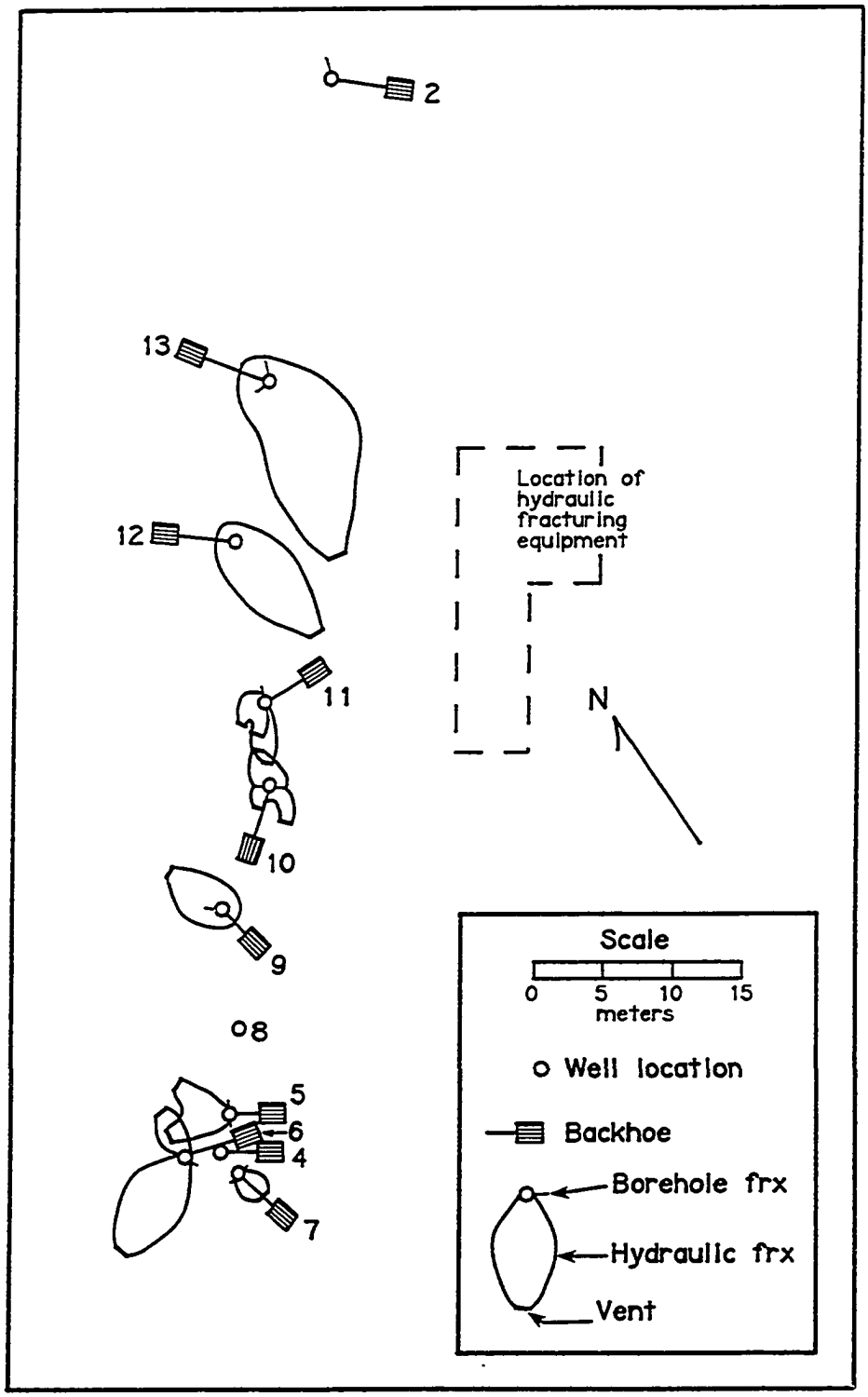

Figure 4.12 Outlines of hydraulic fractures and locations of a backhoe at the time of fracturing.

the front wheels of the vehicle (Fig. 4.5). No fractures propagated beneath the backhoe.

Theoretical analyses indicate that hydraulic fractures will propagate in directions of decreasing confining stress. Apparently the weight of the backhoe resulted in vertical stress gradients that were great enough to affect the propagation of the underlying hydraulic fracture.

The dominant direction of propagation is related to the strikes of the hydraulic fracture at the vent, and to the vertical hydraulic fractures adjacent to the borehole. Strikes of vertical fractures at the vent are nearly perpendicular to the dominant direction of propagation in every fracture (Fig. 4.12 and Table 4.5). At most fractures, the strike of a vertical fracture at the borehole is also nearly perpendicular to the propagation direction.

In a few cases, however, the strikes of fractures adjacent to the borehole (e.g. HF9, HF11) are at high angles to the direction of propagation, and in one case (HF13), two vertical fractures differing in strike by 125° were observed.

DISCUSSION

The development of the fractures created during the field test presumably share a similar history. When pumping begins at the start of the fracturing procedure, the pressure within the borehole increases, affecting the state of stress until failure occurs in the till enveloping the open interval of the borehole. The initial failure results in a vertical fracture, which contains the axis of the borehole and apparently is unrelated to the notch.

Several investigators have reported results from the lab indicating that hydraulic fractures nucleated from cylindrical holes in rock will contain the axis of

the hole, even though the applied far-field state of stress favored an orientation normal to the axis (Medlin and Masse, 1979; Daneshy, 1973; Haimson and Fairhurst, 1969). Similar results occurred when hydraulic fractures were created from cylindrical holes in soil using the apparatus described in Chapter One.

This result can be explained by an analysis of stresses in the vicinity of a long (e.g. ignoring effects at the ends) pressurized cylindrical hole in an elastic medium where the principal confining stresses act parallel or normal to the axis of the hole (Poulos and Davis, 1974). The analysis shows that pressure within the hole can induce tensile stresses in the enveloping medium that act parallel to the circumference of the hole. Stresses acting parallel to the axis of the hole, however, are unaffected by pressure within the hole. Accordingly, tensile stress adjacent to a vertical borehole develop normal to a vertical plane, regardless of the relative magnitudes of the principal confining stresses. The vertical fractures observed adjacent to the boreholes apparently result from those tensile stresses.

A disk-shaped notch should favor the nucleation of a fracture in the plane of the notch, assuming the minimum applied compression is normal to the notch. Indeed, this was the reason the notches were created. It is clear from the results of the field test that the notches had little effect on the nucleation of hydraulic fractures. Failure to nucleate a horizontal fracture at the borehole is a significant shortcoming of the design of the borehole because it reduces the overall size of the hydraulic fractures. This occurs because the vertical fractures at the borehole grow upward before rolling over, essentially reducing the depth of initiation and limiting the length of the fracture prior to venting.

The development of a vertical fracture could be inhibited by decreasing the length of the open interval in the boring, and by increasing the depth of penetration

of the notch. Recently, I have used a high-velocity water jet to cut notches that extend 15 to 25 cm into till, many times larger than the ones cut mechanically during the field test.

Once formed, the vertical fracture grows outward and upward climbing above the open interval of the borehole. At some point, either adjacent to or several dm to one meter above the basket, the vertical fracture changes orientation, or rolls over, flattening abruptly to a shallow dip. Typically, the fractures roll over to a nearly flat-lying orientation, but in some cases they dip 15° to 25° toward the borehole. This change of orientation appears to occur as the fracture grows out of a zone where stresses are influenced by the pressurized borehole and into a zone influenced by the far-field stresses.

The idealized fracture then grows roughly horizontally as much as several m away from the borehole and changes orientation again, curving upward to dip roughly 20° toward the borehole. This change in orientation is inferred to result from a mechanical interaction between the fracture and the overlying ground surface. The interaction has several effects on the propagating fracture, all of which are related to the lack of resistance of material at the ground surface. Perkins and Kern (1961), for example, analyze one effect of mechanical interaction by comparing the aperture of a shallow circular horizontal fracture, which dilates by lifting the overburden, to the aperture of a deep circular fracture, which dilates by compressing the overburden. They show that fracture apertures depend on the size of the fracture relative to its depth, expressed as the ratio of radial length a to depth of initiation d. Apertures of the two fractures are equal when $a/d = 1.33$, but the aperture of the fracture that lifts the overburden greatly exceeds that of the other fracture when $a/d > 1.33$.

Pollard and Holzhausen (1979) show how mechanical interaction could cause a fracture to turn upward and propagate toward the ground surface. They calculated the stress intensity factors, K_I and K_{II}, for a two-dimensional, static, planar fracture of half-length a in an elastic medium bounded by a free surface (the ground surface). The direction of propagation of the fracture can be predicted using the relative magnitudes of K_I and K_{II}, according to theories proposed by Cottrell and Rice (1980) or other investigators cited by Pollard and Holzhausen (1979). Those theories state that non-zero values of K_{II} lead to propagation out of the plane of the original fracture. The results of Pollard and Holzhausen indicate that K_{II} of a horizontal fracture increases as a/d increases; K_{II} is negligible when $a/d < 0.3$, it increases gradually when $0.3 < a/d < 1.0$, and it increases rapidly when $a/d > 1.0$ (Pollard and Holzhausen, 1979; fig 5). This is because the upper surface of a horizontal fracture is displaced further from the axial plane than the lower surface, resulting in shear at the tip and non-zero values of K_{II}.

Those results suggest that the depth of initiation is critical to the propagation path. A horizontal fracture considerably shorter than the depth of initiation will propagate horizontally, but as the fracture length approaches the depth the fracture will tend to curve out of plane and propagate upward.

The analyses described in the previous paragraph are for static fractures, and as such they are limited to the favored direction of a miniscule extension of a stationary planar fracture. Dynamic analyses, which track the movement of a fracture as it propagates, show how the interactions described above affect fracture form. Narandren and Cleary (1983) present the results of a dynamic analysis predicting the path of propagation of a horizontal hydraulic fracture beneath a free surface. The results (Narandren and Cleary 1983; fig. 9) show that the fracture is nearly flat-lying when it is short relative to its depth, but the dip increases noticeably

when $a/d > 0.7$. The analysis was terminated when $a/d = 1.55$ and the fracture curves upward yielding a shape suggestive of the cross-section of the idealized fracture (Fig. 4.5b and Narandren Cleary 1983; fig. 9).

The idealized fracture grows at nearly a constant dip once it begins to propagate toward the ground surface (neglecting vertical growth at the borehole). Processes causing the dip to remain constant are unclear because available analyses (i.e. Pollard and Holzhausen, 1979; Narandren and Cleary, 1983) suggest that the dip will increase as the fracture climbs and the effect of the ground surface increases. One possibility is that during upward growth the vertical stress, resulting from the weight of the overburden at the fracture tip decreases, whereas the lateral stress remains constant. Thus the tendency to steepen, due to effects of the ground surface, is balanced by a tendency to flatten, due to an increase in the ratio of lateral to vertical stress at the tip (Cottrell and Rice, 1980).

The dip of the idealized fracture is uniform in general, but it varies slightly in detail, resulting in gentle step-like features. The steps suggest that slight deviations from the average dip are rapidly corrected by the fracture curving back to the initial orientation. Cottrell and Rice, who analyze the stability of slightly-curved Mode I cracks, show how a small deviation from the optimal path will result in a step-like form in a fracture (Cottrell and Rice, 1980; fig. 10).

Many analyses of hydraulic fractures assume that they are symmetric with respect to the axis of the borehole, but all of the fractures created in the field test were asymmetric. The hydraulic fracture created beneath sloping ground (HF13) is elongate in the downslope direction. Where the ground is level, however, applied loads seem to influence the direction of propagation because the dominant directions of propagation are typically away from the backhoe parked near each

when $a/d > 0.7$. The analysis was terminated when $a/d = 1.55$ and the fracture curves upward yielding a shape suggestive of the cross-section of the idealized fracture (Fig. 4.5b and Narandren Cleary 1983; fig. 9).

The idealized fracture grows at nearly a constant dip once it begins to propagate toward the ground surface (neglecting vertical growth at the borehole). Processes causing the dip to remain constant are unclear because available analyses (i.e. Pollard and Holzhausen, 1979; Narandren and Cleary, 1983) suggest that the dip will increase as the fracture climbs and the effect of the ground surface increases. One possibility is that during upward growth the vertical stress, resulting from the weight of the overburden at the fracture tip decreases, whereas the lateral stress remains constant. Thus the tendency to steepen, due to effects of the ground surface, is balanced by a tendency to flatten, due to an increase in the ratio of lateral to vertical stress at the tip (Cottrell and Rice, 1980).

The dip of the idealized fracture is uniform in general, but it varies slightly in detail, resulting in gentle step-like features. The steps suggest that slight deviations from the average dip are rapidly corrected by the fracture curving back to the initial orientation. Cottrell and Rice, who analyze the stability of slightly-curved Mode I cracks, show how a small deviation from the optimal path will result in a step-like form in a fracture (Cottrell and Rice, 1980; fig. 10).

Many analyses of hydraulic fractures assume that they are symmetric with respect to the axis of the borehole, but all of the fractures created in the field test were asymmetric. The hydraulic fracture created beneath sloping ground (HF13) is elongate in the downslope direction. Where the ground is level, however, applied loads seem to influence the direction of propagation because the dominant directions of propagation are typically away from the backhoe parked near each

borehole. Apparently gradients in vertical stress, caused by either topography or applied loads, affect the dominant direction of propagation of horizontal or shallowly-dipping hydraulic fractures. This conclusion raises the intriguing possibility of artificially loading the ground surface to cause fractures to propagate in a particular direction.

It is reasonable to expect that hydraulic fractures of similar size and shape as those described here could be created under conditions similar to the ELDA site. It would be misleading, however, to suggest that similar hydraulic fractures can be expected at any site. The relatively large horizontal compression in the overconsolidated till inhibits upward growth (e.g. Cottrell and Rice, 1980) and favors the creation of flat-lying fractures. At sites where the direction of maximum compression is vertical (e.g. underlain by normally consolidated deposits) there should be a strong tendency for hydraulic fractures to climb upward, perhaps vertically.

CONCLUSIONS

Hydraulic fractures that are several times longer than they are deep were created at shallow depths in a deposit of overconsolidated, silty clay till. The fractures were slightly elongate in plan and dipped gently toward their parent borehole. They covered several tens of square meters and ranged to more than 10 m in maximum length. Sand was injected into several of the fractures, suggesting that the technique could be used to create permeable layers that would increase fluid flow in the subsurface.

The borehole design described in Figure 4.4 nucleated a vertical hydraulic fracture that contained the axis of the borehole and grew upward. A larger notch

and a shorter interval of open hole would promote the nucleation of a horizontal hydraulic fracture at the borehole.

The general field observations can be explained using the principals of linear elastic fracture mechanics. This indicates that the large body of analyses of hydraulic fracture propagation through rock published by workers in the energy industry, and reviewed in Appendix A, will offer important guidelines in the formulation of a theoretical analysis of field-scale hydraulic fracturing of soil.

REFERENCES

Aamodt, R.L. and M. Kuriyagawa. 1982. Measurement of instantaneous shut-in pressure in crystalline rock.

Abe, H., T. Mura, and L.M. Keer. 1976. Growth rate of a penny-shaped crack in hydraulic fracturing of rocks. J. Geop. Res. 81:5335-5340.

Abou-Sayed, A.S. 1977. Fracture toughness triaxially loaded Indiana limestone. in: Proc. 18th U.S. Sym. Rock Mech. 1-8.

Abou-Sayed, A.S., C.E. Brechtel and R.J. Clifton. 1978. In-situ stress determination by hydrofracturing: A fracture mechanics approach. J. Geop. Res. 83:2851-2862.

Abou-Sayed, A.S., K.P. Sinha and R.J. Clifton. 1984. Evaluation of the influence of in-situ reservoir conditions in the geometry of hydraulic fractures using a 3-D simulator: Part 1--Technical Approach, SPE Paper 12877. In: Proc. Uncon. Gas Rec. Sym., Pittsburg, PA.(May) 433-438.

Abramowitz, M. and I.A. Stegun. 1964. eds. Handbook of Mathematical Functions with Formulas, Graphs, and Mathematical Tables. U.S. Govt. Printing Office. Washington, DC. 1046.

Acharya, A. 1988. Hydraulic-fracture-treatment design simulation. SPE Production Engineering. 40:139-142.

Advani, S.H., H. Khattab and J.K. Lee. 1985. Hydraulic fracturing geometry, modeling, prediction and comparisons, SPE Paper 13863. In: Proc. Low Perm. Gas Res. Sym., Denver, CO.(May) 135-139.

Ahmed, U., J. Strawn, M. Wilson and J. Schatz. 1983. Effect of stress distribution on hydraulic fracture geometry: A laboratory simulation study in one meter cubic blocks, SPE Paper 11637. In: Proc. SPE Sym. Low Permeability, Denver, CO. 1-5.

Anderson, G.D. 1979. Laboratory experiments on hydraulic fracture growth near an interface. In: Proc. U.S. Sym. Rock Mech., Golden, CO. 19:333-339.

Anderson, R.A. 1974. Slurry injection of vein materials in the Coeur d'Alene district. Economic Geology. 69:414-415.

Anderson, R.W. and A.M. Phillips. 1988. Practical application of economic well-performance criteria to the optimization of fracturing treatment design. SPE Production Engineering. 40:223-228.

Babcock, R.E., C.L. Prokop and R.O. Kehle. 1967. Distribution of propping agents in vertical fractures. Prod. Monthly. 11-18.

Barenblatt, G.I. 1962. The mathematical theory of equilibrium cracks in brittle fracture. Adv. Appl. Mech. 7:55-129.

Baski, H. 1987. Hydrofracturing of water wells. Water Well J. 41:6:34-35.

Biot, M.A., L. Masse and W.L. Medlin. 1982. A two-dimensional theory of fracture propogation, SPE Paper 11067. In: Proc. Ann. SPE Fall Tech. Conf., New Orleans, LA. 1-15.

Biot, M.A., W.L. Medlin and L. Masse. 1983. Fracture penetration through an interface. Soc. Petr. Eng. J. 857-869.

Bjerrum, L. and K.H. Andersen. 1972. In-situ measurement of lateral pressures in clay. Geotechnique. 15:11-20.

Bjerrum, L., J.K.L. Nash, R.M. Kennard and R.E. Gibson. 1972. Hydraulic fracturing in field permeability testing. Geotechnique. 22:319-332.

Boone, T.J., A.R. Ingraffea and J.C. Roegiers. 1989. Visualization of hydraulically driven fracture propagation in poroelastic media using a superworkstation. J. Petr. Tech., Trans. AIME. 41:574-580.

Bouteca, M.J. 1988. Hydraulic fracturing model based on a three-dimensional closed form: Tests and analysis of fracture geometry and containment. SPE Production Engineering. 3:445-454.

Bouwer, H. 1978. Groundwater Hydrology. McGraw-Hill Book Co. New York. 480.

Briones, A.A. and G. Uehara. 1977a. Soil Elastic Constants: I. Calculations from sound velocities. Soil Sci. Soc. Am. J. 41:22-25.

Briones, A.A. and G. Uehara. 1977b. Soil Elastic Constants: II. Application to analysis of soil cracking. Soil Sci. Soc. Am. J. 41:26-29.

Brooker, E.W. and H.O. Ireland. 1965. Earth pressures at rest related to stress history. Canadian Geotech. J. 2:1-15.

Brunsing, T.P. 1987. The block displacement method field demonstration and specifications. U.S. EPA Project Summary. 600-S2-87-023:1-6.

Brunsing, T.P. and R.B. Henderson. 1984. A laboratory technique for assessing the in-situ constructability of a bottom barrier for waste isolation. In: Proc. Nat. Conf. Manag. Uncont. Haz. Wast. Sites, Washington, DC. 135-140.

Bryant, D.G. 1968. Intrusive breccias associated with ore, Warren (Bisbee) Mining District, Arizona. Economic Geology. 63:1-12.

Cinco-Ley, H., V.F. Samaniego and N.A. Dominguez. 1978. Transient pressure behavior for a well with a finite-conductivity vertical fracture. Soc. Petr. Eng. J. 253-264.

Cinco-Ley, H., V.F. Samaniego and A. Dominguez. 1981. Transient pressure analysis for fractured wells. J. Petr. Tech., Trans. AIME. 1749-1764.

Clark, J.B. 1949. A hydraulic process for increasing the productivity of wells. Petr. Trans. AIME. 2510:1-8.

Cleary, M.P. 1978a. Primary factors governing hydraulic fractures in heterogeneous stratified porous formations. In: Proc. ASME Energy Tech. Conf. & Exh., Houston, TX.(Nov.) 1-12.

Cleary, M.P. 1978b. Some deformation and fracture characteristics of oil shale. In: Proc. U.S. Sym. Rock Mech., Rapid City, SD. 72-82.

Cleary, M.P. 1980a. Analysis of mechanisms and procedures for producing favourable shapes of hydraulic fractures, SPE Paper 9260. In: Proc. 55th Ann. SPE Fall Tech. Conf. Exh., Dallas, TX. 1-12.

Cleary, M.P. 1980b. Comprehensive design formulae for hydraulic fracturing, SPE Paper 9259. In: Proc. 55th Ann. SPE Fall Tech. Conf. Exh., Dallas, TX. 1-16.

Cleary, M.P. 1988. The engineering of hydraulic fractures: State of the art and technology of the future. J. Petr. Tech., Trans. AIME. 13-21.

Cleary, M.P. and S.K. Wong. 1985. Numerical simulation of unsteady fluid flow and propagation of a circular hydraulic fracture. Int. J. Num. Anal. Meth. Geomech. 9:1-14.

Cleary, M.P., A.R. Crockett, J.I. Martinez and V.M. Narendran. 1983a. Surface integral schemes for fluid flow and induced stresses around fractures in underground reservoirs, SPE Paper 11632. In: Proc. SPE Sym. Low Permeability, Denver, CO. 283-292.

Cleary, M.P., M. Kavvadas and K.Y. Lam. 1983b. Development of a fully three-dimensional simulator for analysis and design of hydraulic fracturing, SPE Paper 11631. In: Proc. SPE Sym. Low Permeability, Denver, CO. 271-278.

Clifton, R.J., E.R. Simonson, A.H. Jones and S.J. Green. 1976. Determination of the critical-stress-intensity factor K from internally pressurized thick-walled vessels. Experimental Mechanics. 233-238.

Cornet, F.H., J.M. Hosanski, F. Bernaudat and E. Ledoux. 1982. Shallow depth experimentation on the concept of energy extraction from deep hot dry rocks. Hydraulic Fracturing and Geothermal Energy. Nemat-Nasser, S., H. Abe and S. Hirakawa.(eds.) Martinus Nijhoff Pub. The Hague. 75-93.

Cottrell, B. and J.R. Rice. 1980. Slightly curved or kinked cracks. Int. J. Fracture. 16:155-169.

Crockett, A.R., R.M. Willis and M.P. Cleary. 1989. Improvement of hydraulic fracture predictions by real-time history matching on observed pressures. SPE Production Engineering. 4:408-416.

Daneshy, A.A. 1973a. Experimental investigation of hydraulic fracturing through perforations, SPE Paper 4333. In: Proc. 2nd Ann. SPE European Meeting, London, England. 1-12.

Daneshy, A.A. 1973b. On the design of verticla hydraulic fractures. J. Petr. Tech., Trans. AIME. 83-97.

Daneshy, A.A. 1973c. A study of inclined hydraulic fractures. Soc. Petr. Eng. J. 13:61-68.

Daneshy, A.A. 1973d. Three-dimensional propagation of hydraulic fractures extending from open holes. Rock Mechanics. 157-179.

Daneshy, A.A. 1976a. Hydraulic fracture propagation in layered formations. Soc. Petr. Eng. J. 33-41.

Daneshy, A.A. 1976b. Rock properties controlling hydraulic fracture propagation, SPE Paper 5752. In: Proc SPE European Spring Meeting, Amsterdam, The Netherlands.(April) 1-8.

Daneshy, A.A. 1978a. Hydraulic fracture propagation in layered formations. Soc. Petr. Eng. J. 33-41.

Daneshy, A.A. 1978b. Numerical solution of sand transport in hydraulic fracturing. J. Petr. Tech., Trans. AIME. 132-140.

Davis, P.M. 1983. Surface deformation associated with a dipping hydrofracture. J. Geop. Res. 88:5826-5834.

Dean, R.H. and S.H. Advani. 1984. An exact solution for pistonlike leak-off of compressible fluids. J. Energy Res. Tech., Trans. ASME. 106:539-542.

DeGraff, J.M. and A. Aydin. 1987 Surface morphology of columnar joints and its significance to mechanics and directions of joint growth. Geological Society of America Bulletin 99, 605-617.

De Laguna, W. 1966a. Disposal of radioactive wastes by hydraulic fracturing, Part I: General concept and first field experiments. Nuclear Eng. & Design. 3:338-352.

De Laguna, W. 1966b. Disposal of radioactive wastes by hydraulic fracturing, Part II: Mechanics of fracture formation and design of observation and monitoring wells. Nuclear Eng. & Design. 3:432-438.

Detournay, E. 1979. The interaction of deformation and hydraulic conductivity in rock fracture. Improved stress determination proceedures by hydraulic fracturing. Univ. of Minn., Civil & Mineral Eng. Dept. Minneapolis. 1-42.

Dickinson, R.M. 1988. Review of consolidation grouting of rock masses and methods for evaluation. U.S. Army Corps of Eng. Final Report REMR-GT-8. 86.

Dugdale, D.S. 1960. Yielding of steel sheets containing slits. J. Mech. Phys. Solids. 8:100-104.

Dyes, A.B., C.E. Kemp and B.H. Claude. 1958. Effect of fractures on sweep-out pattern. Petr. Trans. AIME. 213:245-248.

Elbel, J.L. and P.A. Sookprasong. 1987. Use of cumulative-production type curves in fracture design. SPE Production Engineering. 2:191-198.

Ernst, P. 1980. Linking of boreholes. Meded. Rijks. Geol. Dienst. 33:35-40.

Fairhurst, C. 1964. Measurement of in-situ rock stresses, with particular reference to hydraulic fracturing. Felsmechanik. 2:129-147.

Farmin, R. 1934. Pebble dikes and associated mineralization at Tintic, Utah. Economic Geology. 29:356-370.

Farrell, D.A., E.L. Greacen and W.E. Larson. 1967. The effect of water content on axial strain in a loam soil under tension and compression. Soil Sci. Soc. Am. Proc. 31:445-450.

Geertsma, J. and F. de Klerk. 1969. A rapid method of predicting width and extent of hydraulically induced fractures. J. Petr. Tech., Trans. AIME. 1571-1581.

Geertsma, J. and R. Haafkens. 1979. A comparison of theories for predicting width and extent of vertical hydraulically induced fractures. J. Energy Res. Tech., Trans. ASME. 101:8-19.

Gidley, John L., Stephen A. Holditch, Dale E. Nierode, and Ralph W. Veatch. 1989. Recent Advances in Hydraulic Fracturing. Society Petroleum Engineers Monograph. 452.

Griffith, A.A. 1920. The phenomena of rupture and flow in solids. Phil. Trans. Roy. Soc. London. 221:163-198.

Griffith, A.A. 1924. The theory of rupture. In: Proc. 1st Int. Cong. Appl. Mech., Delft. 55-63.

Griffiths, S.K., R.H. Nilson and F.A. Morrison. 1983. Hybrid analytical/numerical computation of heat transfer in a gas driven fracture. Paper No. 83-WA/HT-35, Winter Meeting, Boston, MA. 1-9.

Gringarten, A.C. 1982. Flow-test evaluation of fractured reservoirs. Geol. Soc. Amer. Spec. Paper. 189:237-263.

Gringarten, A.C. and H.J. Ramey. 1973. The use of source and Green's functions in solving unsteady flow problems in reservoirs. Soc. Petr. Eng. J. 285-296.

Gringarten, A.C. and H.J. Ramey. 1974. Unsteady-state pressure distributions created by a well with a single horizontal fracture, partial penetration, or resticted entry. Soc. Petr. Eng. J. 413-426.

Gringarten, A.C., H.J. Ramey and R. Raghaven. 1974. Unsteady-state pressure distributions created by a well with a single infinite-conductivity vertical fracture. Soc. Petr. Eng. J. 347-360.

Gronseth, J.M. 1979. Stress determination by hydraulic fracturing. Improved stress determination procedures by hydraulic fracturing. Univ. of Minn., Civil & Mineral Eng Dept. Minneapolis. 1-114.

Haimson, B. and C. Fairhurst. 1967. Initiation and extension of hydraulic fractures in rocks. Soc. Petr. Eng. J. 7:310-318.

Haimson, B. and C. Fairhurst. 1969. Hydraulic fracturing in porous-permeable materials. J. Petr. Tech., Trans. AIME. 21:811-817.

Haimson, B. and C. Fairhurst. 1970. In-situ stress determination at great depth by means of hydraulic fracturing. (28) Rock Mechanics: Theory and Practice. Somerton, W.H.(ed.) The American Institute of Mining, Metallurgical, and Petroleum Engineers, Inc. New York. 559-584.

Haimson, B. and E.J. Stahl. 1970. Hydraulic fracturing and the extraction of minerals through wells. In: Proc. 3rd Sym. on Salt, Northern Ohio Geol. Soc., Cleveland, OH. 2:421-432.

Hanson, M.E., G.D. Anderson, R.J. Shaffer, D.N. Montan, B. Haimson and M.P. Cleary. 1978a. LLL gas stimulation program quarterly progress report January through March 1978. Lawrence Livermore Laboratories Report. No. UCRL 536-78-1-2:1-25.

Hanson, M.E., G.D. Anderson, R.J. Shaffer, D.N. Montan, L.D. Thorson, W. Lin, C. Haimson and M.P. Cleary. 1978b. LLL gas stimulation program quarterly progress report October through December 1977. Lawrence Livermore Laboratories Report. UCRL 50036-78-4:1-25.

Hanson, M.E., G.D. Anderson, R.J. Shaffer, D.F. Towse, A.G. Duba, N.R. Burkhard, W. Lin, M.P. Cleary and B.C. Haimson. 1979. LLL gas stimulation program quarterly progress report January through March 1979. Lawrence Livermore Laboratories Report. UCRL 50036-79-1:1-24.

Harrison, E., W.F. Kieschnick and W.J. McGuire. 1954. The mechanics of fracture induction and extension. Petr. Trans. AIME. 20:252-263.

Hartley, R. and M.G.R. Bosma. 1985. Fracturing in chalk completions. J. Petr. Tech., Trans. AIME. 73-79.

Hartsock, J.H. and J.E. Warren. 1961. The effect of horizontal hydraulic fracturing on well performance. J. Petr. Tech., Trans. AIME. 1050-1056.

Helmer, O. 1957. Mechanical analysis of the dike pattern of the Spanish Peak area, Colorado. Geol. Soc. Am. Bull. 68:567-576.

Holzer, T.L., T.L. Youd and T.C. Hanks. 1989. Dynamics of liquefaction during the 1987 Superstition Hills, California Earthquake. Science. 244:56-59.

Holzhausen, G.R., C.C. Card, J.M. Raisbeck and T.L. Dobecki. 1985a. Hydraulic fracture growth during steam stimulation in a single-well test, SPE Paper 13619. In: Proc. SPE Regional Meeting, Ventura, CA.

Holzhausen, G.R., C.S. Haase, S.H. Stow and G. Gazonas. 1985b. Hydraulic-fracture growth in dipping anisotropic strata as viewed through the surface deformation field. In: Proc. 26th U.S. Sym. Rock Mech., Rapid City, SD.

Horsrud, P., R. Risnes and R.K. Bratli. 1982. Fracture initiation pressures in permeable poorly consolidated sands. Int. J. Rock Mech. Min. Sci. Geomech. Abs. 19:255-266.

Howard, G.C. and C.R. Fast. 1957. Optimum fluid characteristics for fracture extension. Drilling & Prod. Prac., API. 261-270.

Howard, G.C. and C.R. Fast. 1970. Hydraulic Fracturing. Society of Petroleum Engineers AIME. New York. 198.

Hubbert, M.K. and D.G. Willis. 1957. Mechanics of hydraulic fracturing. Petr. Trans. AIME. 210:153-168.

Huck, P.J., M.J. Waller and S.L. Shimondle. 1980. Innovative geotechnical approaches to the remedial in-situ treatment of hazardous materials disposal sites. In: Proc. Nat. Conf. Control Haz. Mater. Spills, Louisville, KY. 421-426.

Hurlburt, S. 1989. Moving ahead with hydrofracing. Water Well J.(Feb.) 37-40.

Inglis, C.E. 1957. Stresses in a plate due to the presence of cracks and sharp corners. Inst. Naval. Architects, Trans., London. 55:1.

Irwin, G.R. 1957. Analysis of stresses and strains near the end of a crack traversing a plate. J. Appl. Mech., Trans. ASME. 361-364.

Jaworski, G.W., J.M. Duncan and H.B. Seed. 1979. An experimental study of hydraulic fracturing, Report UCB/GT/79-02. U.S. Bur. Reclam.(Oct.) 234.

Jaworski, G.W., J.M. Duncan and H.B. Seed. 1981. Laboratory study of hydraulic fracturing. J. Geotech. Eng. GT6:713-732.

Johnson, A.M. 1970. Physical Processes in Geology. Freeman Cooper and Company. San Fransisco. 577.

Kaufman, J.G. and F.G. Nelson. 1974. More on specimen size effects in fracture toughness testing. Fracture Toughness and Slow-Stable Cracking, ASTM STP 559. Irwin, G.R.(ed.) Amer. Soc. for Testing & Materials. Baltimore. 74-85.

Keck, R.G., M.P. Cleary and A. Crockett. 1984. A lumped numerical model for the design of hydraulic fractures, SPE Paper 12884. In: Proc. SPE Unconventional Gas Recovery Sym., Pittsburgh, PA. 507-514.

Kehle, R.O. 1964. The determination of tectonic stresses through analysis of hydraulic well fracturing. J. Geop. Res. 69:259-273.

Kerr, R.A. 1987. Hot dry rocks: Problems, Promise. Science. 238:1226-1228.

Kesler, S.E., N. Russell, M. Seaward, M. Rivera, K. McCurdy, G.L. Cumming and J.F. Sutter. 1981. Geology and geochemistry of sulfide mineralization underlying the Pueblo Viejo gold-silver oxide deposit, Dominican Republic. Economic Geology. 76:1096-1117.

Khristianovic, S.A. and Y.P. Zheltov. 1955. Formation of vertical fractures by means of highly viscous liquid. In: Proc. 4th World Petroleum Congress, Rome. 2:579-586.

Kirkham, D., M.F. De Boodt and L. De Leenheer. 1959. Modulus of rupture determination on undisturbed soil core samples. Soil Science. 87:141-144.

Klepaczko, J.R., M.N. Bassim and T.R. Hsu. 1984. Fracture toughness of coal under quasi-static and impact loading. Eng. Frac. Mech. 19:305-316.

Knauss, W.G. 1976. Fracture of solids possessing deformation rate sensitive material properties. In: Proc. ASME Winter Ann. Meeting, New York. AMD-19:70-103.

Koenig, L. 1960. Survey and analysis of well stimulation performance. J. Am. Water Works Assoc. 52:333-350.

Lam, K.Y. and M.P. Cleary. 1984. Slippage and re-initiation of hydraulic fractures at frictional interfaces. Int. J. Num. Anal. Meth. Geomech. 8:589-604.

Lambe, T.W. and R.V. Whitman. 1969. Soil Mechanics. John Wiley and Sons. New York. 553.

Landrum, B.L. and P.B. Crawford. 1961. Horizontal fractures do affect ultimate recovery. The Petroleum Engineer. 80-98.

Lawn, B.R. and T.R. Wilshaw. 1975. Fracture of Brittle Solids. Cambridge University Press. Cambridge.

Leach, R.E. 1977. Hydraulic fracturing of soils: A literature review. Misc. Paper S-77-6 U.S. Army Waterway Experiment Station.(Mar.) 1-25.

Luiskutty, C.T., L. Tomusta and I.D. Palmer. 1989. A three-dimensional semianalytical model of hydraulic fracture growth through weak barriers. SPE Production Engineering. 4:226-232.

Macaulay, D. 1987. Hydrofracturing the hard rock well. Ground Water Age. 21:22-25,28,30.

Massarch, K.R., R.D. Holtz, B.G. Holm and A. Fredriksson. 1975. Measurement of horizontal in-situ stresses. In: Proc. ASCE-GED Spec. Conf. In-situ Meas. Soil Prop., Raleigh, NC. 1:266-286.

Massarsch, K.R. 1978. New aspects of soil fracturing in clay. J. Geotech. Eng. Div. GT8:1109-1123.

McGuire, W.J. and V.J. Sikora. 1960. The effect of vertical fractures on well productivity. Petr. Trans. AIME. 219:401-403.

McLennan, J.D. and J.C. Roegiers. 1982. Do instantaneous shut-in pressures accurately represent the minimum principal stress? Proceedings of Workshop on Hydraulic Fracturing Stress Measurements. Zoback, M.D. and B.C. Haimson.(eds.) U.S. National Comm. for Rock Mechanics. Menlo Park, CA. 181-207.

Medlin, W.L. and L. Masse. 1979. Laboratory investigation of fracture initiation pressure and orientation. Soc. Petr. Eng. J. 129-144.

Medlin, W.L. and L. Masse. 1982. Plasticity effects in hydraulic fracturing, SPE Paper 11068. In: Proc. Ann. SPE Fall Tech. Conf., New Orleans, LA. 1-14.

Medlin, W.L. and L. Masse. 1984. Laboratory experiements in fracture propagation. Soc. Petr. Eng. J. 256-268.

Mendelsohn, D.A. 1984. A review of hydraulic fracture modeling, Part I: General concepts, 2D models, motivation for 3D modeling. J. Energy Res. Tech., Trans. ASME. 106:369-376.

Meyer, B.R. 1989. Heat transfer in hydraulic fracturing. SPE Production Engineering. 4:423-429.

Mony, P.M. 1989. Hydro-frac: One Man's Opinion. Water Well J.(Feb.) 48-50.

Morgenstern, N.R. and P.R. Vaughan. 1963. Some observations on allowable grouting pressures. In: Proc. Conf. Grouts and Drill. Muds, Instit. Civ. Eng., London. 36-42.

Mori, A. and M. Tamura. 1987. Hydrofracturing pressure of cohesive soils. Soils and Foundations. 27:14-22.

Morita, N., D.L. Whitfill and H.A. Wahl. 1988. Stress-intensity factor and fracture cross-sectional shape predictions from a three-dimensional model for hydraulically induced fractures. SPE Production Engineering. 40:1329-1342.

Morrisson, T.E. and J.H. Henderson. 1960. Gravity drainage of oil into large horizontal fractures. Petr. Trans. AIME. 219:7-15.

Murdoch, L.C., G. Holzhausen, J.C. Roegiers and B.K. Naceur. 1987. Innovative delivery and recovery systems: Hydraulic fracturing. EPA Center Hill Research Facility Interim Report, WA #3379 0-8. 205.

Murdoch, L.C., G. Losonsky, P. Cluxton, B. Patterson, I. Klich, B. Braswell. 1990. The feasibility of hydraulic fracturing of soil to improve remedial action. Final Report USEPA 600/2-91-012. NTIS Report PB91-181818. 298.

Murphy, H. 1982. Hot dry rock reservoir development and testing in the USA. Hydraulic Fracturing and Geothermal Energy. Nemat-Nasser, S., H. Abe and S. Hirakawa.(eds.) Martinus Nijhoff Pub. The Hague. 33-58.

Muskat, M. 1937. Use of data on build-up of bottom hole pressures. Trans. AIME. 123:44-48.

Nakatsuka, K., H. Takahashi and M. Takanohashi. 1982. Hydraulic fracturing experiment at Nigorikawa and fracture mechanics evaluation. Hydraulic Fracturing and Geothermal Energy. Nemat-Nasser, S., H. Abe and S. Hirakawa.(eds.) Martinus Nijhoff Pub. The Hague. 95-111.

Narendran, V.M. and M.P. Cleary. 1983. Analysis of growth and interaction of multiple hydraulic fractures, SPE Paper 12272. In: Proc. SPE Sym. Res. Sim., San Francisco, CA. 389-397.

Narendran, V.M. and M.P. Cleary. 1984. Elastostatic interaction of multiple arbitrarily shaped cracks in plane inhomogeneous regions. Eng. Frac. Mech. 19:481-506.

Natrella, Mary Gibbons. 1963. Experimental Statistics. U.S. Department of Commerce, National Bureau of Standards Handbook 91.

NAVFAC. 1982. Soil Mechanics Design Manual 7.1. Dept. of Navy, Navy Facilities Eng. Command. Alexandria. 348.

Nilson, R.H. 1981. Gas-driven fracture propagation. J. Appl. Mech., Trans. ASME. 48:757-762.

Nilson, R.H. 1986. An integral method for predicting hydraulic fracture propagation driven by gases or liquids. Int. J. Num. Anal. Meth. Geomech. 10:191-211.

Nilson, R.H. and S.K. Griffiths. 1986. Similarity analysis of energy transport in gas-driven fractures. Int. J. Fracture. 30:115-134.

Nilson, R.H., W.J. Proffer and R.E. Duff. 1985. Modelling of gas-driven fractures induced by propellant combustion within a borehole. Int. J. Rock Mech. Min. Sci. Geomech. Abs. 22:3-19.

Nolte, K.G. 1979. Determination of fracture parameters from fracturing pressure decline, SPE Paper 8341. In: Proc. 54th Ann. SPE Fall Tech. Conf. Exh., Las Vegas, NV. 1-16.

Nolte, K.G. 1982. Fracture design considerations based on pressure analysis, SPE Paper 10911. In: Proc. SPE Cotton Valley Sym., Tyler, TX.

Nolte, K.G. 1984. Determination of proppant and fluid schedules from fracturing pressure decline, SPE Paper 13278. In: Proc. 59th SPE Ann. Tech. Conf. & Exh., Houston, TX.

Nolte, K.G. 1986. A general analysis of fracturing pressure decline with application to three models. SPE Formation Evaluation. December. 571-583.

Nolte, K.G. 1988a. Application of fracture design based on pressure analysis. SPE Production Engineering. 3:31-42.

Nolte, K.G. 1988b. Principles for fracture design based on pressure analysis. SPE Production Engineering. 3:22-30.

Nolte, K.G. and M.B. Smith. 1981. Interpretation of fracturing pressures. J. Petr. Tech., Trans. AIME. 1767-1775.

Nolte, K.G. and M.B. Smith. 1987. Hydraulic Fracturing Pressure Analysis. 1st NSI Technologies, Inc. Tulsa. 96.

Nordgren, R.P. 1972. Propagation of a vertical hydraulic fracture. Soc. Petr. Eng. J. 306-314.

Northrop, D.A., N.R. Warpinski, R.A. Schmidt and C.W. Smith. 1978. Stimulation and mineback experiment project: The direct observation of hydraulic and explosive fracturing tests. In: Proc. Sym. Enhanced Oil & Gas Recovery & Improved Drilling Meth., Tulsa, OK. 1-14.

Novotny, E.J. 1977. Proppant transport, SPE Paper 6813. In: Proc. SPE Ann. Tech. Meeting & Exh., Denver, CO.

Ode, H. 1957. Mechanical analysis of the dike pattern of the Spanish Peak area, Colorado. Geol. Soc. Am. Bull. 68:567-576.

Ouchterlony, F. 1982. Review of frature toughness testing of rock. SM Archives. 7:131-211.

Paillet, F.L. 1985. Problems in fractured-reservoir evaluation and possible routes to their solution. The Log Analyst. 26:26-41.

Palmer, I.D. and C.T. Luiskutty. 1986. Comparison of hydraulic fracture models for highly elongated fractures of variable height. J. Energy Res. Tech., Trans. ASME. 108:107-115.

Papadoloulos, J.M., V.M. Narendran and M.P. Cleary. 1983. Laboratory simulations of hydraulic fracturing, SPE Paper 11618. In: Proc. SPE Sym. Low Permeability, Denver, CO. 161-168.

Pascal, H. 1986. Rheological behavior effects of non-newtonian fracturing fluids on propagation of vertical hydraulic fracture. Int. J. Num. Anal. Meth. Geomech. 10:443-448.

Perkins, T.K. and L.R. Kern. 1961. Widths of hydraulic fractures. J. Petr. Tech., Trans. AIME. Sept. 937-949.

Phillips, W.J. 1972. Hydraulic fracturing and mineralization. J. Geol. Soc. London. 128:337-359.

Phillips, W.J. 1973. Mechanical effects of retrograde boiling and its probable importance in the formation of some porphyry ore deposits. Instit. Mining Metallurgy Trans. 82:B90-B98.

Pollard, D.D. 1973. Derivation and evaluation of a mechanical model for sheet intrusions. Tectonophysics. 19:233-269.

Pollard, D.D. 1978. Forms of hydraulic fractures as deduced from field studies of sheet intrusions. United States Symposium of Rock Mechanics. Kim, Y.S.(ed.) University of Nevada. Reno. 1-9.

Pollard, D.D. and G. Holzhausen. 1979. On the mechanical interaction between a fluid-filled fracture and the earth's surface. Tectonophysics. 53:27-57.

Pollard, D.D., O.H. Muller and D.R. Dockstader. 1975. The form and growth of fingered sheet intrusions. Geol. Soc. Am. Bull. 86:351-363.

Pollard, D.D., P. Segall and P.T. Delaney. 1982. Formation and interpretation of dilatant echelon cracks. Geol. Soc. Am. Bull. 93:1291-1303.

Poulos, H.G. and E.H. Davis. 1974. Elastic Solutions for Soil and Rock Mechanics. John Wiley & Sons, Inc. New York. 411.

Prats, M. 1961. Effect of vertical fractures on reservoir behavior--incompressible fluid case. Soc. Petr. Eng. J. 1:105-118.

Prats, M. 1981. Effect of burial history on the subsurface horizontal stresses of formations having different material properties. Soc. Petr. Eng. J. 21:658-662.

Press, W.H. B.P. Flannery, S.A. Teukolsky and W.T. Vetterling. 1986. Numerical Recipes. Cambridge University Press.

Ramey, H.J. 1967. Application of the line source solution to flow in porous media: A review. Producers Monthly. May. 4-27.

Rice, J.R. 1968. A path independent integral and the approximate analysis of strain concentration by notches and cracks. J. Appl. Mech., Trans. ASME. 379-386.

Rice, J.R. 1979. The mechanics of quasi-static crack growth. In: Proc. 8th U.S. Nat. Cong. Applied Mechanics. 191-216.

Richards, Cedric, W. 1961. Engineering Materials Science. Brooks/Cole Publishing Co. Belmont, CA.

Robinson, B.M., S.A. Holditch and W.S. Whitehead. 1988. Minimizing damage to a propped fracture by controlled flowback procedures. SPE Production Engineering. 40:753-759.

Roegiers, J.C., J.D. McLennan and D.L. Murphy. 1982. Influence of pre-existing discontinuities on the hydraulic fracturing propagation process. Hydraulic Fracturing and Geothermal Energy. Nemat-Nasser, S., H. Abe and S. Hirakawa.(eds.) Martinus Nijhoff Pub. The Hague. 413-430.

Rogowski, A.S., W.C. Moldenhauer and D. Kirkham. 1968. Rupture parameters of soil aggregates. Soil Sci. Soc. Am. Proc. 32:720-724.

Ruina, A. 1978. Influence of coupled deformation-diffusion effects on the retardation of hydraulic fracture. In: Proc. U.S. Sym. Rock Mech., Rapid City, SD. 19:274-282.

Rummel, F. and O. Kappelmeyer. 1982. The Falkenberg geothermal frac-project: Concepts and experimental results. Hydraulic Fracturing and Geothermal Energy. Nemat-Nasser, S., H. Abe and S. Hirakawa.(eds.) Martinus Nijhoff Pub. The Hague. 59-74.

Scheidegger, A.E. 1960. On the connection between tectonic stresses and well fracturing data. Geofisica Pura e Applicata. 46:66-76.

Scheidegger, A.E. 1965. Discussion of paper by P.E. Gretener, "Can the state of stress be determined from hydraulic fracturing data?". J. Geop. Res. 70:6213.

Schlichting, H. 1960. Boundary Layer Theory. McGraw Hill. New York. 647.

Schmidt, R.A. 1977. Fracture mechanics of oil shale: Unconfined fracture toughness, stress corrosion cracking, and tension test results. In: Proc. 18th U.S. Sym. Rock Mech. 1-6.

Schmidt, R.A. 1980. A microcrack model and its significance to hydraulic fracturing and fracture toughness testing. in Proceedings 21st U.S. Symposium Rock Mech. Univ. Missouri, Rolla, Mo. 581-590.

Scott, P.P., W.G. Bearden and G.C. Howard. 1953. Rock rupture as affected by fluid properties. Petr. Trans. AIME. 198:111-124.

Secor, D.T. and D.D. Pollard. 1975. On the stability of open hydraulic fractures in the earth's crust. Geophysical Research Letters. 2:510-513.

Settari, A. 1980. Simulation of hydraulic fracturing processes. Soc. Petr. Eng. J. 487-500.

Settari, A. 1983. A new general model of fluid loss in hydraulic fracturing, SPE Paper 11625. In: Proc. SPE Sym. Low Permeability, Denver, CO. 219-228.

Settari, A. 1985. Quantitative analysis of factors influencing vertical and lateral fracture growth, SPE Paper 13862. In: Proc. Low Perm. Gas Res. Sym., Denver, CO.(May) 117-128.

Settari, A. 1988. Quantitative analysis of factors influencing vertical and lateral fracture growth. SPE Production Engineering. 3:310-322.

Settari, A. and M.P. Cleary. 1982a. Development and testing of a pseudo-three-dimensional model of hydraulic fracture geometry, SPE Paper 10505. In: Proc. 6th SPE Sym. Res. Sim., New Orleans, LA. 187-215.

Settari, A. and M.P. Cleary. 1982b. Three-dimensional simulation of hydraulic fracturing, SPE Paper 10504. In: Proc. 6th SPE Sym. Res. Sim., New Orleans, LA. 159-186.

Settari, A. and M.P. Cleary. 1984. Three-dimensional simulation of hydraulic fracturing. J. Petr. Tech., Trans. AIME. 1177-1190.

Settari, A. and M.P. Cleary. 1986. Development and testing of a pseudo-three-dimensional model of hydraulic fracture geometry. SPE Production Engineering. 449-466.

Settari, A. and H.S. Price. 1984. Simulation of hydraulic fracturing in low permeability reservoirs. Soc. Petr. Eng. J. 24:141-150.

Shaffer, R.J., R.K. Thorpe, A.R. Ingraffea, and F.E. Heuze. 1984 Numerical and physical studies of fluid-driven fracture propagation in jointed rock. SPE Paper 12881, In: Proc. SPE/DOE/GRI Unconventional Gas Recovery Symp., Pittsburg, PA. 471-476.

Sherard, J.L. 1973. Embankment dam cracking. Embankment Dam Engineering. Hirschfeld, R.C. and S.J. Poulos.(eds.) John Wiley & Sons. New York. 271-353.

Shockey, D.A., K.C. Dao and R.L. Jones. 1979. Effect of grain size on the static and dynamic fracture behavior of titanium. Mechanisms of Deformation and Fracture. Easterling, K.E.(ed.) Permagon Press. Oxford. 77-85.

Shoji, T. and S. Takenouchi. 1982. Hydraulic fracturing in geological processes: A review. Hydraulic Fracturing and Geothermal Energy. Nemat-Nasser, S., H. Abe and S. Hirakawa.(eds.) Martinus Nijhoff Pub. The Hague. 175-190.

Smart, P. and J.W. Dickson. 1979. Deformation and shear of normally consolidated flocculated kaolin. Mechanisms of Deformation and Fracture. Easterling, K.E.(ed.) Permagon Press. Oxford. 129-136.

Smith, E. 1981. Some observations on the viability of crack tip opening angle as a characterising parameter for plane strain crack growth in ductile materials. Int. J. Fracture. 17:443-448.

Smith, M.B., W.K. Miller, and J. Haga. 1987. Tip screenout fracturing: A technique for soft unstable formations. SPE Production Engineering. 2:95-103.

Smith, S. 1989. Rock fracturing methods: Their development and use. Water Well J.(Feb.) 41-47.

Sneddon, I.N. 1946. The distribution of stress in the neighborhood of a crack in an elastic solid. Proc. Royal Soc. London. 187:229-260.

Snyder, V.A. 1980. Theoretical Aspects and Measurement of Tensile Strength in Unsaturated Soils. Ph.D. Cornell University. 94.

Snyder, V.A. and R.D. Miller. 1985. Tensile strength of unsaturated soils. Soil Sci. Soc. Am. J. 49:58-65.

Spence, D.A. and D.L. Turcotte. 1985. Magma-driven propagation of cracks. J. Geop. Res. 90:575-580.

Stewart, G.W. 1974. Hydraulic fracturing of crystalline rock stimulates yield of two test wells drilled in New Hampshire. Ground Water. 12:46-47.

Stewart, G.W. 1978. Hydraulic fracturing of drilled water wells in crystalline rocks of New Hampshire. New Hampshire Dept. of Resources and Econ. Devel., and Water Resources Research Center. New Hampshire. 161.

Stierman, D.J. 1988. Geophysical monitoring of shallow hydraulic fractures, Unpublished draft report. Univ. of Toledo, Geology Dept.

Stow, S.H., S. Haase and H.O. Weeren. 1985. Waste disposal by hydrofracture and application of the technology to the management of hazardous wastes. In: Proc. Int. Conf. New Frontiers Haz. Waste Manag. EPA/600/9-85/025:138-144.

Streeter, V.L. 1971. Fluid Mechanics. 5th McGraw-Hill Book Co. New York. 755.

Strickland, F.G. 1985. Reasons for production decline in the diatomite, Belridge Oil Field: A rock mechanics view. J. Petr. Tech., Trans. AIME. 521-526.

Strubhar, M.K., W.L. Medlin, S.M. Nabi and F.S. Andreani. 1984. Fracturing results in diatomaceous earth formations, South Belridge Field, California. J. Petr. Tech., Trans. AIME. 495-502.

Sun, Y. and C. Ting. 1988. Introduction to a new apparatus for hydraulic fracturing tests. Geotech. Test. J. 11:288-292.

Tada, H., P.C. Paris and G.R. Irwin. 1985. The Stress Analysis of Cracks Handbook. 2nd Paris Productions Inc. St. Louis. 475.

Tavenas, F.A., G. Blanchette, S. Laroueil, M. Roy and P. La Rochelle. 1975. Difficulties in the in-situ determination of Ko in soft sensitive clays. In: Proc. ASCE-GED Spec. Conf. In-situ Meas. Soil Prop., Raleigh, NC. 1:450-476.

Telelman, A.S. and A.J. McEvily. 1967. Fracture of Structural Materials. John Wiley & Sons, Inc. New York. 697.

Thiem, A. 1906. Hydrologische Methoden. Gebhardt. Leipzig. 56.

Thiercelin, M., R.G. Jeffrey and K.B. Naceur. 1989. Influences of fracture toughness on the geometry of hydraulic fractures. SPE Production Engineering. 4:435-442.

Tyler, L.D. and W.C. Vollendorf. 1975. Physical observations and mapping of cracks resulting from hydraulic fracturing in situ stress measurements, SPE Paper 5542. In: Proc. 50th Ann. Fall Meeting SPE-AIME, Dallas, TX. 1-16.

Vandamme, L., R.G. Jeffrey and J.H. Curran. 1988. Pressure distribution in three-dimensional hydraulic fractures. SPE Production Engineering. 3:181-186.

van Eekelen, H.A. 1980. Hydraulic fracture geometry--Fracture containment in layered formations, SPE Paper 9261. In: Proc. 55th Ann. SPE Fall Tech. Conf. Exh., Dallas, TX. 1-9.

van Poolen, H.K., J.M. Tinsley and C.D. Saunders. 1958. Hydraulic fracturing: Fracture flow capacity vs. well productivity. Petr. Trans. AIME. 213:91-95.

Veatch, R.W. 1983a. Overview of current hydraulic fracturing design and treatment technology--Part 1. J. Petr. Tech., Trans. AIME. 677-687.

Veatch, R.W. 1983b. Overview of current hydraulic fracturing design and treatment technology--Part 2. J. Petr. Tech., Trans. AIME. 853-863.

Vomocil, J.A. and W.J. Chancellor. 1967. Compressive and tensile failure strengths of three agricultural soils. Trans. ASAE. 771-774, 779.

Waltz, J. and T.L. Decker. 1981. Hydro-fracturing offers many benefits. Johnson Driller's Journal. 53:4-9.

Waltz, J.P. 1988. Hydro-frac Basics. Ground Water Age. 22:26-29.

Wang, T., J.A. Stodt, D.J. Stierman, and L.C. Murdoch. Mapping hydraulic fractures using a borehole-to-surface electrical resistivity method. in Symposium on Borehole Geophysics, Society of Exploration Geophysicists, Tucson, AZ, Feb. 1-3.

Warpinski, N.R. 1983. Investigation of the accuracy and reliability of in-situ stress measurements using hydraulic fracturing in perforated cased holes. In: Proc. 24th U.S. Sym. Rock Mech., Golden, CO. 773-786.

Warpinski, N.R. and P.T. Branagan. 1989. Altered-stress fracturing. J. Petr. Tech., Trans. AIME. 41:990-997.

Warpinski, N.R., J.A. Clark, R.A. Schmidt and C.W. Huddle. 1982. Laboratory investigation on the effect of in-situ stresses on hydraulic fracture containment. Soc. Petr. Eng. J. 333-340.

Weertman, J. 1980. The stopping of a rising, liquid-filled crack in the earth's crust by a freely slipping horizontal joint. J. Geop. Res. 85:967-976.

Weidmann, G.W. and W. Doell. 1979. Crazes and the fracture of glassy thermoplastics. Mechanisms of Deformation and Fracture. Easterling, K.E.(ed.) Permagon Press. Oxford. 385-391.

Williams, B.B. 1970. Fluid loss from hydraulically induced fractures. J. Petr. Tech., Trans. AIME. 882-888.

Williams, J.G. 1984. Fracture Mechanics of Polymers. John Wiley and Sons. New York. 302.

Williamson, W.H. and D.R. Woolley. 1980. Hydraulic fracturing to improve the yield of bores in fractured rock. Australian Water Resources Council Technical Paper. 55:1-76.

Wolff, R.G., J.D. Bredehoeft, W.S. Keys and E. Shuter. 1975. Stress determination by hydraulic fracturing in subsurface waste injection. Water Tech. Res., J. AWWA. 519-523.

Wong, H.Y. and I.W. Farmer. 1973. Hydrofracture mechanisms in rock during pressure grouting. Rock Mechanics. 5:21-41.

Yuster, S.T. and J.C. Calhoun. 1945. Pressure parting of formations in water flood operations. The Oil Weekly. March 9. 34-40.

Zhang, Z.M. 1989. Application of hydrofracture principals to grouting in deep foundation. Pile Buck. 1-12.

Zoback, M.D. and D.D. Pollard. 1978. Hydraulic fracture propagation and the interpretation of pressure-time records for in-situ stress determinations. U.S. Symposium of Rock Mechanics. Kim, Y.S.(ed.) University of Nevada. Reno. 14-22.

Zoback, M.D., F. Rummel, R. Jung and C.B. Raleigh. 1977. Laboratory hydraulic fracturing experiments in intact and pre-fractured rock. Int. J. Rock Mech. Min. Sci. Geomech. Abs. 14:49-58.

APPENDIX A

POTENTIAL REMEDIAL APPLICATIONS OF HYDRAULIC FRACTURING

The final decision on the use of hydraulic fractures during remediation will depend on whether the benefits they produce outweigh the effort of creating them. Most of the dissertation deals with the processes and problems of creating hydraulic fractures in soil, but here I will review some of the potential applications and estimate the order of benefits that can be expected. I will assume that fractures of useful size can be created and filled with a permeable proppant.

Most remedial systems that require fluid flow either into or out of the subsurface could benefit from the effects expected to accompany hydraulic fracturing. Pump and treat systems are obvious candidates, as are systems involving vapor extraction, soil flushing, or steam stripping. Hydraulic fractures offer the novel possibility of delivering solid material, formed into granules and mixed with proppant, to the subsurface. Nutrients for microorganisms, or the microorganisms designed for bio-remediation themselves, could be delivered as solid grains to contaminated regions.

Filling a hydraulic fracture with material of low permeability, such as a bentonite-rich soil or grout, was proposed by Huck and others (1980) as a method of isolating contaminated material. This proposal has been investigated experimentally in the lab (Brunsing and Henderson, 1984), and tested in the field at a site near Whitehouse, Florida (Brunsing, 1987). The ability to place a flow barrier beneath a contaminated region without removing overburden is the principal advantage of this application. The principal drawback lies in the inability to verify

continuity of a low permeability layer. It seems to be inevitable that hydraulic fractures break into segments, with unfractured gaps between the segments (e.g. Pollard, 1978). That property, combined with the presence of objects such as tree roots, will cause discontinuities in the fracture-filling that would be impossible to predict and difficult to detect using current methods. It is feasible that hydraulic fractures filled with grout could act as short-term barriers, or impediments to flow, but the likelihood of undetectable discontinuities inhibits their use as long-term barriers.

Increasing the rate of flow from a well is expected to be the most widespread application of hydraulic fracturing in remediation. The magnitude of increase will be site-specific, but a general estimate of what to expect can be obtained from the results of related applications and from theoretical analyses.

DATA FROM FRACTURED WELLS

Records of oil production are irrefutable testimony of the benefits of hydraulic fracturing, and ratios of production rates are a suitable yardstick with which to measure those benefits. According to data from several dozen oil wells (Howard and Fast, 1970; Table A.1), production ratios (production rate after fracture/initial rate) are at least 1.5 and range up to very large values. In general, the ratios range from 1.5 to roughly 10 for wells that were producing before fracturing, and the ratios are very large for wells showing negligible production prior to fracturing.

Production rates, from either fractured or unfractured wells, typically decrease as a function of time due to depletion of the reservoir, clogging of pores, or other processes. Behaviors of fractured wells through time were characterized by Howard and Fast (1970) in their classic monograph,

STATE	FORMATION	RATE OF OIL PRODUCTION in Barrels of Oil per Day Before frx	After frx	Ratio (after/before)
Alaska	Kenai sand	1128	1584	1.4
Calif.	Stephans sand	20	120	6.0
	Vaqueros sand	10	70	7.0
Canada	Beaverhill ls.	0	75	-
	Cardium sand	50	204	4.1
	Villenuve quartz	0	4‡	-
Colorado	Weber sand	20	110	5.5
Illinois	Cypress sand	4	35	8.7
	McCloskey ls.	4	50	12.5
Kansas	Arbuckle ls.	10	40	4.0
	Herrington ls.	670‡	2050‡	3.1
	Kansas City ls.	6	30	5.0
Louisiana	Annona Chalk	5	20	4.0
	Hackberry sand	30	115	3.0
	Marguilana sand	15	104	6.9
Michigan	Richfield ls.	22	150	6.8
New Mex.	Grayburg ls.	15	110	7.3
	San Andres ls.	20	60	3.0
	Mesa Verde	490‡	5000‡	10.2
N.Dakota	Madison ls.	111	295	2.6
Ohio	Berea sand	0	60	-
Oklahoma	Bartlesville sand	25	275	11.0
	Basal sand	80	350	4.4
	Granite wash	120	550	4.6
	Mississippi ls.	trace	168	-
	Pennsylvanian	130	475	3.6
Penn.	Bradford sand	6	55	9.1
Texas	Brown dolomite	6	65	10.8
	Camerina sand	26	230	8.8
	Canyon limestone	50	130	2.6
	Reklaw sand	72	113	1.6
	Strawn sand	10	35	3.5
	Wilcox sand	15‡	1100‡	73.0
West Va.	Benson sand	3.5‡	66.1‡	18.9
Wyoming	Dakota sand	25	125	5.0
	Frontier sand	16	70	4.4
	Madison limestone	473	715	1.5
	Phosphoria ls.	1050‡	3050‡	2.9
	Tensleep saand	20	65	3.2

‡ units of (Mcubic ft./day)

Table A.1. Data describing the production rates from oil wells before and after hydraulic fracturing. From Howard and Fast (1970).

"The effect of [hydraulic] fracturing on both short and long term well productivity has been studied by many investigators, most of whom conclude that, regardless of the kind of treatment, four basic patterns of production behavior have been observed.

Type A: Sustained increase in well production accompanied by a flattening of the production decline curve following treatment.

Type B: Sustained increase in production with the well's highest rate of production after the treatment declining essentially at the same rate established before treatment.

Type C: Transitory increase in production lasting from a few months to several months, after which the well continues to follow the production decline trend observed prior to treatment.

Type D: No increase in production, with the well continuing to follow its established, normal production history.

In no case did a treatment have a discernibly detrimental effect on the production performance of the well."

In one example of a Type A or B result (Fig. A.1), the production rate at a well in North Texas increased by a factor of four, from 20 to 80 barrels of oil per day (bopd), and then gradually decreased to 30 bopd over the subsequent seven months. Interestingly, a second hydraulic fracturing job increased the production rate to 80 bopd (Fig. A.1).

Yields of water wells are also increased by hydraulic fracturing (e.g. review by Smith, 1989). Thirty years ago Koenig (1960) examined data from wells used for waterflooding or waste disposal and reported that 78 percent of those wells showed an increase in yield following hydraulic fracturing. The ratio of yields ranged up to 100, with a median of 5.0. More recently, Stewart (1974, 1978) observed increases in yields from water wells drilled in granite or schist formations in New Hampshire. Yields of one well reported by Stewart increased from 0.30 to 1.82 l/s, (ratio of 6.0),

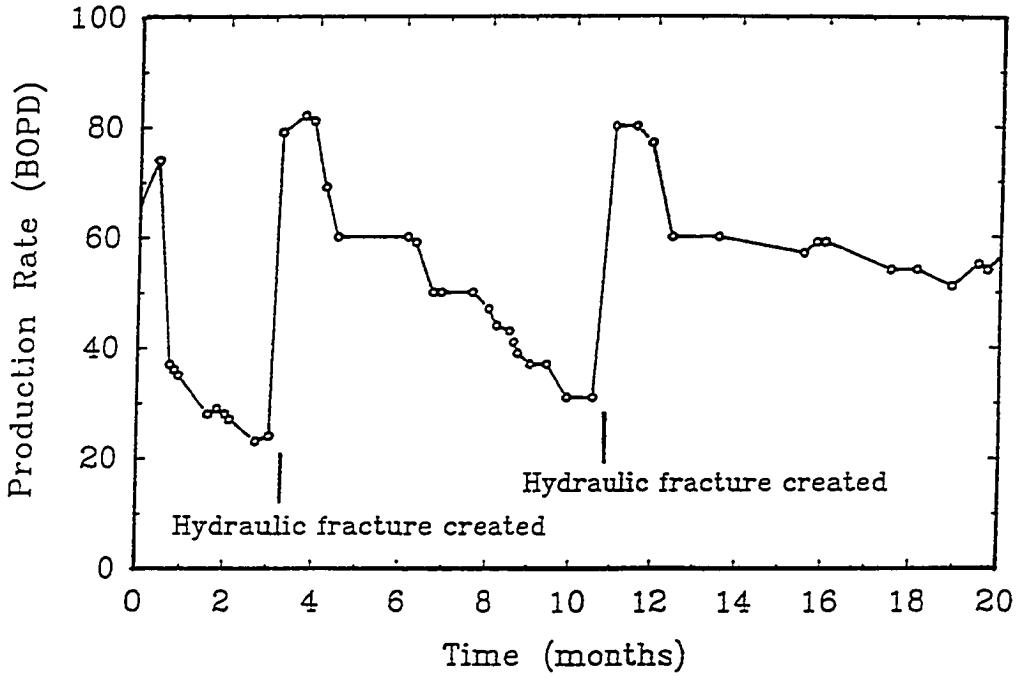

Figure A.1. Production rate of an oil well in Northern Texas. From Howard and Fast (1970).

and at another well yields increased from 0.26 to 1.14 l/s (ratio of 4.4). A particularly impressive increase in yield of 22 to 25 times is described by Mony (1989), who cites a water well drilled in gneiss that yielded 0.0077 l/s prior to fracturing and 0.16 to 0.19 l/s after fracturing. Waltz and Decker (1981) used hydraulic fracturing to stimulate wells in crystalline rock in Colorado and reported ratios of yields of 1.5 to 2.0. Williamson and Woolley (1980) created hydraulic fractures from water wells penetrating igneous or metamorphic rocks in Australia, and cited improvements in specific yield by factors of 5.0 to 6.0. Several other authors (Hurlburt, 1989; Waltz, 1988; Baski, 1987; Macaulay, 1987) have recently claimed that hydraulic fracturing of water wells consistently results in increased yields that are economically significant.

Rates of inflow into wells used for waste disposal (Stow and others, 1985; Wolff and others, 1975; De Laguna, 1966 a and b), or as infiltration galleries are increased by hydraulic fracturing. For example, rates of inflow were measured from five open boreholes intersecting sand-filled hydraulic fractures created in unsaturated glacial till. The fractures were flat-lying, typically 1 cm in maximum thickness and as much as 8 m in maximum dimension (Murdoch and others, 1990).

For comparison, inflow rates were measured from three similar boreholes penetrating unfractured till. Boreholes intersecting hydraulic fractures are EL2, EL5, EL6, EL7, whereas those in unfractured ground are TB1, TB2, TB3.

All boreholes were 5 cm in diameter and 2 m deep. Tests were conducted using Guelph Borehole Permeameter, manufactured by SoilMoisture Inc., Santa Barbara, Ca. Flow rates were measured while maintaining a constant water depth of one meter above the bottom of the borehole using the permeameter.

Rate of inflow into unfractured boreholes diminished slightly with volume, approaching steady-state rates after one to three liters. The steady-state rates were between 0.04 and 0.07 l/min, depending on the well, and the average rate was 0.055 l/min.

The rate of inflow into the wells intersecting hydraulic fractures also diminished with time, but larger volumes, as much as several tens of liters, were required to achieve steady-state. Initially, inflow rates were as rapid as 2 to 3 l/min, the upper limit that could be supplied by the permeameter. The rates diminished with volume, but they were greater than those of the unfractured wells even after large volumes. For example, the rate of inflow was roughly 0.4 l/min after 200 liters of water flowed into EL7, and the rate was 0.175 after 350 liters flowed into EL4. Steady inflow into the fractured wells occurred at 0.30 l/min.

In the previous works cited above, effects of a hydraulic fracture were illustrated using the ratio of flow after fracturing to flow prior to fracturing. The method used to create the hydraulic fractures precluded measuring inflow at a well before it was fractured, so the average inflow into an unfractured well will be used to determine the ratios (Table A.2). Values range from 3.1 to 9.0 for steady-state conditions, and they are typically several times greater than that for unsteady state (Fig. A.2).

Inflow into the boreholes that intersect fractures probably would have been greater if screen and gravel packing was used to prevent collapse. The boreholes filled with mud to depths of several dm while they contained water during inflow testing. Nevertheless, the data do suggest that hydraulic fractures in unsaturated ground could provide marked improvements to remedial systems based on soil flushing.

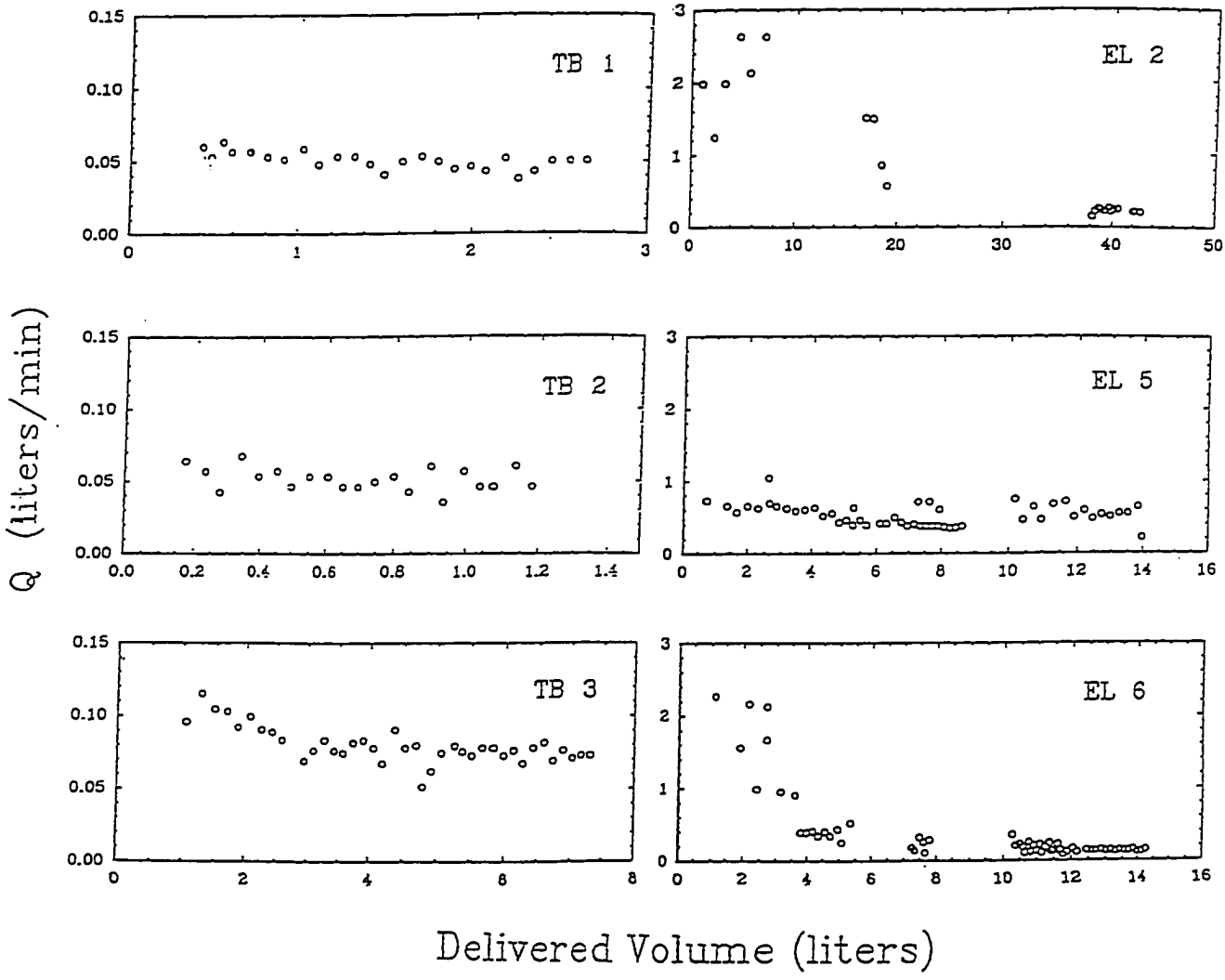

Figure A.2. Rates of inflow into boreholes in silty clay till. TB1, TB2, TB3, are in virgin ground, whereas EL2 through EL7 are borings in ground that has been hydraulically fractured.

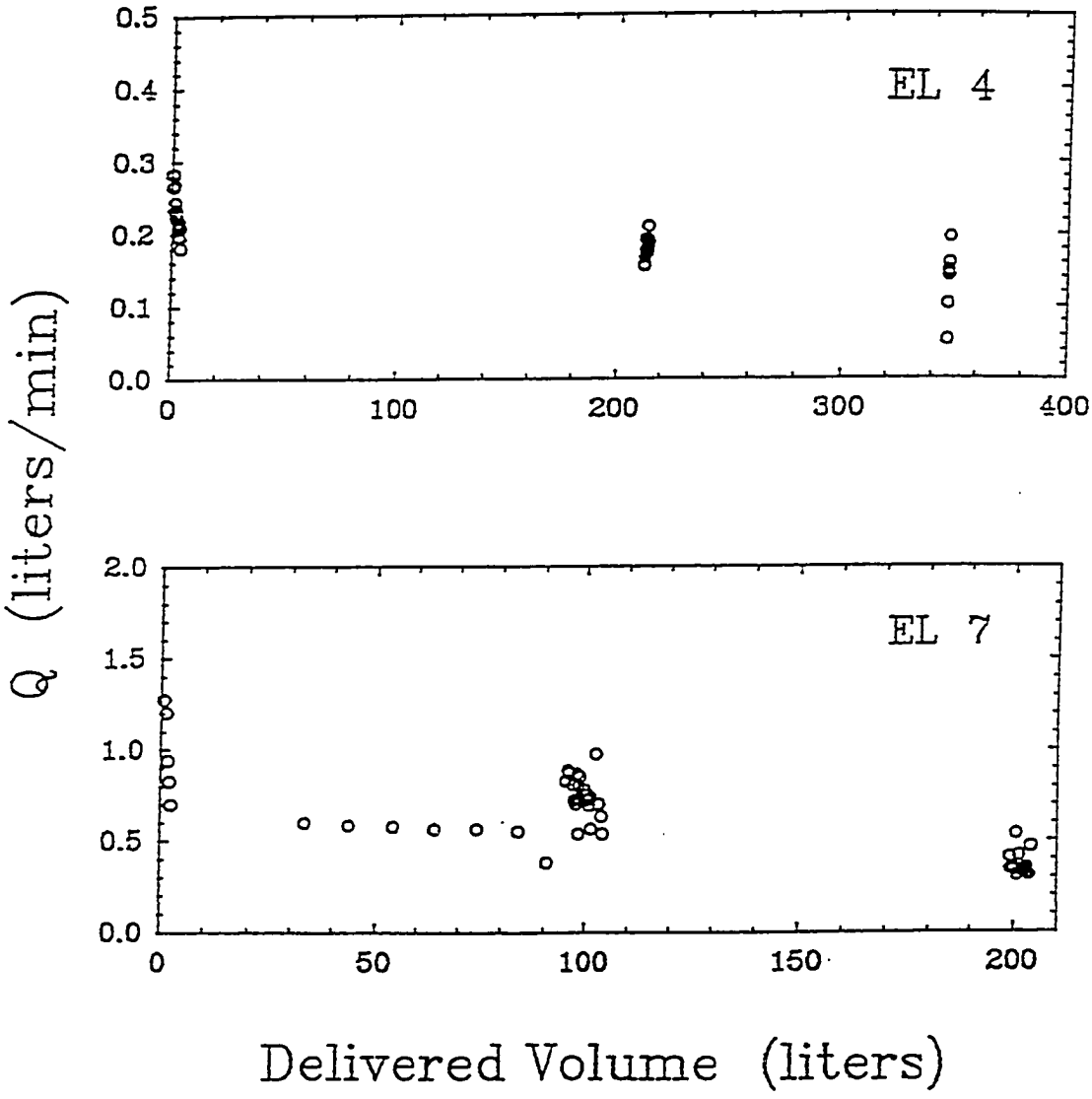

Figure A.2. (continued)

Table A.2 Inflow Rates Into Glacial Till

Borehole	Steady inflow l/min	Average	Ratio
TB1	0.04		
TB2	0.05		
TB3	0.075	0.055	
EL2	0.20		3.6
EL4	0.175		3.1
EL5	0.50		9.0
EL6	0.20		3.6
EL7	0.40	0.30	7.3

Wells used for purposes ranging from delivery of water in unsaturated soil to recovery of oil in reservoirs have shown strikingly similar responses after hydraulic fracturing: their yield is consistently increased, and the magnitude of increase ranges up to several orders of magnitude or more. Typically, the ratio of yields is roughly 1.5 to 8 or 10 for wells that are producing prior to fracturing, but it can be greater than 10 for wells that are initially poor producers.

PREDICTING FLOW TO WELLS THAT INTERSECT FRACTURES

Early schemes of predicting flow to wells that intersect hydraulic fractures were based on empirical studies, electrical analogs, and simple theory. Results were obtained for fractures that were either vertical and rectangular in shape (Prats, 1961, McGuire and Sikora, 1960; Dyes and others, 1958; van Poolen and others, 1958), or horizontal and circular in shape (Landrum and Crawford, 1961; Hartsock and Warren, 1961; Morrisson and Henderson, 1960). Today, those schemes are

important for simple calculations, but more sophisticated numerical models (Gringarten, 1982; Cinco-Ley and others, 1981, 1978) are available for detailed analyses.

Many of the available analyses can be used to obtain the specific yield of a well intersecting a hydraulic fracture, which when divided by the specific yield of the well without a fracture results in a dimensionless measure of the improvement of the well. This ratio will be termed the recovery capacity J in the following pages. Recovery capacity in general depends on conditions of the fracture, such as its size, shape, aperture, location, and permeability of proppant, and on conditions of the reservoir or aquifer, such as its permeability, dimension, and the location of the well within it.

Two analyses will provide useful insights: one that shows the importance of fracture length, relative transmissivity, and radius of influence at steady-state, and another that shows the importance of fracture length as a function of time. Prats (1961) analyzed the effect of a vertical fracture of finite permeability k_f and thickness d in a confined aquifer bounded laterally by surfaces of constant pressure (an alternative solution to the one described by Prats is presented in Appendix C). Relative transmissivity T_r is defined by Prats (1961) as

$$T_r = 2k_f d/\pi k_s a \qquad (1.1)$$

where k_s is the permeability of enveloping soil or rock, a is fracture half-length. Prats describes T_r as the ratio of the ability of fluid to travel along the fracture to the ability of fluid to travel through the enveloping material and reach the fracture. The flow at the fracture increases with relative transmissivity for values of T_r between 0 and 1.0. For values of T_r greater than 1.0, however, the effect of T_r is negligible

(Prats, 1961) and the fracture behaves at steady-state as if its permeability were infinite. This result is important because it indicates that in many field cases the permeability of a propped hydraulic fracture can be assumed to be essentially infinite, thereby avoiding analytical difficulties associated with fractures of finite permeability.

Assuming that the relative transmissivity is essentially infinite, the steady-state recovery capacity is

$$J = ln(r_e/r_w)/ln(r_e/(L/4)) \qquad (A.2)$$

in which r_w is the actual radius of the well, and r_e is the effective radius of the area drained by the well, and L is the total fracture length. In a field of regularly-spaced wells, for example, the effective radius is roughly half the spacing between wells.

According to eq. (A.2) the steady-state behavior of the fracture is the same as that of a well whose radius is equivalent to $L/4$. A vertical fracture 10 m long would behave as a well 2.5 m in radius, so that the equivalent radius of a fracture can be much larger than most wells.

Recovery capacity certainly increases with fracture length, but its magnitude depends on the ratio of fracture length to effective radius. According to this analysis, the recovery capacity will be greatest when the fracture extends across the area drained by the well. Assuming $L = 2r_e$, the maximum J is

$$J_{smax} = 1.44\ ln(L/2r_w) \qquad (A.3)$$

For example, 2.3 is the maximum recovery capacity of a fracture 10 times as long as the radius of the unfractured well, whereas the value increases to 5.6 for a fracture 100 times the well radius, according to this analysis.

As the effective radius increases, the steady-state recovery capacity decreases and approaches unity. For a single well in a large aquifer, therefore, the steady-state yield from a fractured well will approach that of one from an unfractured well. This conclusion is misleading, however, because it ignores potential increases in yields during the transient period of recovery before steady-state is achieved.

Recovery capacity is typically greatest shortly after fracturing and then it decreases with time, as shown in Figure A.1 for example. A solution to the transient recovery capacity can be obtained in analytical form from dimensionless drawdown functions for a well and for a fracture. Dimensionless drawdown of a vertical well in a confined aquifer of thickness h is obtained by assuming the well behaves as a line sink (Ramey, 1967), so

$$2\pi hKp/Q = s_{dw}(1/t_{dw}) \qquad \text{(A.4)}$$

where

$$t_{dw} = 4tKh/Sr^2 \qquad \text{(A.5)}$$

and K and S are the hydraulic conductivity and the storage coefficient of the aquifer, respectively; p, Q, and r are the drawdown, pumping rate and radius of the well, respectively. The drawdown function $s_{dw}(1/t_d)$ is an exponential integral given by Ramey (1967) and polynomial approximations of the integral are in Abramowitz and Stegun (1964).

Hydraulic fractures are commonly idealized as planar sinks in flow problems because analytical solutions to several relevant geometries are available. Solutions to dimensionless drawdowns due to planar sinks can be reduced to forms similar to those for a line sink

$$2\pi hKp/Q = s_{df}(t_{df}) \tag{A.6a}$$

where

$$t_{df} = t_{dw}/n \tag{A.6b}$$

and

$$n = (2a/r)^2 \tag{A.6c}$$

in which a is a characteristic length, such as the radius of a circular sink (fracture). Drawdown functions s_{df} have been published for an envelope-shaped vertical fracture (Gringarten, and others, 1974), a circular horizontal fracture (Gringarten and Ramey, 1974), and functions for other shapes can be determined using methods given by Gringarten and Ramey (1973).

Solving eqs. (A.4) and (A.6) for recovery capacity leads to

$$J(t_{df}) = Q_f p_w / p_f Q_r = s_{dw}(1/nt_{df})/s_{df}(t_{df}) \tag{A.7}$$

where the drawdown function used for $s_{df}(t_{df})$ depends on the geometry of the problem. Accordingly, in this formulation improvements in recovery indicated by $J > 1.0$ are a result only of the difference in geometry between a sheet-like fracture and a line-like well.

Many hydraulic fractures created at shallow depths (less than roughly 300 m) are flat-lying and roughly equant, a geometry that can be approximated by a planar sink that is flat-lying and shaped like a circular disk. The drawdown function for a fracture of that geometry in a confined aquifer (e.g. Gringarten and Ramey, 1974; eqs. 51 and 53) was used in eq. (A.7) to produce Figure A.3. The ratio of aquifer thickness T to well radius r was held constant and equal to 250, and the fracture was assumed to be at mid-height in the aquifer (z/T = 0.5 where z is the height of the fracture above the bottom of the aquifer). Recovery capacity was determined as a function of time for ratios of a/r between 50 and 1000. The radius of the fracture equals the aquifer thickness when a/r equals 250, and it is four times the aquifer thickness when a/r equals 1000. Although the dimensionless form is valuable for many applications, a reference value of t_{df} may be helpful in some cases: if K = 10^{-4} cm/sec, S = 0.001, a = 10 m, T = 11.6 m; then t_{df} x 10 = t in days.

Results of the analysis indicate that the recovery capacity at any given time increases with relative fracture length. Recovery capacity is roughly unity when a/r = 50, indicating that the recovery from a fracture 50 times the radius of a well will be similar to that of an unfractured well. As the ratio a/r increases to 1000, the value of J increases to 8.0, and even greater values of J are obtained for earlier times or longer fractures.

Magnitudes of J diminish with time because geometric advantages of a planar sink decrease compared with those of a line sink as water is removed from regions at increasingly greater distances from the sinks. Even at relatively large values of t_{df}, however, the recovery capacity is significantly greater than 1.0 (Fig. A.3), indicating that the fracture is performing better than the well. The performance of the fracture would be even better if it was assumed that the well draining the fracture was screened for the full thickness of the aquifer, which is a reasonable assumption

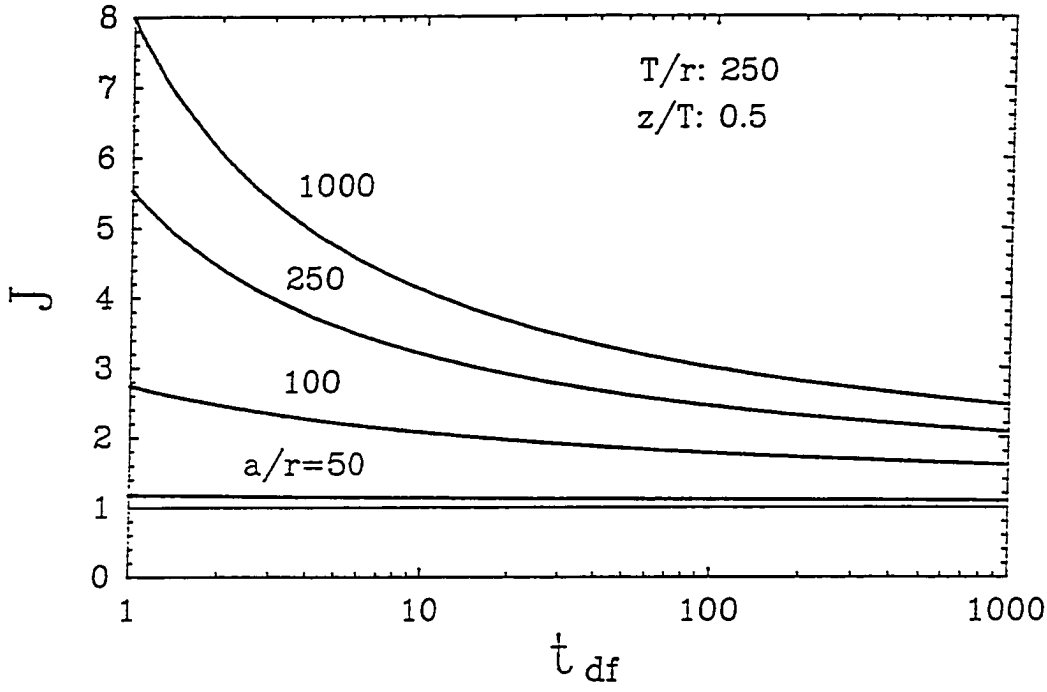

Figure A.3. Recovery capacity of a flat-lying, circular fracturing in a confined aquifer.

for most applications. That case can be approximated by adding 1.0 to the right hand side of eq. (1.7), or to values of J shown in Figure A.3.

SUMMARY

In the previous section we have seen that hydraulic fracturing increases the yields (or inflow rates) of oil and gas wells, water wells, and infiltration wells. The magnitude of increase is consistently between 1.5 and 5 times, routinely as much as 10 times, and in some cases much more than 10 times. In general, hydraulic fracturing offers the greatest relative increase to wells which show poor yields prior to fracturing. Of course, if the initial yield of a recovery well is extremely low, even the improvement offered by hydraulic fracturing may be insufficient to make recovery a viable remedial solution. That judgement will depend on analyses of costs, which exceed the scope of this investigation.

Observations indicate that yields of fractured wells diminish with time, just as they do at unfractured wells. The relative improvement of the well diminishes following fracturing, but the effect of the fracture can be important even after many months or longer. In some cases, wells can be re-stimulated and their yields increased by creating another hydraulic fracture.

A simple theoretical analysis, based on the difference in shape between plane and line sinks, predicts improvements in specific yield that are similar, both in magnitude and behavior with time, to improvements observed in the field. It follows that improvements in yield result principally from the geometric effects of the fractures.

It seems reasonable to expect that the magnitude of increase in yields of contaminant recovery wells will be similar to that of wells used to recover oil,

natural gas, or water from rock. Hydraulic fractures are expected to increase the yields of recovery wells in soil or rock by several times, or perhaps up to an order of magnitude. Detailed predictions of the effects of hydraulic fractures at a particular site will require more sophisticated analyses, but the general magnitude of the improvement in yield predicted by the data and analyses described above justifies further investigation into this process.

APPENDIX B

OTHER STUDIES OF HYDRAULIC FRACTURING

To some investigators hydraulic fracturing is a blessing, to others it is a curse. The difference depends on the effect of fracturing on particular processes, and it has resulted in two different approaches to studying hydraulic fracturing. When hydraulic fracturing produces useful results, such as increasing the yield of a well, providing a measure of in-situ stress, or generating insight into a geologic process, investigators generally focus on predicting characteristics of the fracture (e.g. size, shape, orientation). When hydraulic fracturing causes problems, such as collapsing a dam, compromising a permeability test, or bleeding off grout or waste from a borehole, however, investigators generally focus on predicting, and thus preventing, initiation. To the latter group, the characteristics of hydraulic fractures are of little interest.

A thorough review of the vast body of published work related to hydraulic fracturing would fill several volumes, so the following section is intended only as a brief overview. Other reviews relevant to the present work have been published by Cleary (1988), Mendelsohn (1984), Veatch (1983 *a* and *b*), Geertsma and Haafkens (1979). The classic SPE monograph on hydraulic fracturing by Howard and Fast (1970) is a valuable source, and a revision of that monograph will be published in the near future.

THE HYDRAULIC FRACTURE AS A TOOL

As early as the mid-1930s it was widely recognized by workers in the petroleum industry that pressurizing a well could fracture the enveloping formation (Yuster and Calhoun, 1945). The first use of proppants to hold fractures open, however, was the key to developing a technique of widespread importance. The first

description of the creation of propped fractures is generally attributed to Clark (1949), who outlined a process that closely resembles the ones used today. Clark claimed that hydraulic fractures had been created at 32 wells when his paper was submitted for publication in 1948. Several years later in 1953, a patent of the hydraulic fracturing method was reissued to R.F. Ferris, a colleague of Clark (Howard and Fast, 1970).

During the 20 years following Clark's paper the application of hydraulic fracturing to oil and gas wells became routine, and by 1968 the technique had been used at roughly 500,000 wells (Howard and Fast, 1970). Success rates, indicated by an increased yield after fracturing, were between 75 and 80 percent during the early years, but they increased to nearly 90 percent by the late 1960s, according to Howard and Fast (1970).

Typical fracturing operations pumped volumes on the order of several thousand to several tens of thousands of gallons prior to 1970, but in the following years the sizes of fracturing jobs increased to a miliion or more gallons. These so-called massive hydraulic fractures opened oil reserves that could not be economically produced using previous methods. The costs of creating massive hydraulic fractures spurred the modern era of research into methods, materials, analyses and designs of hydraulic fracturing.

Petroleum companies are the primary users of hydraulic fractures, but they are by no means the only ones. The generation of thermal energy from hot dry rocks is a technology that makes use of hydraulic fractures to create flow paths in basement rock. In principle, two wells drilled into hot rock are linked together by one or more hydraulic fractures (e.g. Murphy, 1982; Ernst, 1980). Cold water is injected into one well, it flows through the hydraulic fractures and is heated by the

wall rocks, and then is recovered at the other well where it is used to drive turbines for electrical power. This application was successfully implemented in a small-scale test at Fenton Hill, New Mexico, where two wells 2.75 km in depth were connected by a fracture 0.3 km in height (Kerr, 1987; Murphy, 1982). The hydraulic fracture acted as a heat exchange producing 3 megawatts of power. A second phase of that project, intended to create larger fractures and produce more power, encountered difficulties. Two boreholes were drilled to depths of 4.6 km, but hydraulic fractures created at one well failed to intersect the neighboring well. Presumably injection resulted in slippage along many natural joints rather than dilation of a single fracture (Kerr, 1987). In a related project in Cornwall, England, investigators used gel to open natural fractures, successfully creating a circulation loop between two wells. This project was producing 5 megawatts of thermal power after two years of operation (Kerr, 1987). Similar projects involving the circulation of water through hydraulic fractures linking two boreholes have been evaluated in France (Cornet and others, 1982), and Germany (Rummel and Kappelmeyer, 1982).

Proppant was omitted from fractures created during the projects cited above, because thermal breakdown of the guar gum-based gel used to transport proppant could cause sand to plug the well casing during fracturing. A modified gel, intended for use at high temperatures, was employed by Nakatsuka and others (1982), who created hydraulic fractures used to recover wet steam at the Nigorikawa geothermal field in Japan. They injected as much as 81 metric tons of sand per fracture, and increased the yields of steam or hot water by factors as great as 2.3.

Water wells can be stimulated by hydraulic fracturing, as indicated by data cited in a previous section. Most of the applications are to water wells in igneous or metamorphic rock, where the natural permeability is low and the wells are initially nearly dry (Hurlburt, 1989; Waltz, 1988; Baski, 1987; Macaulay, 1987; Williamson

and Wooley, 1980; Stewart, 1974, 1978). The use of proppant in hydraulic fractures at water wells is unnecessary in many cases because sufficient yields can often be achieved using water alone (Smith, 1989; Baski, 1987; Williamson and Woolley, 1980). Presumably this occurs because fractures in hard rock can be held open by asperities on fracture surfaces (Paillet, 1985; Detournay, 1979). Omitting proppant from a fracture eliminates the need for a blender and a sand supply, considerably reducing the expense of the fracturing operation.

Several other industries that use wells to gain access to the subsurface have applied hydraulic fracturing. The mining industry, for example, extracts soluble minerals such as halite, sylvite, sulfur, or uraninite by circulating fluids through natural ore deposits. Solution mining operations commonly employ two wells, one to produce and another to inject fluid. Hydraulic fractures are used to increase the flow rate between the two wells, in a design similar to that of geothermal energy operations (Haimson and Stahl, 1970).

Various industries have disposed of wastes by injecting them into hydraulic fractures. In 1958, injecting radioactive waste into hydraulic fractures was first considered by the Atomic Energy Commission as a means of disposal (De Laguna, 1966). This application was evaluated for 20 years at the Oak Ridge National Laboratory (Stow and others, 1985), where radionuclides were mixed with cement-based grout and injected into a shale formation. The grout formed nearly flat-lying hydraulic fractures roughly 300m below the ground surface (Stowe and others, 1985; Holzhausen and others, 1985 *a* and *b*; De Laguna, 1966).

Deep well injection is a popular technique of waste disposal that can either benefit or suffer from hydraulic fracturing. On one hand, hydraulic fracturing during deep well injection will increase the rate of injection (Bouwer, 1978) and

thereby reduce the cost of disposal. On the other hand, hydraulic fractures can propagate upward from the bottom of the disposal well, cutting through low permeability formations intended to isolate the waste and possibly contaminating overlying aquifers (Wolff and others, 1975).

The state of stress in the earth's crust is a central topic of interest to investigators of tectonics, structural geology, earthquake prediction, mining, well stimulation, soil or rock mechanics, and related disciplines. Hydraulic fracturing has been used by those scientists since the early 1960s, when Scheidegger (1960, 1965), Kehle (1964), and Fairhurst (1964) proposed that the pressure required to initiate a hydraulic fracture from a well bore was related to the magnitude of in-situ stress. Their method idealizes a wellbore as a pressurized cavity and assumes that hydraulic fracturing occurs when the magnitude of tensile stress in the wall of the cavity exceeds the tensile strength S of the formation. Assuming the wellbore is a long cylindrical cavity in a porous formation, the maximum horizontal compressive stress is given by

$$s_{Hmax} = S + 3s_{Hmin} - p_w - p_o \qquad (A.8)$$

in which p_w is the pressure in the wellbore at the onset of fracturing, s_{Hmin} is the minimum horizontal compressive stress, and p_o is the pressure of pore-fluid in the formation.

To solve eq. (A.8), tensile strength S is determined by testing core samples and the pressures p_o and p_w are obtained from transducer measurements before and during fracturing. The minimum confining stress s_{Hmin} is generally equated to the wellbore pressure at the instant the fracture closes shut after pumping has ceased (termed the instantaneous shut-in pressure, or ISIP). Kehle (1964) presents an

eloquent argument supporting the use of the ISIP in determining s_{Hmin}. Most investigators agree that the ISIP is marked by a subtle change in slope of the pressure record after pumping has ceased, but there are a variety of methods of estimating this pressure (e.g. Aamodt and Kuriyagawa, 1982; McLennan and Roegiers, 1982; Gronseth, 1979; Nolte, 1979; Bjerrum and Anderson, 1972). The methods of Nolte and Smith (Nolte, 1979, 1982; Nolte and Smith, 1981, 1987; Smith, 1981) are particularly robust, yielding not only s_{Hmin} but leakoff coefficients, proppant schedules, and other parameters used to design hydraulic fracture treatments.

Flaws in the walls of boreholes, either natural fractures or cracks created during drilling or perforating a well, will nucleate hydraulic fractures and cause errors in in-situ stress measurements if they are overlooked (Warpinski, 1983). Abou-Sayed and others (1978) present theoretical analyses based on linear elastic fracture mechanics that account for pre-existing cracks in a borehole during in-situ stress measurement. Their analysis requires knowing the size and shape of pre-existing fractures intersecting the borehole, information that is generally difficult to obtain for naturally-occurring fractures. This difficulty is avoided by deliberately cutting a notch of known dimension in the wall of the borehole to dominate the effects of natural fractures.

Geologists have recognized natural features that formed by processes closely resembling hydraulic fracturing. The features are tabular in form and are filled by materials that differ in composition or texture from enveloping material. Igneous sheet intrusions (Pollard, 1978), clastic dikes (Shoji and Takenouchi, 1982), hydrothermal breccia dikes (Bryant, 1968; Farmin, 1934), and some mineralized veins (Kesler and others, 1981; Anderson, 1974; Phillips, 1972 and 1973) are interpreted as resulting from natural processes related to hydraulic fracturing. High

pore pressures induced by seismic shocks accompanying earthquakes (Holzer and others, 1989) can fracture overlying sediments and erupt at the ground surface as sand blows, or sand boils (Shoji and Takenouchi, 1982).

Studies of those natural features have certainly benefited from research conducted by the petroleum industry, but it has by no means been a one-way street. Natural analogs to hydraulic fractures can be studied directly where they are exposed at the ground surface, a luxury seldom afforded investigators in the petroleum industry. Much of what is known about the details of large-scale fractures has been derived from studies of exposures of igneous dikes and sills. In their argument for the state of stress as a fundamental control of the orientation of hydraulic fractures, for example, Hubbert and Willis (1957) first noted the mechanical similarity between dikes and hydraulic fractures. Then they cited the similarity between the pattern of dikes at Spanish Peaks, Colorado, and the pattern of principal stresses calculated by Ode (1957). Later, Pollard (1978, 1973) and Pollard and others (1975) showed that dikes and sills are tabular in gross form, but are discontinuous in detail. The discontinuities are particularly well-developed near leading edges, where they appear as segments, or elongate lobes. Pollard (1978) argues, by analogy, that hydraulic fractures should also be discontinuous, and his argument is supported by later theoretical analyses (Pollard and others, 1982) showing how a fracture could break into segments in response to small fluctuations in the in-situ state of stress. This insight is significant because it suggests that hydraulic fractures filled with grout and used as barriers to flow (Huck and others, 1980; Brunsing, 1987) could be plagued by imperfections that compromise the integrity of the barrier. Furthermore, the performance of fractures filled with sand and used as drains could be reduced if some of the sand is isolated in discontinuous lobes (Pollard, 1978).

Experiments

Experiments conducted in the laboratory or the field have contributed to useful applications of hydraulic fracturing. Laboratory experiments are designed to measure material properties, to test theories, or to illustrate effects of processes that are difficult to analyze theoretically. Fracture toughness is a material property, which was introduced to predict fracture in metals (Irwin, 1957), but has been applied the prediction of fracture in rock as well. Traditionally, fracture toughness has been ignored (set to zero) because the energy required to overcome viscous forces in large fractures is several orders of magnitude greater than the energy required to overcome material toughness (Cleary, 1980a). Recently, however, it has been recognized that fracture toughness can affect aperture and shape in cross-section (Spence and Turcotte, 1985; Nilson and Griffiths, 1986; Abe and others, 1976), and that natural variations in toughness can affect the shape of the leading edge of a hydraulic fracture (Thiercelin and others, 1989).

Methods of measuring fracture toughness of rock differ widely in specimen geometry and type of loading, but they all have one feature in common: the use of a large notch, or starter slot, cut in the sample. The starter slot nucleates failure at a pre-existing fracture of known dimension, thereby avoiding the problem of characterizing effects of naturally-occurring cracks or flaws. Some methods are adaptations of ASTM techniques, which apply external loads to measure fracture toughness of metal specimens (Klepaczko and others, 1984; Ouchterlony, 1982; Cleary, 1978b; Schmidt, 1977), whereas others are patterned after the hydraulic fracturing process and inject fluid to measure fracture toughness (Clifton and others, 1976; Abou-Sayed, 1977).

Early theories (e.g. Haimson and Fairhurst 1967; Kehle, 1964; Harrison and others, 1954) predicted that hydraulic fracturing would initiate when the

circumferential stress on the wall of a borehole exceeded the tensile strength of the formation. This theory was tested by Haimson and Fairhurst (1969) by injecting fluid into cylindrical samples of hydrostone, a gypsum cement exhibiting properties similar to natural rock. They observed that during injection the fluid pressure increased and then abruptly decreased, and they assumed that fracturing, or *breakdown*, initiated at the maximum pressure. According to the elastic solution of Haimson and Fairhurst (1967), breakdown pressure increases linearly with confining pressure, but both the slope and intercept of breakdown as a function of confining pressure decrease if injection fluid penetrates the sample prior to fracturing. Results of their experiments (as well as those of early studies by Harrison and others, 1954; and Scott and others, 1953) showed that fluid penetration reduces the breakdown pressure, similar to the theoretical results. In detail, results of the elastic theory predicted slightly lower breakdown pressures than were actually observed by Haimson and Fairhurst (1969), a difference they attributed to plastic deformation in the walls of the borehole that was omitted by their analysis. Medlin and Masse (1979) performed similar experiments. Their results show that the elastic theory predicts breakdown pressures at relatively low confining stress, but tends to overestimate breakdown when confining pressures exceed some critical value, which depends on rock type. Medlin and Masse (1979) attribute this deviation to plastic deformation induced by the confining stresses, and they offer a modified theoretical analysis that is consistent with their results.

Haimson and Fairhurst (1969) also reported that the breakdown depended on the rate of pressurization; it increased as the rate increased. Zoback and others (1977) offered an explanation by using an increase in acoustic emissions (AE), rather than a change in slope of the pressure record, to indicate the onset of fracturing. According to Zoback and others (1977), during relatively low rates of

pressurization an increase in AE occurred at the same time as the breakdown pressure. As the rate of pressurization increased, the pressure of fracturing (as indicated by AE) remained roughly constant, although the breakdown, or maximum pressure increased dramatically.

Theoretical analyses of fracture propagation have been tested in the laboratory since the first analyses were proposed. Harrison and others (1954) created hydraulic fractures in photoelastic gelatin to verify an analysis of hydraulic fracturing based on elasticity theory and originally published by Sneddon (1946). Fractures they created experimentally had ratios of length to width that were similar to those predicted by the simple theory (Harrison and others, 1954; fig, 6). Moreover, photographs of the experiments revealed fractures that were elliptical in cross-section, the shape predicted by Sneddon's theory. More recently, Medlin and Masse (1984) created fractures in rectangular blocks fitted with ultrasonic transducers to sense the fracture during propagation. Their results show that the injection fluid lags slightly behind the leading edge, resulting in an unwetted zone at the tip of the hydraulic fracture. The existence of an unwetted tip was long suspected on theoretical grounds (Khristianovich and Zheltov, 1955; Barenblatt, 1962). Rates of growth, dilation, and the pressure record during fracturing in the experiments were shown to be consistent with two-dimensional, plane-strain theories of fracture propagation (e.g. Khristianovich and Zheltov, 1955; Geerstma and de Klerk, 1969; Spence and Turcotte, 1985). Those rates were also shown to depend on confining stress, and a possible explanation of this dependence is suggested in Chapter Three.

The orientation of hydraulic fractures normal to the least principal stress is a result obtained nearly universally, from the early studies of Hubbert and Willis (1957), or Haimson and Fairhurst (1969) to the more recent work of Hanson and

others (1979), and Medlin and Masse (1979). Daneshy (1973) showed that the local state of stress induced by a cylindrical borehole can cause the initial orientation of a hydraulic fracture to differ from that favored by far-field conditions. In most of Daneshy's experiments, fractures contained the axis of the borehole where they were adjacent to the hole, but the fractures curved or twisted out of their original plane until they were normal to the direction of least far-field compression at some distance from the hole. Similar results were obtained by Medlin and Masse (1979), who report that the initial orientation of fractures would contain the axis of the borehole and ignore the presence of shallow notches cut in the wall of the hole at orientations favorable to the far-field conditions. Deeper notches overcame the effects of the borehole, nucleating hydraulic fractures in the plane of the notch instead of parallel to the axis of the borehole. The results of those studies are important to field applications, such as the tests described in later chapters, where horizontal fractures are created from vertical boreholes.

Model studies have contributed to the understanding of how hydraulic fractures behave at interfaces between different materials. This behavior is important to applications in the petroleum industry where vertical fractures can be *contained* within a thin formation by overlying and underlying units that inhibit propagation. Daneshy (1976) describes results of some of the first experiments where hydraulic fractures were created in layered media in the lab. He found that the shear strength of the interface was important, with hydraulic fractures cutting across well-bonded interfaces but unable to cut across poorly-bonded ones. Anderson (1979) confirmed this result, presenting qualitative evidence that it is the relative tensile strengths of the materials on either side of the interface, as well as the shear strength and normal loading on the interface itself that determine whether a fracture will cross an interface. Other experiments describing the behavior of a

hydraulic fracture approaching an interface are described by Papadapolous and others (1983), Biot and others (1983), Hanson and others (1978 a and b, 1979), and Pollard (1973).

The distribution of in-situ stresses plays an important role in the forms of hydraulic fractures, according to the results of several laboratory investigations. Warpinski and others (1982) designed a test cell that allowed the radial load on a cylindrical rock sample (20 cm in diameter and 20 cm long) to be varied along the axis of the cylinder. Hydraulic fractures were created in homogeneous samples where radial loads at the ends of the cylindrical axis were 2.0 to 2.75 MPa greater than loads at the center of the axis. They found that a stress contrast of that magnitude alone was sufficient to inhibit growth of a hydraulic fracture out of the zone of diminished confining stress. Similar results were obtained by Ahmed and others (1983), who created fractures in large (1.0 m on a side) blocks of cement grout to reduce effects of exterior boundaries.

The experiments cited above were conducted to examine effects of nucleation and growth; other experiments address processes occurring after a fracture has been created. Of particular interest are processes that could cause a reduction in permeability of the fracture, either by embedment, or crushing of proppant grains (Howard and Fast, 1970). A propped fracture may tend to close if the normal stress on the fracture is great relative to the strength of the formation, leading to embedment of the proppant grains. Results from experimental studies using either chalk or diatomite (Hartley and Bosma, 1985; Strubhar and others, 1984; Strickland, 1985) indicate that embedment is limited to roughly one-half a grain diameter. Permeability is seriously reduced by embedment when the proppant layer is one to two grains thick, but it is only moderately reduced when the proppant is three grains thick, and fracture permeability is unaffected when proppant is

greater than five grains thick (Hartley and Bosma, 1985). Studies of embedment of proppant grains into soil have not been published.

Proppant crushing can occur when the confining stress on the wall of the fracture exceeds the strength of the proppant particles. According to results of experiments reported in Howard and Fast (1970), for example, quartz sand can be crushed at pressures equivalent to depths of two km. At greater depths a high strength proppant, such as aluminum oxide, is generally recommended. Crushing of quartz sand should be of no concern to the relatively shallow applications of remediation.

Experimental investigations of hydraulic fracturing are by no means limited to the laboratory. Field experiments of most of the applications described in the previous section have been conducted to test new ideas or verify new theories. In most field experiments, data are obtained from wells intersecting the fractures, but in a few experiments data have been obtained from the fractures themselves. The pioneering paper by Clark (1949) begins with a description of a shallow hydraulic fracture exposed by excavation. A photograph of the excavation showing a wellbore intersecting a horizontal fracture propped with sand provided Clark with irrefutable evidence that fractures could be created using the process he describes.

An extensive suite of field experiments were conducted at the DOE Nevada Test Site, where hydraulic fractures were created in ash-fall volcanic tuff and excavated using mining procedures (Northrop and others, 1978). The objectives of this program were to evaluate proppant distribution, examine characteristics of a fracture intersecting an interface between different formations, evaluate results of small-volume fractures as a tool for measuring in-situ stress, and compare the size and geometry of actual fractures to those predicted by theory. Results are described

by Warpinski (1983), Northrop and others (1978), Tyler and Vollendorf (1975), and references cited therein.

Analyses

Hydraulic fracturing was proven as a technique of increasing the yields of oil wells long before the physics of the process were understood. As the cost of the fracturing operation increased, however, it became clear that analyses predicting fracture geometry (size, shape, orientation) could be used to maximize recovery performance and minimize expenses. Khristianovich and Zheltov (1955) recognized that the basic physics of hydraulic fracturing involves two processes: the flow of liquid within the fracture, and the dilation of the fracture walls due to deformation of enveloping material. The processes are coupled, though, in that the pressure distribution resulting from viscous losses during flow is strongly dependent on the fracture aperture, but the aperture depends on the amount of dilation caused by the pressure distribution. Dilation of the fracture resulting from material deformation is calculated, with few exceptions, using elastic, or poro-elastic theory. One of the exceptions, a study by Medlin and Masse (1982), showed that effects of plastic deformation during fracturing are detectable in the lab, but are undetectable in field applications of hydraulic fracturing in sedimentary rock. Effects of plastic deformation are generally ignored. Fluid flow within the fracture is commonly assumed to be laminar and governed by a linear viscous behavior. Many fracturing fluids are thixotropic, so nonlinear flow laws have been incorporated into solutions of hydraulic fracture propagation (Pascal, 1986).

Two-dimensional analytical solutions to the problem of a linear viscous fluid driving a fracture in an elastic medium have been derived that yield length, aperture, and driving pressure as functions of time for the following geometries:

1.) Vertical, circular (Perkins and Kern, 1961; Geerstma and de Klerk, 1969 Abe and others, 1976);

2.) Horizontal, circular (Perkins and Kern, 1961);

3.) Vertical, rectangular with large ratio of length to height (Perkins and Kern, 1961; Nordgren, 1972);

4.) Vertical, rectangular with small ratio of length to height (Khristianovich and Zheltov, 1955; Geerstma and de Klerk, 1969; Geerstma and Haafkens, 1979; Nilson, 1981; Spence and Turcotte, 1985; Nilson, 1986; Nilson and Giffiths, 1986) .

Analytical solutions show that the growth of an idealized hydraulic fracture, that is the characteristic length (half-length or radius), L, aperture, A, and fluid pressure, P, as functions of time, t, can be expressed as simple power functions

$$L = C_1 t^b \tag{1.9a}$$

$$A = C_2 t^c \tag{1.9b}$$

$$P = C_3 t^d \tag{1.9c}$$

assuming loss of the injected fluid by flow through the walls of the fractures, or *leakoff*, is negligible. The constants C_1, C_2, C_3 depend on details of each solution (e.g. references cited above), but in general they depend on properties of the injection system and the material containing the fracture. The superscripts b, c, and d, are constants that depend on fracture geometry (Table A.3). The lengths and apertures of both types of vertical fractures, for example, are predicted to grow faster than those of either of the circular fractures. Curiously, however, the pressure record of the Case A (Table A.3) circular fracture would be indistinguishable from the vertical, rectangular fracture of small length:height ratio; pressures would decrease as negative one-third powers of time in both cases.

A horizontal, circular fracture is expected to grow by increasing its radius and compressing adjacent material early in its propagation history, and thus behave as Case A. With continued pumping, however, the fracture could cease to grow radially and increase in volume by lifting its overburden (Case B, Table A.3), either

TABLE A.3. Some Possible Constants In Eq. (A.9)

Geometry	b	c	d
Circular			
Case A*	4/9	1/9	-1/3
Case B**	0	1	1
Vertical, Rectangular			
small L/H	2/3	1/3	-1/3
large L/H	4/5	1/5	1/5

* Vertical fracture, or deep horizontal fracture. Assumes dilation only by elastic deformation of adjacent material.

** Shallow, horizontal fracture. Assumes volumetric growth only by lifting overburden, no radial growth.

because of a mechanical advantage achieved with increasing radius (Pollard, 1973) or because leakoff near the tip increases the sand concentration preventing flow. In either case, the change in mode of growth could be detected because the pressures would begin to increase, approaching a slope of unity for Case B in Table A.3. Similar applications of principles derived from analytical solutions of vertical fractures have been described by Nolte and Smith (1981; 1987).

Analytical solutions require that the fracture geometry is known, and it is simple. Furthermore, details of the fracturing procedure, such as effects of

nonlinear fluid rheologies, transport of proppant grains, leakoff, or back stress, fracture toughness, material interfaces, and nonuniform stress distribution in the host rock cannot be investigated by most analytical solutions. In practice, the fracture geometry is unknown and effects of those and other details can be crucial in a design strategy. As a result, sophisticated computer programs have been developed that offer predictions of the shape of the leading edge of a fracture, and are able to estimate how a wide range of design parameters affects the length, thickness, and distribution of proppant within a hydraulic fracture. There are many dozen, or perhaps more, published descriptions of computer programs used to simulate hydraulic fractures. The capabilities of those descriptions are reviewed and compared by Cleary (1988), Palmer and Luiskutty (1986), Advani and others (1985), Mendelsohn (1984), and Veatch (1983 a and b), so a detailed review seems unnecessary in the present work. Contributions to the development of computer codes that predict fracture geometries in three dimensions have been made by Luiskutty and others (1989), Vandamme and others (1988), Settari (1988; 1985), Bouteca (1988), Acharya (1988), Morita and others (1988), Settari and Cleary (1986; 1984; 1982 a and b),, Abou-Sayed and others (1984), Cleary and others (1983 a and b), Cleary (1978a), and Daneshy (1973). Carter (in Howard and Fast, 1957) presented the first analysis of leakoff, which was refined by Williams (1970), and generalized to include nonlinear effects by Settari (1983). Analyses of relevant effects, including fluid rheology (Settari and Price, 1984; Cleary, 1980 a and b), back stress due to pressure of pore-fluids (Keck and others, 1984; Cleary, 1980 a and b; Ruina, 1978), and heat transfer (Meyer, 1989; Keck and others, 1984; Griffiths and others, 1983; Settari, 1980), proppant transport (Settari and Price, 1984; Daneshy, 1978; Novotny, 1977), and fracture toughness (Theircelin and others, 1989; Morita, and others, 1988; Settari, 1985; van Eekelen, 1980) are commonly included in computer programs analyzing fracture propagation. One of those programs,

described by Boone and others (1989), represents fracture shape, pore-fluid pressure, and stress in the vicinity of a vertical fracture as a color image that changes with time on a video monitor.

Interactions between a hydraulic fracture and the ground surface, a topic of particular interest to the proposed applications, have been analyzed by Pollard and Holzhausen (1979), and Narendran and Cleary (1983). In related work, interactions between multiple hydraulic fractures have been analyzed by Narendran and Cleary (1984), and Hanson and others (1979), and consequences of fracture interactions have been utilized in design concepts by Warpinski and Branagan (1989), Ernst (1980), and Huck and others (1980). Theoretical solutions of a fracture encountering interfaces between materials of differing properties are described by Lam and Cleary (1984), Weertman (1980), van Eekelen (1980), and Hanson and others (1978 a and b).

In addition to forecasting the geometry of hydraulic fracture, the results of theoretical analyses are matched against field measurements, such as injection pressure or deformation of the ground surface, to estimate geometry after the fracture has been created. Methods of inverting pressure records were developed in a series of papers by Nolte and Smith (Nolte, 1988 a and b, 1984, 1982, 1979; Nolte and Smith, 1987, 1981), and other investigators (e.g. Crockett and others, 1989) have made contributions as well. The inversion of measurements of surface deformation--commonly obtained using tiltmeters--to obtain estimates of the location, orientation, and dimensions of a hydraulic fracture was described by Davis (1983), and applied by Holzhausen and others (1985 *a* and *b*).

Another application is the optimization of fracture designs, where the output of a fracture simulator is used as the input of a program that evalutes flow to the

fracture (Anderson and Phillips, 1988) and possibly economic considerations, such as costs of fracturing materials and rate of return (Howard and Fast, 1970; Veatch, 1983 a and b). A simple method of optimization, based on the cumulative volume of recovery and described by Elbel and Sookprasong (1987), is relevant to the application of hydraulic fracturing during remediation.

The work cited above includes some notable contributions, but it is by no means an exhaustive survey of papers that address useful applications of hydraulic fracturing; there are many more. With few exceptions, those papers are targeted to applications where hydraulic fractures are created in rock at depths in excess of several hundred meters. Use of the significant body of existing information for the purposes of this research, therefore, will depend on the extent to which hydraulic fracturing of rock at great depth resembles hydraulic fracturing of soil at shallow depths.

THE HYDRAULIC FRACTURE AS A PROBLEM

Hydraulic fracturing of soil at shallow depths has, in the past, generally been regarded as a problem. This is because many soil engineering techniques, which require increasing ambient pore pressures, will be ruined if they induce hydraulic fracturing--with the exception of hydraulic fractures created to measure in-situ stresses in soil (Leach, 1977; Massarsch and others, 1975; Tavenas and others, 1975; Bjerrum and Anderson, 1972).

Applications

The collapse of a dam is perhaps the most severe consequence of accidental hydraulic fracturing. One example occurred at the Teton Dam, Idaho, where excessive rates of seepage were noted downstream of the dam shortly after the reservoir behind it was filled in 1976. Seepage rates increased and soon a muddy

flow appeared at the downstream toe of the dam. The flow eroded a gully, which cut through the dam from the downstream toe upward to the crest. Fourteen people died and 400 million dollars of property damage resulted from the subsequent failure. An investigation of the tragedy concluded that hydraulic fracturing, due to increases in pore pressure accompanying filling of the reservoir, probably contributed to the dam failure (Jaworski and others, 1979; and references therein). Elsewhere, hydraulic fracturing was attributed as the cause of leaks that ultimately led to the failure of 14 dams in Oklahoma and Mississippi, and other dams in California, Brazil, and China, according to Sherard (1972), and Jaworski and others (1979).

Ironically, hydraulic fracturing was known to workers in the oil industry as a problem during waterflooding before it was used to stimulate wells. Yuster and Calhoun (1945) recognised that a sudden increase in the rate of inflow during a waterflooding operation (a technique of injection water in one well to sweep oil toward a recovery well) without an increase in pressure could be caused by hydraulic fracturing, or in their terminology, pressure parting. Hydraulic fracturing caused by excessive injection pressures can reduce the area swept out by the waterflood. New methods of estimating the maximum allowable pressure without causing fracturing continue to be developed (Singh and Agarwal, 1990).

In-situ permeability of soil is commonly calculated by holding a constant pressure and measuring the rate at which water flows into a borehole. Bjerrum and others (1972) show that hydraulic fractures can be created if the borehole pressure used in a permeability test is greater than a critical value, which they relate theoretically to the overburden load and these soil properties: Poisson's ratio, coefficient of lateral pressure, tensile strength, and compressibility. They point out that hydraulic fracturing can go undetected during a test, but values of permeability

calculated from the resulting data can be as much as three orders of magnitude greater than the actual in-situ permeability.

In some applications, hydraulic fracturing can be either an asset or a liability, depending on the details of the application. The disposal of liquid waste by injection into wells, outlined in the previous section, is one example. Injection grouting is another. Some designs require grout to uniformly permeate pores in the vicinity of an injection point (borehole), and the specifications of these designs cannot be met if grout flows preferentially into hydraulic fractures (Wong and Farmer, 1974). Moreover, hydraulic fracturing during grouting could result in problems, such as deforming a neighboring foundation, lifting a concrete cut-off from its seat, or markedly increasing the amount of grout required to complete a job (Morgenstern and Vaughn, 1963). Interestingly, however, hydraulic fracturing can also play a useful role in grouting practices. Zhang (1989) indicates that intentionally creating hydraulic fractures during grouting increases the rate of penetration of grout in some formations, and it effectively seals formations by creating an interlocking network of grout sheets. The technique is especially useful in formations, such as karstic limestone cut by clay- and sand-filled caves, where conventional grouting techniques are ineffective. Moreover, the load-bearing capacity of large diameter piles in silty sand is increased by creating grout-filled fractures following pile driving, according to Zhang (1989).

Experiments

The goal of many experimental investigations of the applications described above is to predict the pressure at which hydraulic fracturing occurs under a particular set of laboratory conditions. A noteworthy set of experiments is described by Jaworski and others (1979 and 1981), who examined hydraulic fractures in the

vicinities of model wellbores and dam faces. They injected water into cubic blocks of soil, slowly increasing injection pressure and recording flow rate until a marked increase in flow rate indicated the onset of fracturing. This technique is common for other investigations of hydraulic fracturing of soil, although it differs from studies of hydraulic fracturing of rock (e.g. Medlin and Masse, 1979; Zoback and others, 1977; Haimson and Fairhurst, 1967, 1970; Harrison and others, 1954; Scott and others, 1953), which hold flow rate constant and monitor pressure. Jaworski and others (1979) cut slots in the faces of samples and applied pressure to the slots to simulate the role of joints or pre-existing cracks as stress concentrators. Cutting a slot in a sample to nucleate a fracture is common practice in tests designed to measure fracture toughness, as mentioned above.

Significant results of Jaworski and others (1979 and 1981) are as follows:

1. The pressure required to induce hydraulic fracturing from a cylindrical borehole is linearly related to confining stress. A similar relation was observed for the pressure required to induce hydraulic fracturing in rock by Medlin and Masse (1979), and Haimson and Fairhurst (1967, 1970).

2. A large amount of variation was observed in the fracturing pressures, suggesting that fracturing pressure from an open borehole would be difficult to predict. Fracturing pressure was affected by many factors, such as pre-existing flaws in the soil, that could neither be eliminated nor characterized.

3. The fracturing pressure depended on soil properties, increasing with the number of blows used to compact the sample. It increased as the water content decreased.

4. A discontinuity, such as a slot, will nucleate a hydraulic fracture in soil, and the presence of the discontinuity reduces the pressure required to induce fracturing.

In a later study, Mori and Tamura (1987) created hydraulic fractures from cylindrical holes in cylindrical soil samples, using much the same technique as

Jaworski and others (1979). Their results confirm the linear relation between fracturing pressure and confining stress. Mori and Tamura conducted tests using various rates of injection, concluding that the fracturing pressure increased as the rate of pressurization increased. Hydraulic fracturing pressures in rock also increase with rate of pressurization, according to Haimson and Fairhurst (1967 and 1970), and Zoback and others (1977).

In one suite of tests, Mori and Tamura applied an axial load that was less than the radial load. Hydraulic fractures were formed either inclined or normal to the axial hole, leading Mori and Tamura to conclude that shear failure controls hydraulic fracturing of cohesive soil. This conclusion contradicts a large body of solid evidence for hydraulic fracturing being a tensile phenomenon in other materials. It seems likely that the peculiar orientations of fractures observed by Mori and Tamura resulted from boundary conditions on their test samples. As Medlin and Masse (1979) point out, a cylindrical hole will tend to create a hydraulic fracture containing the axis of the hole. The fracture will change orientations, however, as it grows away from the hole and into a region of different stresses--such as would have been the case under the applied stress conditions used by Mori and Tamura. Large changes in orientations during propagation are accomplished by curving, twisting, or breaking into segments (Pollard and others, 1982), resulting in irregular or intricate fracture forms. The results that are briefly described by Mori and Tamura are consistent with behavior as tensile, or Mode I fractures (Lawn and Wilshaw, 1975), propagating in an abruptly changing stress field; their conclusion that hydraulic fractures in cohesive soil behave as shear failures is unconvincing.

An apparatus used to create hydraulic fractures is described by Sun and Ting (1988), who claim that it offers advantages over apparatuses described previously. Their device is designed to create a hydraulic fracture from a cylindrical hole in a

cylindrical sample, which is a standard configuration. The principal novelty appears to be that the pressure acting on the cylindrical hole can be controlled independently from pore pressure in soil adjacent to the hole. This is done by lining the hole with a permeable layer and then inserting a flexible bladder along the length of the lined hole; inflating the bladder controls pressure on the wall of the hole, whereas wetting the liner controls pore pressure in the soil.

Analyses

Studies seeking methods of preventing fracture initiation commonly employ analyses of stresses in the vicinity of pressurized holes. Hydraulic fracturing is assumed to occur when tensile stress exceeds the tensile strength of the material. Analyses of this type were first based on elastic solutions and used to predict hydraulic fracturing of rock (e.g. Harrison and others, 1954; Schiedegger, 1960; Kehle, 1964; Haimson and Fairhurst, 1967), but have been applied directly to predict hydraulic fracturing of soil (Mori and Tamura, 1987; Jaworski and others, 1979 and 1981). Jaworski and others (1979) point out some discrepancies between theory and data, not the least of which is a large amount of variability in the data. This observation leads them to conclude that the criteria represented by the simple theory were insufficient to reliably predict the pressure required to cause fracturing from an open borehole in soil.

Bjerrum and others (1972), who were concerned with inhibiting hydraulic fracturing during field permeability tests, included in their analysis the effect that driving a piezometer would have on state of stress prior to fracturing. They assume that when a piezometer is inserted, the soil adjacent to it yields, and the radial and circumferential stresses change by an amount that depends on the compressibility of the soil. The radial stress always increases when a piezometer is inserted; by a

factor of 1.5 for highly compressible soil to as much as 5.2 for relatively incompressible soil. The circumferential stress at the wall of the piezometer, however, will decrease by a factor of as much as 0.6 for highly compressible soil, or increase by as much as 2.1 for relatively incompressible soil. Deformation resulting from pushing a piezometer into the ground, thus, could either increase or decrease--depending on the compressibility of the soil--the pressure required to initiate fracturing, according to the analysis of Bjerrum and others (1972).

An analysis of the conditions required to create a hydraulic fracture specifically in unconsolidated sediment is presented by Horsrud and others (1982), who use coupled elastic and plastic solutions. Fracture initiation pressures can be reduced by plastic deformation to roughly 10 percent less than that predicted by elastic theory, according to their results. Medlin and Masse (1979) presented both experimental and theoretical evidence confirming that plastic deformation around a borehole reduces the pressure required for fracture initiation.

Predicting the maximum pressure achievable without causing a hydraulic fracture during injection grouting has been an elusive task. The limiting pressure is recognized to increase with depth; values of 1.0 to 4.5 psi/ft of depth are used in regulations defining maximum allowable pressure (Dickinson, 1988). Those gradients apparently are determined empirically. Morgenstern and Vaughn (1963) suggest that a Mohr-Coulomb failure criterion could be adopted to predict hydraulic fracturing during grouting, although the mode of failure--shear--implied by that criterion is unfounded for hydraulic fractures. The analysis of Wong and Farmer (1973) assumes tensile failure and uses an elastic analysis, which includes pore-pressure effects, to examine the initiation of a hydraulic fracture during grouting. This approach is consistent with established methods (e.g. Haimson and Fairhurst, 1967), although it is unclear how well it predicts grouting pressures.

Analyzing the propagation of an unwanted hydraulic fracture has received little attention. A notable exeception is the analysis of a hydraulic fracture cutting the core of the Fontana dam in Tennessee (Shaffer and others, 1984; and references therein). In that study a detailed finite element code, which coupled elastic deformation of the medium and fluid flow in the fracture, was used to predict the path of the hydraulic fracture with remarkable accuracy, as compared with field observations made at the dam site.

APPENDIX C

THE STEADY STATE DRAWDOWN DUE TO A WELL INTERSECTING VERTICAL HYDRAULIC FRACTURE IN A CONFINED AQUIFER

Steady flow to a well intersecting a vertical hydraulic fracture filled with sand will be idealized by considering the well as a line sink and the fracture as an elliptical-shaped body of hydraulic conductivity K_I embedded in a matrix of conductivity K_{II}. The elliptical body has a major axis a, a minor axis b, and a focus f, where

$$f = \sqrt{a^2 - b^2} \tag{C.1}$$

The line sink lies at the center of the elliptical body, which is at the origin of an elliptical coordinate system defined by confocal ellipses, u, and confocal hyperbolas, v. Elliptical coordinates are related to cartesian coordinates according to

$$x = f \cos v \cosh u \tag{C.2a}$$

$$y = f \sin v \sinh u \tag{C.2b}$$

Thus, the ellipse u_e having axes a and b is given by

$$u_e = \cosh^{-1}\left[\frac{a}{\sqrt{a^2 - b^2}}\right] \tag{C.3}$$

The aquifer containing the fracture has a thickness of T and is confined by impermeable boundaries. The fracture will be termed Region I and the enveloping aquifer termed Region II for convenience. Flow in Regions I and II are at steady state and are governed by the Laplace

Equation

$$\nabla^2 \phi_I = 0 \tag{C.4a}$$

$$\nabla^2 \phi_{II} = 0 \tag{C.4b}$$

where we will take ϕ to be the drawdown, and the Laplacian operator in elliptical coordinates is

$$\nabla^2 = \{1/f^2 (\sinh^2 u + \sin^2 v)\} \{\partial^2/\partial u^2 + \partial^2/\partial v^2\} \tag{C.5}$$

Boundary Conditions

Far field boundary conditions require zero drawdown as u approaches the radius of influence of the well R

$$\phi_{II} = 0, \quad u \to R \tag{C.6}$$

The pumping well is defined by the conditions for a line sink, which in radial coordinates require (Bear, 1979)

$$(\partial \phi_I/\partial r) = Q/2\pi r K_I T, \quad r \to 0 \tag{C.7}$$

where Q is the rate of pumping at the well.

Conditions of continuity and equilibrium require that the total head and the flux normal to u are equal at the interface between the fracture and the matrix. The conditions at the interface are

$$\phi_I = \phi_{II}, \quad u = u_e \tag{C.8a}$$

$$K_I (\partial \phi_I/\partial v) = K_{II} (\partial \phi_{II}/\partial v), \quad u = u_e \tag{C.8b}$$

Derivation of a solution to the conditions described above would be cumbersome in the present form. A more manageable form, however, is obtained by separating the problem into two parts, one considering the line sink and the other the interface conditions. The two parts are superposed to obtain the solution.

Superposition

We will decompose the problem to derive separate solutions for the line sink and for the conditions at the interface. One of the solutions, ψ_s, will show the distribution of heads due to the line sink in continuous material having the properties of either the fracture or the matrix. The other solution adjusts the drawdowns to account for the ellitically-shaped discontinuity in hydraulic conductivity, the idealized fracture. The sum of the two solutions

$$\phi_I = \psi_{Is} + \psi_I \tag{C.9a}$$

$$\phi_{II} = \psi_{IIs} + \psi_{II} \tag{C.9b}$$

will satisfy all the boundary conditions, as well as the Laplace Equation, and will be the solution for the drawdowns.

Solution to the Line Sink Part of the Problem

We will first consider the solution for ψ_{Is}, the drawdown due to the line sink in Region I, and the solution to ψ_{IIs} will follow directly. Boundary conditions in cylindrical coordinates are as follows

$$(\partial\psi_{sI}/\partial r) = Q/2\pi r K_I T, \qquad r \to 0 \tag{C.10a}$$

$$\psi_{Is} = 0, \qquad r \to R \tag{C.10b}$$

conditions of the line sink itself.

The conditions of the line sink at the origin are accounted for in the previous section, so in this section there is no drawdown at the origin

$$\psi_I = 0, \qquad u = 0,\ v = \pi/2 \tag{C.16}$$

This is the interior boundary of Region I. The condition at the exterior boundary of Region I is

$$\phi_{II} = \phi_I, \qquad u = u_e \tag{C.16b}$$

However, according to eq. (A.9)

$$\psi_I = \psi_{II} + \psi_{IIs} - \psi_{Is} \tag{C.16c}$$

or

$$\psi_I = \psi_{II} + \psi_{IIs}(1 - K_r), \qquad u = u_e \tag{C.16d}$$

Thus, drawdowns due to the line sink enter the boundary conditions at the interface and provide a coupling between the two parts of the solution.

The interior boundary condition on Region II, where it is adjacent to Region I, is given by

$$K_I(\partial\phi_I/\partial u) = K_{II}(\partial\phi_{II}/\partial u)$$

which can be rewritten using eqs. (A.9) and (A.15)

$$\partial\psi_I/\partial u = K_r(\partial\psi_{IIs}/\partial u + \partial\psi_{II}/\partial u) - \partial\psi_{Is}/\partial u$$

and it reduces further using eq. (A.14)

$$\partial\psi_{II}/\partial u = (1/K_r)\ \partial\psi_I/\partial u \qquad u = u_e \tag{C.16e}$$

The exterior boundary condition on Region II is

$$\psi_{II} = 0, \qquad u = u_R \tag{C.16f}$$

A solution to the conditions described above can be obtained using Fourier series. For convenience, I will assume that the series take the following form

$$\psi_I = \sum_{n=1}^{\infty} A_n \cosh nu \cos nv \tag{C.17a}$$

$$\psi_{II} = \sum_{n=1}^{\infty} B_n \sinh n(R-u) \cos nv \tag{C.17b}$$

Boundary conditions at the origin and at u_R are satisfied by the forms of the series, and the conditions along the boundaries between the regions will be used to obtain the constants A_n and B_n. Substituting the eqs. (A.17) into the boundary conditions for Region I eq. (A.16d) yields

$$\sum_{n=1}^{\infty} A_n \cosh nu_e \cos nv = \sum_{n=1}^{\infty} \left[B_n \sinh n(R - u_e) \cos nv \right] + (1 - K_R)\, \psi_{II}(u_e, v) \tag{C.18}$$

The rightmost term in eq. (A.18) can be written as the following Fourier Series

$$(1 - K_R)\, \psi_{II}(u_e, v) = \sum_{n=1}^{\infty} C_n \cos nv \tag{C.19a}$$

and using standard methods

$$C_n = 2(1 - K_R)/\pi \int_0^{\pi} \psi_{IIs}(u_e, v) \cos nv \, dv \qquad \text{(C.19b)}$$

An analytical evaluation of the integral in (A.19b) was sought, but could not be obtained during this investigation. The integral was evaluated numerically using Gaussian quadrature.

Substituting eqs. (A.19) into (A.18) yields

$$A_n \cosh nu_e = B_n \sinh n(u_R - u_e) + C_n \qquad \text{(C.20)}$$

because the coefficients of each series must be equal for similar values of n. Using similar arguments, it follows from the condition on Region II eq. (A.16e) that

$$A_n = - K_r B_n \cosh n(u_R - u_e)/\sinh nu_e \qquad \text{(C.21)}$$

The coefficients A_n and B_n are

$$A_n = \frac{K_r \cosh n(u_R - u_e)\, C_n}{\sinh nu_e [K_r \cosh n(u_R - u_e) \coth nu_e + \sinh n(u_R - u_e)]} \qquad \text{(C.22a)}$$

$$B_n = - \frac{C_n}{K_r \cosh n(u_R - u_e) \coth nu_e + \sinh n(u_R - u_e)} \qquad \text{(C.22b)}$$

and the problem is solved.